Circuit Models for Standard and PAM Induction Machines

CIRCUIT MODELS AND PARAMETER IDENTIFICATION FOR STANDARD AND POLE AMPLITUDE MODULATED POLYPHASE INDUCTION MACHINES

by

James Forrest Lindsay, B.Sc. (Hons.) (Glasgow)

A thesis submitted to the
Faculty of Graduate Studies and Research
in partial fulfillment of the requirements for the degree of

Doctor of Philosophy

Department of Electrical Engineering,
McGill University,
Montreal, Quebec,

February, 1973.

ABSTRACT

Conventional circuit models for balanced operation of polyphase induction motors are reviewed and augmented to include second order effects. Experimental procedures and instrumentation are developed to measure the characteristics of a machine so that its circuit parameters can be identified. Analytical solutions based on curve fitting are compared with parameter optimizing techniques based on minimization of an error function. Optimizing techniques are shown to yield reliable models which include effects of saturation of main and leakage flux paths and skin effect in the bars of a squirrel cage rotor.

The work on standard machines provides a basis for the development of a dynamic circuit model for pole amplitude modulated machines which normally have high harmonic mmf content and asymmetrical windings. This model includes an orthogonal axis equivalent of a squirrel cage rotor. Experimental results show that harmonic effects are correctly predicted, the difference between measured and computed torques being consistent with stray loss effects.

ABSTRAIT

Les modèles conventionnels des circuits des moteurs asynchrones polyphasés sont revus et accrus pour inclure les effets de second ordre. Des procédures expérimentales et l'instrumentation sont développées pour déterminer les caracteristiques d'une machine afin que les paramètres du circuit puissent être identifiés. Des solutions analytiques basées sur l'ajustement d'une courbe sont comparées avec les techniques d'optimisation des paramètres par la minimisation d'une fonction d'erreur. Il est prouvé que les techniques d'optimisation produisent des modèles fiables qui tiennent compte des effets de la saturation du parcours du flux principal et celui des fuites, aussi bien que l'effet de peau dans les barres de la cage d'écureuil.

Les études sur les machines ordinaires donnent une base pour la développement d'un modèle dynamique pour les machines à fmm modulée qui normalement possèdent de forts harmoniques de la fmm et des enroulements asymétriques. Le modèle employe des axes orthogonaux qui le rendent équivalent à la cage d'écureuil. Les resultats experimentaux montrent que l'effet des harmoniques est prédit correctement, la différence entre les valeurs mésurées et celles des couples calculées est compatible avec les effets des pertes parasites.

PREFACE

This thesis describes a new approach to the parameter identification problem of standard and pole amplitude modulated polyphase induction machines. To the best of the author's knowledge, the following are original contributions:

a) The application of a function minimization technique to optimize a set of parameter values for a circuit model, and the determination of the conditions where this may satisfactorily be done.

b) The development of a suitable circuit model which is enlarged to include second order effects.

c) The use of an equivalent rectangular bar to model skin effect in the bars of a squirrel cage rotor, the depth of the bar being determined by the parameter optimization process.

d) The development of instrumentation for the acquisition of the necessary data. In particular, the instrument used to separate and measure the in-phase and reactive components of input current is an original design which is not commercially available.

e) The complete instrumentation system makes it feasible to operate a machine at normal voltage levels while acquiring the experimental data. As a result it is now possible to obtain reliable parameters applicable to normal operation.

f) The review of pole amplitude modulation is a novel presentation which is particularly concise and in which the existing general theorem of three-phase modulation has been extended to the more general case of q phases

8) The dynamic circuit model for pole amplitude modulated machines involves a new transformation of the variables for a squirrel cage rotor to those of a quasi-stationary set of two-phase coils. The model includes all airgap mmf harmonics and is directly applicable to machines having asymmetrical windings.

ACKNOWLEDGEMENTS

I wish to express my gratitude to Dr. T.H. Barton for his guidance throughout this project. His advice and encouragement have been very much appreciated.

I am grateful also to W. Taal, J. Foldvari, I. Borissov and other technicians of the Department of Electrical Engineering for their assistance in assembling many parts of the equipment, and to Nakra, Peter Morrison and graduate students for many valuable discussions. In addition, Professor P.J. Zsombor-Murray and Mr. L.J. Vroomen of the Data Acquisition Centre were most helpful.

The project received financial support from the National Research Council of Canada, and the pole amplitude modulated machines were provided by Canron Ltd. (Electrical Division). My sincere thanks are offered to these organisations and to McGill University who provided experimental and computational facilities.

I wish also to acknowledge my indebtedness to Sir George Williams University for the freedom and encouragement given me to undertake and complete the project, and also for the use of computational facilities.

With regard to the preparation of this thesis, I am grateful to Miss Geri Phillips, who typed the manuscript, assisted by Miss Jill Commerford.

These acknowledgements would not, however, be complete without a reference to my wife, Judy, whose patience and understanding have given me much needed support.

TABLE OF CONTENTS

LIST OF TABLES

LIST OF ILLUSTRATIONS

CHAPTER I

INTRODUCTION

The formulation of equivalent circuits for induction motors is a problem which has received much attention. Nevertheless standard models and the methods used to measure their parameter values are not entirely satisfactory in that they produce noticeable differences between measured and predicted characteristics. The availability of automatic data acquisition and reduction systems now offers the possibility of improving on existing methods of parameter identification. The facility and rapidity with which such systems can accurately acquire and store large quantities of information should result in the ability to use a wider range of experimental data, thus making it possible to include second order effects in a more detailed model and to consider the effects of temperature rise on performance more effectively.

Among the effects which may require considerable experimental data for their identification are airgap mmf harmonics,[1] skin effect in the rotor bars of a squirrel cage machine,[2] reduction of leakage reactance due to saturation of the leakage flux paths,[3,4] incremental losses in the teeth due to leakage flux,[5] and changes in parameter values due to saturation of the main core. Measurement of parameter values where these effects are significant poses many problems for which no satisfactory solutions have yet been found. For example, the assumption of negligible harmonic effects is often justifiable in the case of modern standard induction motors and from this point of view existing models appear to be satisfactory. However, development of pole amplitude modulated induction motors[6,7] in recent years now provides situations where the harmonic content is invariably large, yet the literature is notably lacking in circuit models. There is therefore a clear need to develop suitable models and parameter identification techniques for such situations. Most of these machines have squirrel cage rotors and therefore skin effect is also likely to be appreciable. The main difficulty in modelling this effect from experimental data is that of estimating the change in part of the rotor resistance and leakage reactance as the speed changes. Since the leakage flux paths include the teeth of both rotor and stator, any tendency for these parts to saturate under the influence of winding currents at high values of slip, irrespective of the terminal voltage, also results in leakage reactances which are speed dependent. In addition to this change in leakage reactance, the leakage flux produces in the teeth incremental core losses which are determined by the winding currents.

The circuit model which is used for the majority of polyphase induction machine problems is based on the similarity between a transformer and a machine having balanced windings, voltages and currents.[8] This model is basically that of a short circuited transformer in which the value of one of the resistive parameters is dependent on the relative velocity between the two sets of windings. Standard tests for the measurement of parameter values for this model do not provide sufficient information to determine the variations in parameter values due to some of the second order effects discussed above. Inclusion of these effects in the model requires additional circuit elements and additional experimental data from operation over a range of speeds rather than at the limited number used in the standard tests. A data acquisition system therefore seems to offer the best means of gathering and interpreting sufficient data so that an enlarged model may include these effects.

Another form of model which is widely used is the set of dynamic circuit equations which results from viewing the machine as a network of coupled coils, some of which are free to move relative to the remainder.[9,10] This model is particularly valuable for situations where windings or source voltages are not balanced. The circuit equations for the actual coils are non-linear and it is usual to seek transformations for some of the variables which yield sets of linear equations for which the total power in terms of the transformed variables is the same as that given by the original variables. These transformations are usually obtained by considering the transformed variables to be associated with another set of coils which produces exactly the same magnetic effect in the airgap, and whose reference frame is chosen to suit the particular situation. The matrices which perform these power invariant transformations are orthogonal, the simplest forms being those having only two axes. Since pole amplitude modulated machines often have asymmetrical windings,[11] a dynamic circuit model is likely to be the most viable form. This, however, requires the determination of a suitable transformation which includes the effects of airgap harmonics.

This thesis presents a new approach to the parameter identification problem. Instrumentation and experimental procedures are developed to provide for the measurement of parameter values of a circuit model which is enlarged to include second order effects. An important feature of this approach is that the time required for a set of measurements is sufficiently small that a machine may safely be operated at its rated voltage, thus making it possible to obtain a reliable set of parameter values applicable to normal operation. In addition, the equipment and experimental procedure are well suited to the measurement of all operating characteristics, including those of machines having significant harmonic content.

After first describing the instrumentation and experimental procedure, the relatively simple situation in a wound rotor machine operated at low voltage is used to develop the augmented circuit model and establish the validity of both model and procedure. Next, skin effect in the rotor bars of a squirrel cage machine is added to the model, and the effect of voltage level on parameter values determined by operating a machine over a range of voltages up to its rated value.

Following a review of the basic principles involved in pole amplitude modulation, a dynamic circuit model is developed for this situation simultaneously involving significant harmonic content and skin effect in the rotor bars. In this case the stator has three axes on each of which there are two sets of harmonic coils to model exactly the magnetic properties of the windings. To complete the model a two-axis equivalent of a squirrel cage rotor is developed. An interesting feature is that although the harmonic coils are electrically orthogonal, their relative mechanical positions are dependent on the order of the harmonic. It may also be noted that the normal simplifications resulting from the absence of groups of harmonics, such as those having even numbers in standard windings, do not apply, and the presence of sub-harmonics makes it desirable to think in terms of a two-pole field which is the fundamental, and a spectrum which has a peak value at the number of poles which it is intended should dominate the airgap field. Finally the model is verified by an experimental investigation of two machines, one having 6/8 poles and the other 6/4 poles.

CHAPTER II

INSTRUMENTATION

2.1 Introduction

The methods which have been devised to obtain parameter values depend on the availability of test facilities incorporating some features not usually found on a dynamometer. The equipment must provide means for changing and measuring speed while the in-phase and reactive components of current are measured. If the speed is changed continuously it is desirable that the acceleration be constant in order to simplify the correction for inertia torque. The speed control system should therefore be capable of providing either a ramp or a constant value of speed. The terminal voltage should be monitored continuously and variations in its value kept to a minimum. To satisfy these requirements, the instrumentation requires several distinct parts, each of which is described below. Figures 2.1 and 2.2 show two views of the system.

2.2 The Dynamometer

The dynamometer has a d.c. work machine which is rated 7½ HP and may be operated at speeds up to 2500 rpm. Speed control is by means of a Ward-Leonard system whose basic reference is obtained from a chopper stabilized operational amplifier which can be operated either as an integrator to provide the ramp reference or as an invertor to provide the constant reference. A thyristor bridge circuit and a motor-generator set provide the necessary power amplification for the d.c. work machine which provides an excellent ramp of speed whose only defect is a slight change of slope on passing through the synchronous speed of the induction machine under test; this is

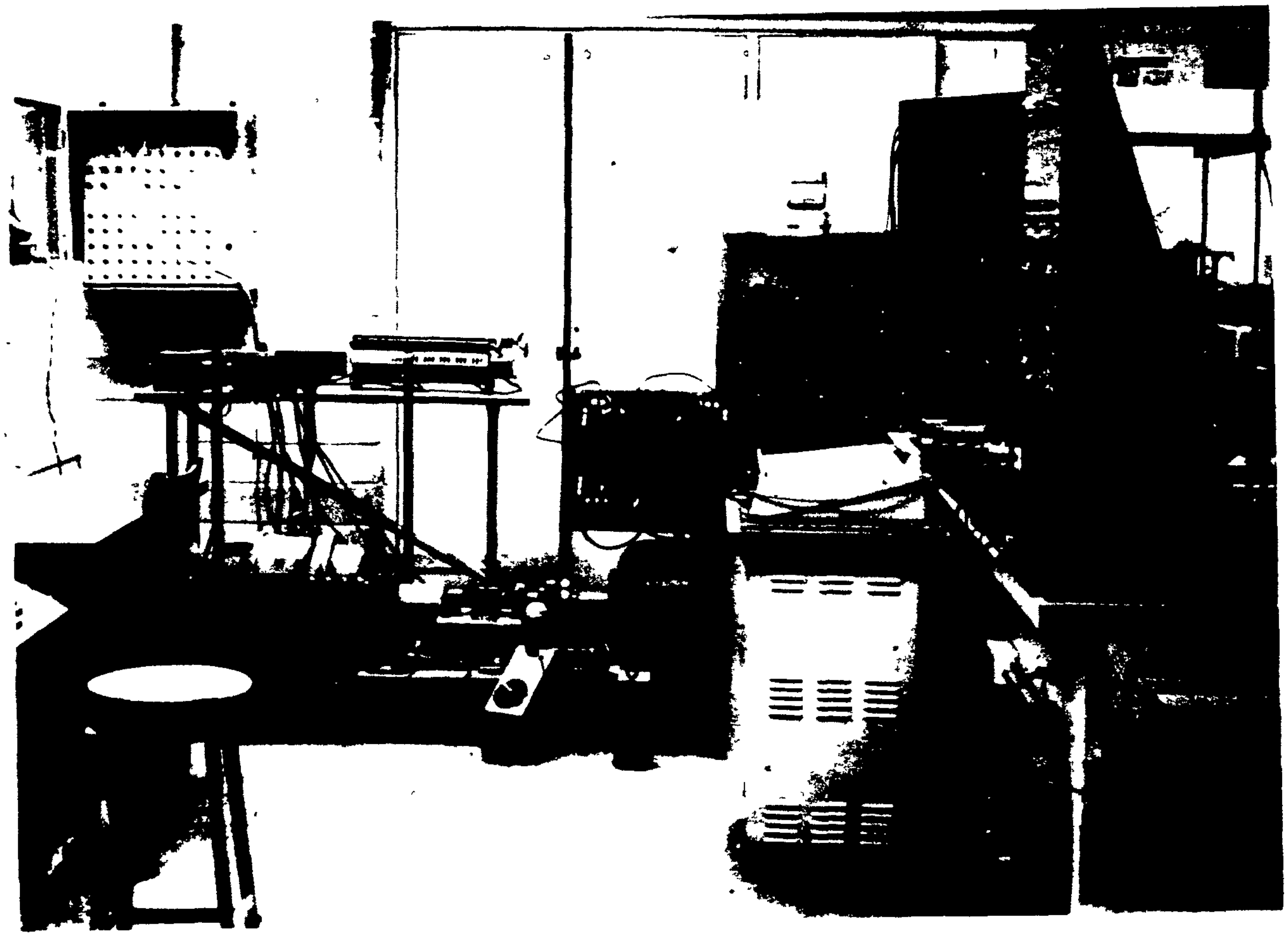

Fig. 2.1 View of Dynamometer

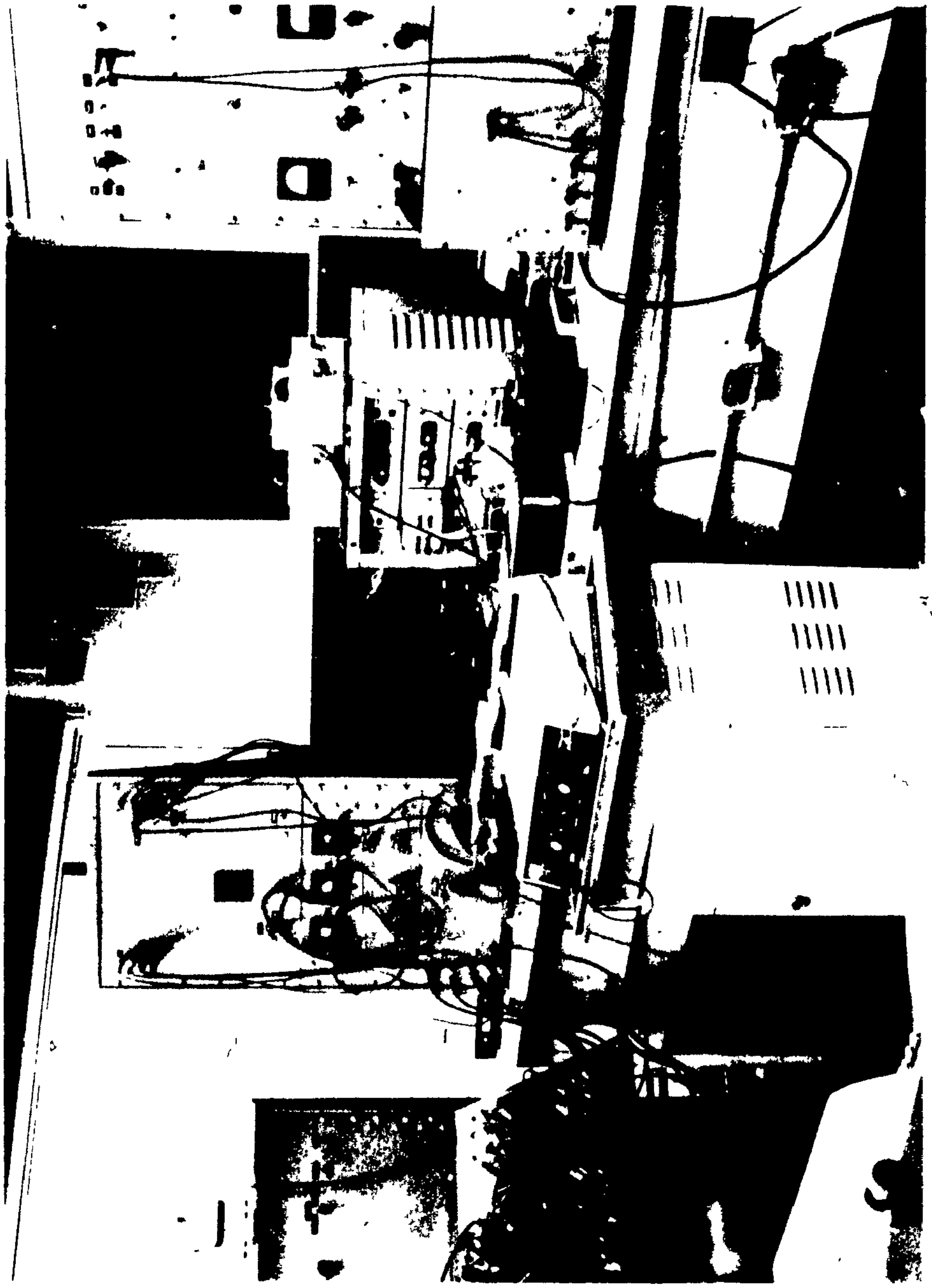

Fig. 2.2 View of Instrumentation

due to hysteresis in the d.c. machines when the power flow reverses.

To achieve the large accelerations required when operating a machine at full voltage, and to overcome the pull-out torque, it is necessary to have a large margin of power reserve in the dynamometer. The speed control of this 7½ HP dynamometer is at the limits of its capability in handling the full voltage pull-out torque of a 2 HP induction motor. Larger machines were operated at reduced voltages where the limiting factor was the current capability of the voltage regulator.

The controller has two ranges for both of its modes of operation. For continuous speeds the maximum values are 250 and 2500 rpm. For ramps of speed the maximum values are 250 and 2500 rpm/sec.

A d.c. tachogenerator provides the measurement of speed. It has an output of 50 V per 1000 rpm and although it has high power capability, it can deliver its rated accuracy of 0.15% only when the load is at least 1 MΩ. A high voltage operational amplifier in simple inverting mode is therefore used as a buffer. The signal is then brought down to a level suitable for the solid state amplifiers which are used throughout the other parts of the system.

Measurement of torque is accomplished by means of a torquemeter of the magnetic anisotropy type which has been developed in previous projects at McGill University.[12] It is excited at 200 Hz to reduce the influence of stray 60 Hz fields and the excitation current is controlled to improve its stability.

To measure stalled torque as a function of position, it is necessary to rotate the machines very slowly with minimal fluctuations in speed. The effect of tooth ripple is such that the main speed control system is unsuitable, and an auxiliary drive system is used for this purpose. It is shown in Figure 2.3.

2.3 Electrical Measurements

The problem of determining parameter values for a circuit model is basically that of measuring either the input impedance or admittance of a machine. If the machine is operated at constant voltage, the real and imaginary components of the input admittance can be determined directly from the in-phase and reactive components of the input current. Since there is no standard instrument capable of performing this function at power frequencies, it was necessary to design and make one having the required accuracy.

The components of input current are detected by two sets of solid state, chopper type, phase sensitive detectors connected to the outputs of three current transformers. One set is switched in phase with the line-to-neutral voltage, and the other set at a phase angle of 90°, this shift being accomplished by a set of three integrators. The components of any one of the three currents or their arithmetic mean are indicated on two d.c. milliammeters and there are corresponding signals available for recording.

Voltage control is by means of a three-phase autotransformer unit. The voltage is measured by a three-phase diode bridge circuit and compared with a zener diode reference. A thyristor bridge circuit provides the necessary amplification of the error signal to operate the drive motor. The rating of the unit is 120 volts (line-to-neutral), 50 amperes.

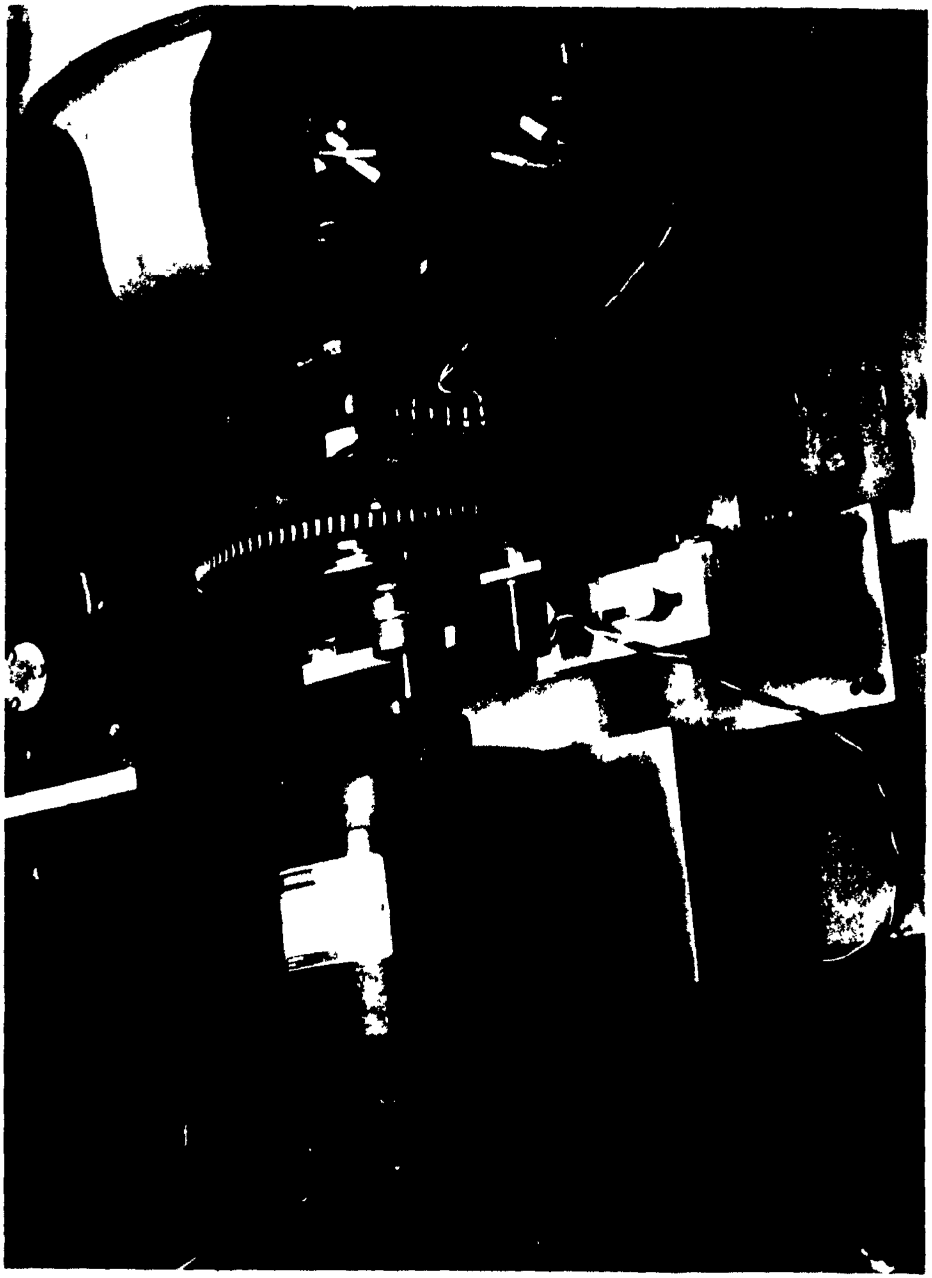

Fig. 2.3 View of Auxiliary Drive System

To determine the temperature of the machine, the d.c. resistance of the stator winding is measured immediately before and after each set of measurements. The method used is the simple one of measuring current and voltage, but for reliable data acquisition the signals must be filtered to eliminate the effects of remanence induced voltage.

2.4 Data Acquisition

Normally the choice of a data acquisition system is determined to a large degree by the quantity of data to be recorded. The data for simultaneous measurement of several characteristics may be recorded in analog or digital form. In this context, the advantages of an analog system include its relative simplicity and the ease of visually smoothing out irrelevant perturbations. Those of a digital system include the possibility of computer control, the fact that the data is already in a form suitable for processing by computer, resulting in reduced time between the measurements and final results, and greater resolution which should be of particular value in determining values for those parameters modelling second order effects. Unfortunately a computer controlled system requires considerable time to set up and must have much repeated use if it is to justify the increased cost of preparation. Nevertheless it seems desirable to use such a system with a view to assessing the feasibility of automatic measurement of parameter values. Digital data acquisition has therefore been used for the development of the parameter determination techniques described in Chapter 4 and also for the experimental study of pole amplitude modulated machines described in Chapter 9. Analog data acquisition has been used for measurements of parameter values at voltage levels up to the rated value, since they must be brief on account of the very rapid rise in temperature. This has provided an opportunity to determine the effect of the lower resolution.

Both the analog and the digital system have difficulty in dealing with one of the natural modes of torsional oscillation of the dynamometer. For example, when coupled to the wound rotor machine there is a natural mode of approximately 30 Hz which appears at several discrete values of speed within the range to be measured. The resulting oscillation in torque is sufficiently high to be hazardous to an X - Y plotter. In addition, there is an oscillatory torque due to mechanical difficulties in aligning the shafts, the frequency being the same as the shaft speed. The torque and speed signals are therefore passed through low-pass active filters.[13] To minimize time lag errors in the recorded data, the signals for the in-phase and reactive components of current are also passed through low-pass filters having the same break point as the speed signal. Since the oscillatory torque is the larger and more troublesome, its filter is fourth order and its break point adjusted so that for the range of frequencies in the signals the time lag is the same as those of the second order filters in all other channels.

In the digital system all the signals derived from the instrumentation are measured by a digital voltmeter and multiplier which are controlled by a General Electric model 4020 process control computer. Range, integration time and scanning rate are programmed to suit the experimental conditions.

In the analog system the signals are measured and recorded by a multi-channel optical recorder. Transcription of the recorded data to digital form is simplified by including the necessary calibration factors in the main computer program.

CHAPTER III

EXPERIMENTAL PROCEDURE

3.1 Introduction

In any process of parameter identification there are two main aspects which are closely interrelated. These are the experimental procedure and the general strategy of computing the parameter values from data obtained by measurement. The development of novel instrumentation specially for the task of measuring parameter values of a novel model inevitably leads to an experimental procedure which has novel features. Although this procedure was developed primarily for use with the models and computational methods described in Chapter 4, it is suitable for the more general task of measurement of all of the characteristics of an induction machine since the conditions applying to these characteristics must be clearly defined. It has therefore been used for the measurement of the characteristics of the pole amplitude modulated machines shown in Chapter 9. An important aspect of any experimental procedure is the error which it introduces. After the detailed description which follows, the remainder of the chapter is devoted to consideration of those effects which are most likely to result in serious experimental error specifically introduced by the procedure.

3.2 Details of the Procedure

The d.c. resistance of the stator winding is measured just before beginning a set of measurements. This is done with the set running at the desired initial speed in order to minimize the time elapsed between the resistance measurement and the first measurement after the machine has been switched on. Measurement of the d.c. resistance while the machine is running minimizes errors in estimating the temperature of the winding during a set of measurements, but unfortunately the effect of remanence in the rotor core results in significant ripple in the voltage which appears across the winding terminals. The elapsed time is measured in the digital system by storing the computer time count at the end of each scan. In the analog system it is measured directly from the recording. After allowing a short time for conditions to become steady, the ramp is switched on or the speed changed point by point and data acquired over the desired range of speed.

Immediately after the machine has reached the ultimate value of speed or, in the case of the digital system, the last scan has been completed, the d.c. resistance is again measured. The speed is then returned to the initial value so that it may be changed again over the same range under the same conditions to determine the inertia and friction torque. With the analog system the data is already recorded on photographic paper and is transcribed to digital form later. With the digital system the data is stored on disc and, if required, the procedure repeated, the only limit being that imposed by the space available on disc. The data is retrieved from the disc after the system has been shut down, and computation follows.

There are two effects which may cause difficulty with the interpretation of the data obtained with this procedure. The expressions given in Appendix A and the normal computation of induction machine characteristics assume that the temperature is constant. This is not correct during a set of measurements and the d.c. resistance is measured so that the temperature variation may be estimated by the method described below. It is also assumed that the machine is electrically in the steady state. If the speed is being changed continuously in the form of a ramp, the slope of the ramp must be small enough that its electrical effects are negligible. This is also considered below.

3.3 Temperature Compensation

One feature of this procedure is the ability to take a complete set of experimental data in a time period sufficiently small that the rise in temperature is kept to a reasonable value. It is tempting to conclude that a change of only a few degrees ought to be negligible. However, the fact that there is a deterministic change in temperature as the measurements proceed rather than a random fluctuation about a mean value results in a swing of some of the characteristics which leads to erroneous results when using the curve fit method described in Appendix A. The swing in the $R_\sigma s$ characteristic can be seen by inspection of Figures 4.5 and 4.6; the uncompensated points show a significant difference in curvature and inspection of the intercepts shows that in one case there is an increase but in the other there is a decrease, leading to values of rotor resistance which are significantly different. For the wound rotor machine used in the investigation it may be noted that the effect of a 5°C increase in temperature is to increase the input conductance by 1¼% and the torque by 1% when stalled. These are significant errors and it is therefore essential to model the variation in temperature and to compensate for it when using measured data to obtain parameter values.

3.3.1 The Thermal Model

Accurate prediction of temperature variations in a rotating machine over a long period of time has been the subject of much investigation in the past [14-16]. A detailed thermal model is complex and experimental determination of its parameters is lengthy and difficult[17]. However, in this case, because of the short time periods involved and the relative constancy of conditions, a simple model in which the machine is regarded as a single homogeneous body with cooling dependent on speed should be sufficiently accurate. Any errors can be minimized by using cooling curve data measured at two or more values of speed to provide the thermal conductance and its speed dependence, and then iterating the computation of the temperature response to seek the thermal capacitance which matches the calculated and measured values of temperature at the end of the measurements.

The basic expression for the temperature variation of a homogeneous body in which the losses are P watts is

$$P = C\frac{d\phi}{dt} + D(\phi - \phi_a) \tag{3.1}$$

where ϕ is the temperature, ϕ_a the ambient temperature, C the thermal capacitance and D the thermal conductance. Hence

$$\frac{d\phi}{dt} = \frac{1}{C}[P - D(\phi - \phi_a)] \tag{3.2}$$

Since the voltage is constant during measurements, and the core losses form a significant part of the total loss during only a small part of the characteristics, the losses may be assumed proportional to the square of the input current, and thus

$$\frac{d\phi}{dt} = K_c[i^2 - K_d(\phi - \phi_a)] \tag{3.3}$$

where K_c and K_d are revised thermal parameters due to the change of variable from power to current. The initial slope of the cooling curve is therefore given by

$$\left[\frac{d\phi}{dt}\right]_0 = -K_cK_d(\phi_o - \phi_a) \tag{3.4}$$

$$= -K_N(\phi_o - \phi_a) \text{ at speed } N$$
$$= -K_S(\phi_o - \phi_a) \text{ when stalled} \qquad (3.5)$$

The values of K_N and K_S are obtained by direct measurement and the initial slope of the cooling curve at any other speed n is given by

$$\left[\frac{d\phi}{dt}\right]_0 = -\left[K_S + (K_N - K_S) \cdot \frac{|n|}{N}\right] (\phi_o - \phi_a)$$
$$= -K_n(\phi_o - \phi_a) \qquad (3.6)$$

This value of K_n replaces $K_c K_d$ in Equation 3.3 and the change in temperature during a time interval can be calculated using the mean value of the square of the current during the interval.

3.4 Acceleration Effects

It has been common practice until recently to assume that any mechanical transient associated with an induction machine would take place so slowly relative to the resulting electrical transients that the electrical transients could safely be ignored and the machine regarded as being in a quasi-steady-state condition. However, recent studies [18,19] have indicated that such a condition does not necessarily exist, especially for the common switching-on transient. It is therefore necessary to establish the errors likely to be introduced by a ramp of speed and note the parts of the characteristics which should be discounted in the modelling process.

The approach used here is to consider the application of a small perturbation, in the form of a ramp, to the normal two-axis model transformed to synchronous reference axes. The machine electrical equations in this reference frame are

$$v = (R + \omega_F F + \omega_m G)\,i + L\,\frac{di}{dt} \qquad (3.7)$$

where R, F, G and L are respectively the resistance, reference frame, torque and inductance matrices of the machine, ω_F is the velocity of the rotating reference frame, ω_m is the rotor velocity and v and i are the voltage and current vectors. For steady-state conditions

$$V = (R + \Omega_F F + \Omega_m G) I = ZI \qquad (3.8)$$

$$I = Z^{-1} V \qquad (3.9)$$

where upper case letters signify the quiescent values. For small perturbations v, i and ω_m

$$v = Zi + \omega_m GI + L \frac{di}{dt} \qquad (3.10)$$

In this case the perturbation is a ramp of slope α, and v = 0 since the applied voltage is constant. Thus

$$Zi + L \frac{di}{dt} = -\alpha GIt \qquad (3.11)$$

The steady-state solution has the form

$$i = At + B \qquad (3.12)$$

where

$$A = -\alpha Z^{-1} GI$$

$$B = \alpha Z^{-1} L Z^{-1} GI \qquad (3.13)$$

$\qquad$ = the error in current due to the ramp.

Computer solutions show errors in current which are completely negligible for the ramps used at all speeds other than close to synchronous speed. A typical set of results for an acceleration of approximately -450 rpm/sec. as used with the experiments on the 2 HP squirrel cage machine is shown in Figure 3.1 for the only range of speed over which the effect is appreciable. It can be seen that the differences between points which include the effect of the ramp and the curve, which is the normal steady-state response, are quite small. At lower values of ramp slope, such as those used

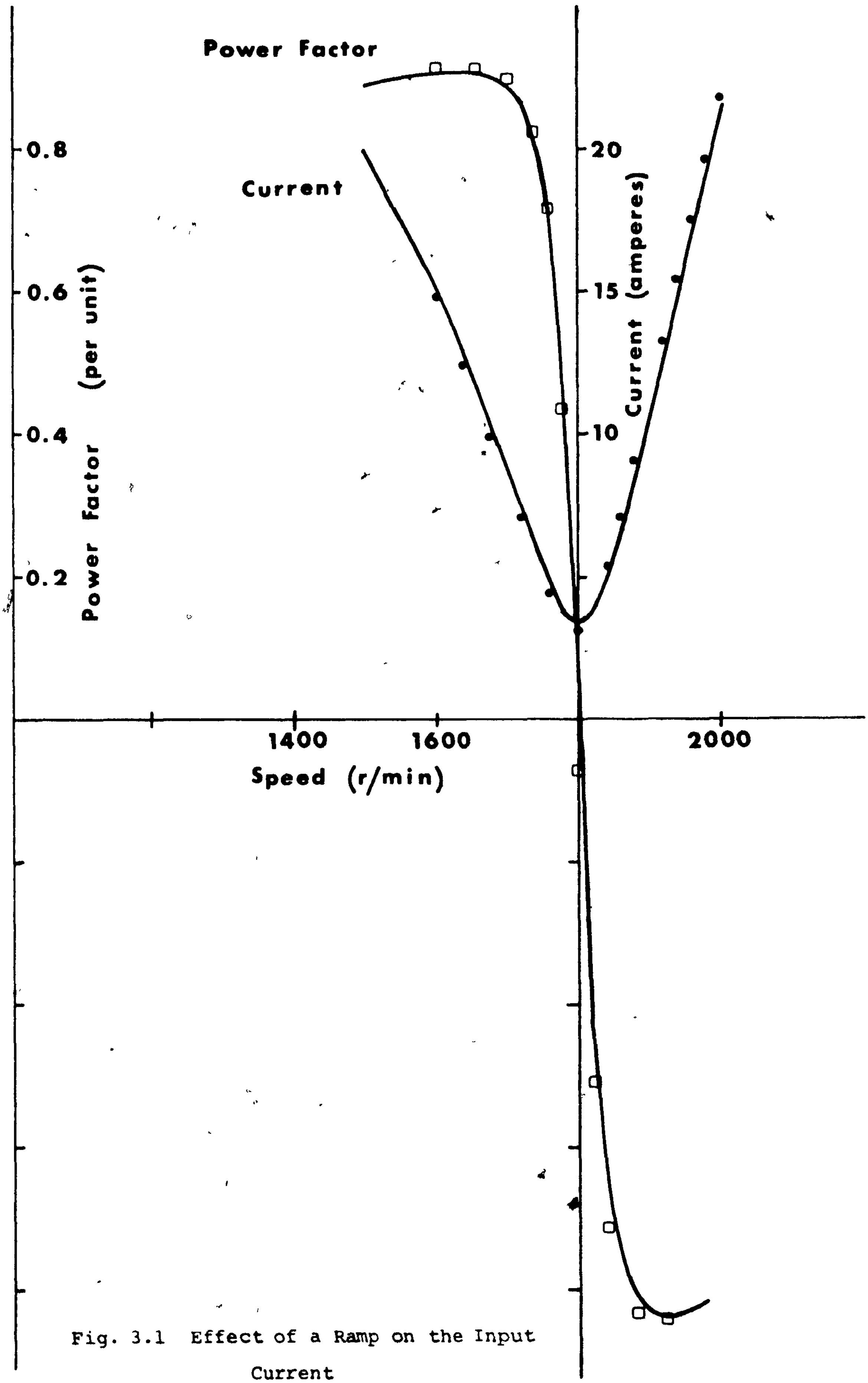

Fig. 3.1 Effect of a Ramp on the Input Current

with the wound-rotor machine, the effect is, of course, less and the only points which need to be discounted are those at very small values of slip.

CHAPTER IV

PARAMETER IDENTIFICATION FOR WOUND ROTOR MACHINES

4.1 Introduction

To complete a process of parameter identification, there must be a satisfactory method of using measured data to calculate numerical values for each of the parameters. In general, it seems desirable to work with an analytical solution for the parameters, but the nature of the model, even in its simplest form, results in sets of non-linear equations which usually are not written explicitly, yet nevertheless are made to yield approximate solutions by means of judicious simplifications[20]. Also, the adequacy of any set of parameters can only be judged if the experimental procedure has included operation over a reasonable range of speeds, preferably including operation in generating, motoring and braking modes. Thus, the computational process should be based on data obtained from the three modes of operation, rather than at a limited number of speeds such as no-load and stalled.

4.2 Circuit Models

The conventional model for balanced operation of a polyphase induction machine is essentially that of a transformer having relative motion between primary and secondary windings. The two most common circuit representations are shown in Figure 4.1 where, for simplicity, all quantities are referred to the primary. The representation of the core loss in Figure 4.1(a) corresponds more closely to physical reality but, if the excitation frequency is constant, the use of the series equivalent magnetizing impedance of Figure 4.1(b) results in somewhat simpler expressions.

This elementary model has certain deficiencies which are related to core losses and saturation of the leakage flux paths in an actual machine.

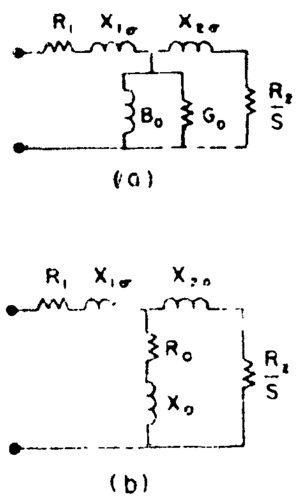

Fig. 4.1 The Simple Equivalent Circuit

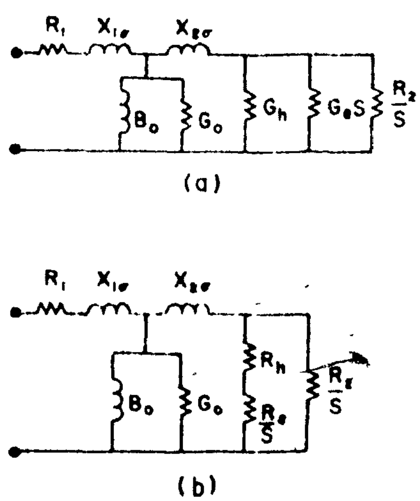

Fig. 4.2 The Additional Core Loss Parameters

$$G_c = G_h + G_e s$$

$$R_c = R_h + \frac{R_e}{s}$$

4.2.1 Core Losses

In a transformer the conductance G_o or resistance R_o of Figure 4.1 represents the total core loss. In an induction motor, because of the energy conversion process applied to all power crossing the airgap, it is necessary to consider separately the primary and secondary core losses. The most recent circuit proposed to model this effect is that shown in Figure 4.2(a).[21] The secondary core loss is represented by a conductance,

$$G_c = G_h + G_e s \tag{4.1}$$

the component G_h representing the loss due to hysteresis and G_e representing that due to eddy currents; G_h changes sign at synchronous speed. Such a formulation, while superficially attractive, is not in accord with observed iron loss behaviour since it suggests that, at constant peak flux density, the eddy current loss increases without limit as the frequency increases. If the frequency dependence of the losses in magnetic sheet steel is to be modelled without any inductance parameter, the series resistance arrangement of Figure 4.2(b),

$$R_c = R_h + \frac{R_e}{s} \tag{4.2}$$

appears to fit the observed behaviour more closely and this representation has therefore been adopted. As for G_h, the hysteresis component of resistance, R_h, changes sign at synchronous speed, being positive for positive slip and negative for negative slip.

4.2.2 Losses Associated with Leakage Fluxes

Since the leakage fields produce significant flux densities in the teeth, a small core loss is associated with them. This can be included in the equivalent circuit by a resistor such as R_c of Figure 4.2(b) in parallel with the leakage reactance. However, this is a small effect and it is more convenient to employ a series equivalent. Since eddy current losses at 60 Hz are usually much smaller than hysteresis losses and the whole effect is small, it is sufficient to take the equivalent primary resistance directly proportional to frequency and the equivalent secondary resistance numerically constant, but having the same sign as the slip.

4.2.3 Effect of Saturation on Leakage Reactance

In addition to the incremental losses described above, the relatively large flux densities in the teeth cause the leakage paths to saturate at high values of current even though the main flux path is well below the knee of its magnetization characteristic.[3] The leakage reactance is therefore reduced as the current increases and this effect can be modelled by the introduction of a negative reactance parameter. Since slip is used as the independent variable with the other variable parameters, it can also be used with this one, the effect being taken as proportional to the magnitude of the slip. Also, since the distribution of the leakage reactance between primary and secondary in the conventional model produces very little difference in calculated performance, it should be sufficient to model this effect using only one parameter in the secondary.

4.2.4 The Equivalent Circuit

Based on the above arguments, the equivalent circuit used for the parameter identification studies is shown in Figure 4.3, where R_{c1} and R_{c2} represent the rotor core losses associated with the main flux and $R_{1\sigma}$ and $R_{2\sigma}$ represent the core loss associated with the leakage fluxes. Direct application of this circuit is limited to the wound rotor machine, and situations

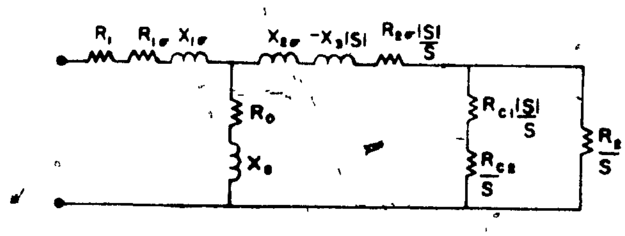

Fig. 4.3 The Complete Equivalent Circuit

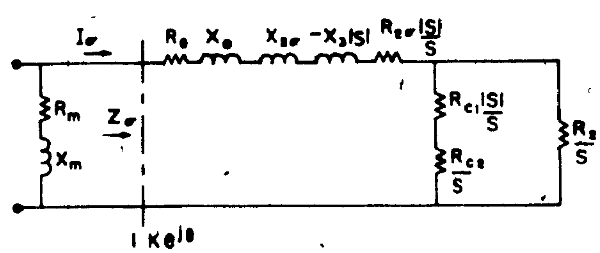

Fig. 4.4 The Modified Morris Model

where harmonic and skin effects are likely to be significant require further consideration.

4.3 Strategy of Computation

The essential purpose of computation is to match a set of data calculated from the parameters of the model with the measured data. There are two ways in which a digital computer may readily be used to achieve this end.

The data points can be considered as a known function of speed or slip and a strategy of least squares curve fitting used to determine the values of the parameters. This process is especially simple when the function is a polynomial although other forms are readily solved, the basic forms being well known.[22] Unfortunately, neither the conventional model of Figure 4.1 nor the more detailed model of Figure 4.3 produces a form of input admittance or impedance expression which is amenable to this approach.

There is, however, an alternate form of the conventional model[23] which has parameters obtainable from simple linear regression. If the[24] same transformation is applied to the model of Figure 4.3 the resulting model is shown in Figure 4.4 and a quadratic curve fitting process yields a set of parameters. Although the model can be used directly in this form, it suffers from the fact that some of its parameters cannot be associated directly with physical concepts such as the resistance of a particular winding or with the leakage flux. It is therefore desirable to transform this model to the form of Figure 4.3. Details of this transformation are given in Appendix A.

This procedure, although rather cumbersome in many respects, therefore provides an analytical solution to the parameter identification problem once the modified input data has been modelled on the statistical basis of the quadratic curve fitting process. Unfortunately, it is of limited value since it is not applicable to a squirrel cage machine in which there is significant skin effect in the rotor bars.

The other way in which a digital computer may be used to obtain a set of parameter values which will match the calculated characteristics with the measured data is to define an error function of the parameters and minimize it in a process of parameter optimization. Of the several methods available[24] one involving the use of conjugate gradients was used for the study.[25] In addition, some of the initial results were checked by using a simpler algorithm based on the method of steepest descent.[26] Since this procedure does not yield an analytic solution, it is prudent to exercise some caution due to the possibility that it may seek and obtain an undesired turning point of the error function. The choice of function is to some extent arbitrary, but is likely to be some form of the standard error,

$$S^2 = \frac{1}{n} \Sigma \Delta^2 \tag{4.3}$$

where Δ is the difference between measured and calculated values, and n is the number of data points. The experimental study of the wound rotor machine has shown that such a function produces a minimum which is sufficiently well defined that an initial parameter set based on extremely crude interpretation of the input admittance at synchronous and zero speeds, together with the arbitrary assignment of initial values to the second order parameters, yields a final set substantially in agreement with the results of the analytic solution above.

4.4 Experimental Results

Tests were carried out on a $7\frac{1}{2}$ HP wound rotor induction motor, details of which are given in Appendix B. The sliprings were short-circuited by means of a bolt to ensure consistency in the value of the rotor resistance. A typical experimental run covered a speed range of -1800 rpm to +2400 rpm at rates ranging from 12.5 to 50 rpm/sec. readings being taken at 100 rpm intervals. The current rating of the voltage regulator limited the applied voltage to approximately 40% of the rated value. This, however, was sufficient to indicate some degree of saturation of the leakage flux paths.

Typical plots of the characteristics R_σs and X_σs used for the curve fitting process are shown in Figures 4.5 and 4.6, the resistive ones being shown with and without temperature compensation. The necessity for temperature compensation can be seen by noting that the curvature of the uncompensated R_σs characteristic is dependent on the initial speed. The most important effect on the resulting parameter values is a significant difference in the indicated value of R_2. When the initial slip is approximately -0.3, the indicated value of R_2 is slightly low, but an initial slip of approximately 2.0 produces a value of R_2 of the order of 10% above the correct value. In addition to these curves the stalled torque is required for the evaluation of $R_{2\sigma}$. Unfortunately it is impractical to measure the stalled torque when the machine is stationary[27] as can be seen by inspection of Figure 4.7 which is a reproduction of a measurement of stalled torque as a function of shaft position. It is therefore necessary to extrapolate the torque-speed characteristic, Figure 4.8, from both sides of zero speed noting that there is a discontinuity due to Coulomb friction. The apparent oscillatory torque is that due to mechanical difficulties in the alignment of the shafts. The effect is the same when the

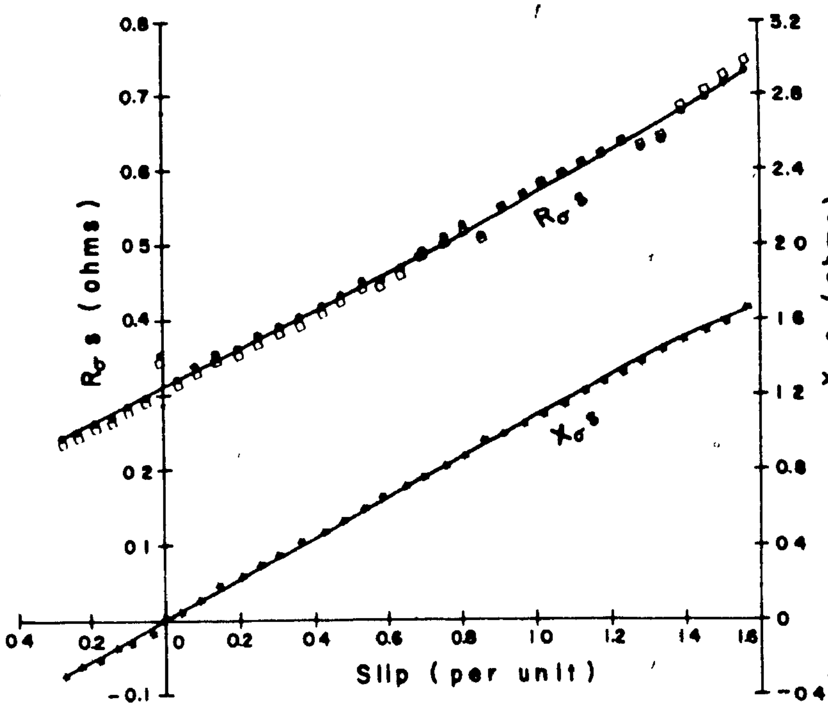

Fig. 4.5 $R_\sigma s$ and $X_\sigma s$ as Fuhctions of Slip.
Initial slip approximately -0.3.
● points compensated for temperature variation.
□ points uncompensated.

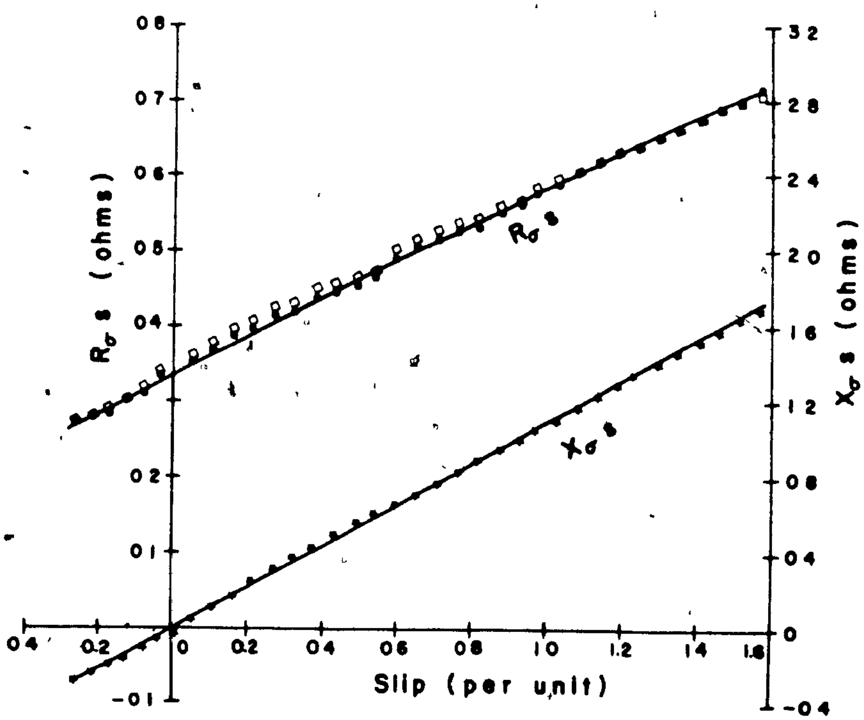

Fig. 4.6 $R_\sigma s$ and $X_\sigma s$ as Functions of Slip.
Initial slip approximately 2.0.
● points compensated for temperature variation.
□ points uncompensated.

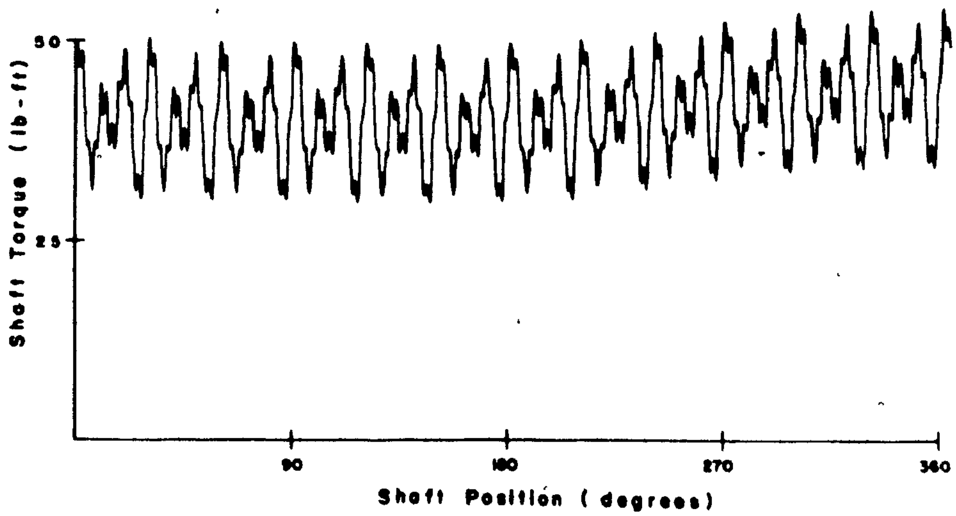

Fig. 4.7 Stalled Torque vs Rotor Position

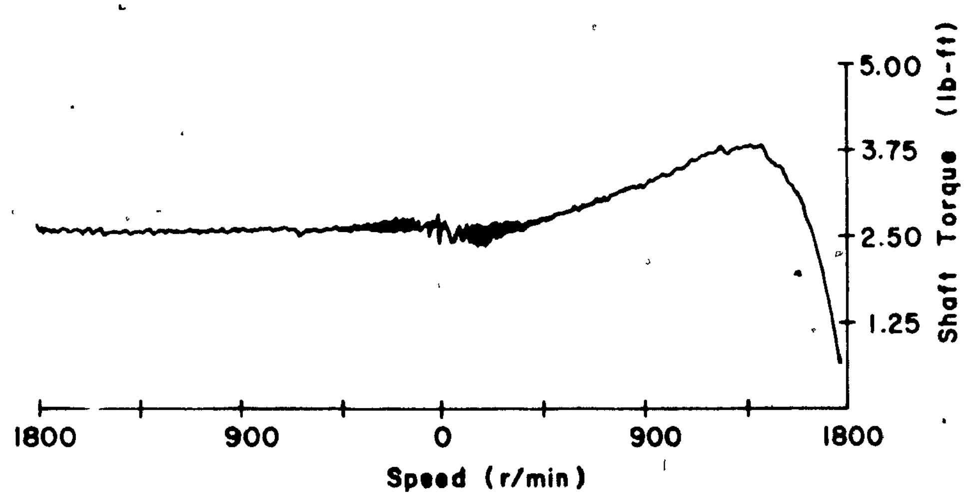

Fig. 4.8 Shaft Torque vs Speed

machines are unexcited and the effect is troublesome only when the machine is operated at low voltages which result in small developed torques. At higher speeds this effect can be filtered but it is impractical to do so at the lowest speeds and therefore measured torques in this region are unreliable.

Comparison of calculated and measured values for the purpose of error function minimization is based on the input conductance and susceptance. To make the value of the function more meaningful, the differences are expressed as a ratio of the admittance corresponding to full scale deflection of the ammeters. An alternate form in which the differences are expressed as a ratio of the measured value is also meaningful and has been used successfully. Since the stalled torque is used in the curve fitting method it can also be included in the error function. However, it is then a small component and makes only a small difference to the final result, this being primarily in the value of the stator resistance, $(R_1 + R_{1\sigma})$.

The results regarding the core loss parameters R_{c1} and R_{c2} are rather inconclusive in that although there is a tendency to reduce the value of the error function, it is quite insensitive to the values of R_{c1} and R_{c2} and therefore the optimization process is unable to change them from their initial arbitrary values. Most of the computation has therefore been done with the 8-parameter model of Figure 4.9 and comparison made with the conventional 6-parameter model of Figure 4.1(b).

A summary of the errors corresponding to different models is shown in Table 4.1. The errors for several possible initial models and those obtained after five searches are shown. The sets of parameter values after the five searches are shown in Table 4.2. The effect of using the value of

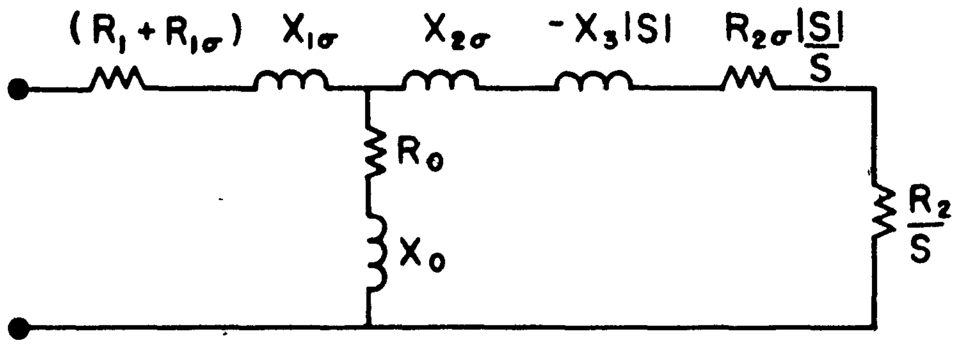

Fig. 4.9 The 8-Parameter Model

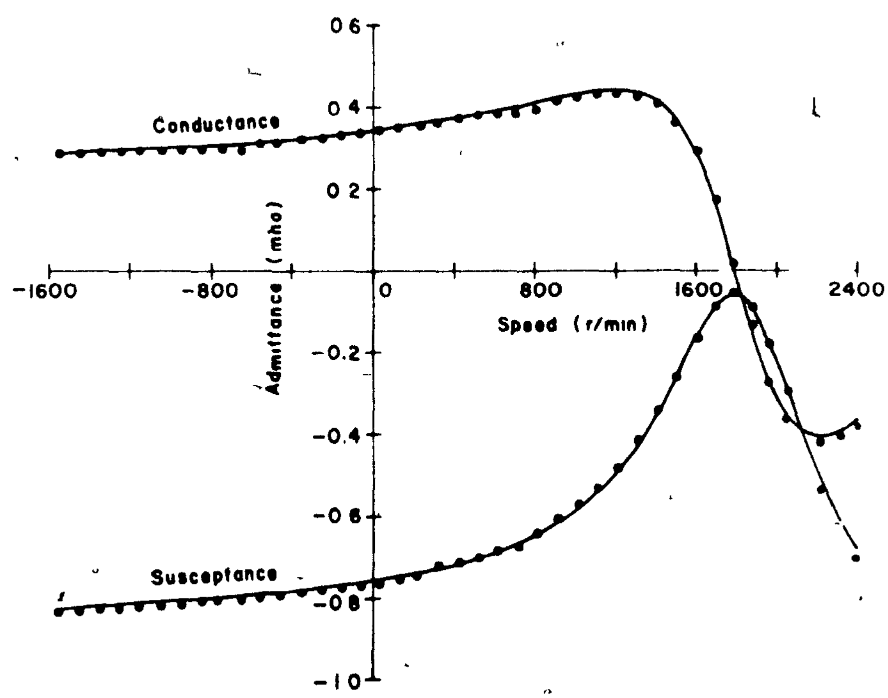

Fig. 4.10 Input Admittance vs Speed

TABLE 4.1

COMPARISON OF MEAN ERRORS OF DIFFERENT MODELS

8-parameter model	Initial Mean Error (%)	Mean Error after 5 Searches (%)
A	12.75	1.28
B	2.32	0.98
C	2.97	0.65
D	0.89	0.59
E	3.88	1.06
F	1.32	0.68
6-parameter model		
A	13.12	1.88
B	3.05	1.79
C	2.77	1.26
D	1.53	0.59

A Initial model based on crude interpretation of data at synchronous and zero speeds.

B Initial model incorporating common refinements to the interpretation of the zero speed data.[20]

C Same a B, but value of stalled torque obtained from X - Y plot of Figure 4.8 used.

D Same as B, but stalled torque is not included in the error function.

E Result of quadratic curve fit used as initial model.

F Same as E, but value of stalled torque obtained from X - Y plot of Figure 4.8 is used.

TABLE 4.2

PARAMETER VALUES AFTER 5 SEARCHES

8-parameter model	$(R_1 + R_{1\sigma})$	R_2	$R_{2\sigma}$	R_0	$X_{1\sigma}$	$X_{2\sigma}$	X_3	X_0
A	0.2015	0.2956	0.0599	1.051	0.5527	0.6055	0.0396	16.11
B	0.1967	0.3014	0.0449	1.051	0.5606	0.5601	0.0131	16.10
C	0.2070	0.2950	0.0325	1.051	0.5615	0.5612	0.0155	16.10
D	0.2120	0.2905	0.0298	1.051	0.5601	0.5601	0.0147	16.10
E	0.1907	0.3001	0.0449	1.059	0.5562	0.5558	0.0078	16.10
F	0.2106	0.2945	0.0335	1.059	0.5581	0.5580	0.0093	16.10

6-parameter model	$(R_1 + R_{1\sigma})$	R_2	$R_{2\sigma}$	R_0	$X_{1\sigma}$	$X_{2\sigma}$	X_3	X_0
A	0.2004	0.3274		1.051	0.5362	0.5353		16.11
B	0.1985	0.3296		1.051	0.5392	0.5396		16.11
C	0.2067	0.3156		1.051	0.5427	0.5434		16.11
D	0.2337	0.2983		1.051	0.5521	0.5530		16.11

the stalled torque interpolated directly from the data, or of using a value obtained from the X - Y plot of Figure 4.8, or of ignoring the stalled torque can be seen. In general, these are not the minima of the error function which can be further reduced although convergence may be slow. For example, the 8-parameter model in Table 4.1 having an error of 0.68% after five searches has an error of 0.67% after ten searches, and it is the results of this model which are shown in Figure 4.10. The parameters, in ohms at 60 Hz normalized to 50°C, of this model are

$R_1 = 0.2045$	
$R_{1\sigma} = 0.0061$	$X_{1\sigma} = 0.5580$
$R_2 = 0.2941$	
$R_{2\sigma} = 0.0340$	$X_{2\sigma} = 0.5590$
	$X_3 = 0.0093$
$R_0 = 1.0592$	$X_0 = 16.0998$

the average value of the terminal voltage during the measurements being 30.2 volts (line-to-neutral). The parameter values vary somewhat with voltage level, but the main investigation of this aspect has been done on a smaller squirrel cage machine and is described in Chapter 5. A further comparison of measured and calculated values, using the input current and power factor, is shown in Figure 4.11. Comparison of developed torque is shown in Figure 4.12 and it can be seen that if allowance is made for the effect of the oscillatory torque at low speeds by extrapolating a smooth curve from the points at higher speeds, the agreement is very good at zero speed since the stray loss torque is zero. At other values of speed the differences are typical of stray losses in a machine of this size and type.

Optimization of the 6-parameter model generally produces values

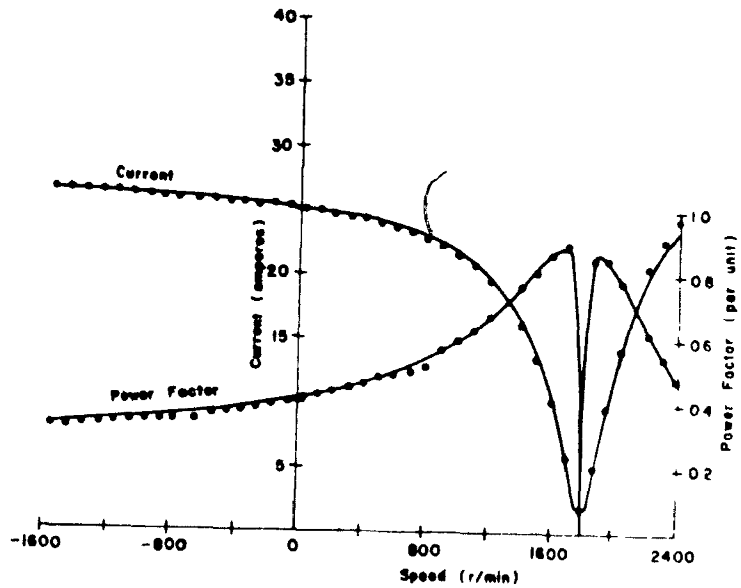

Fig. 4.11 Current and Power Factor vs Speed

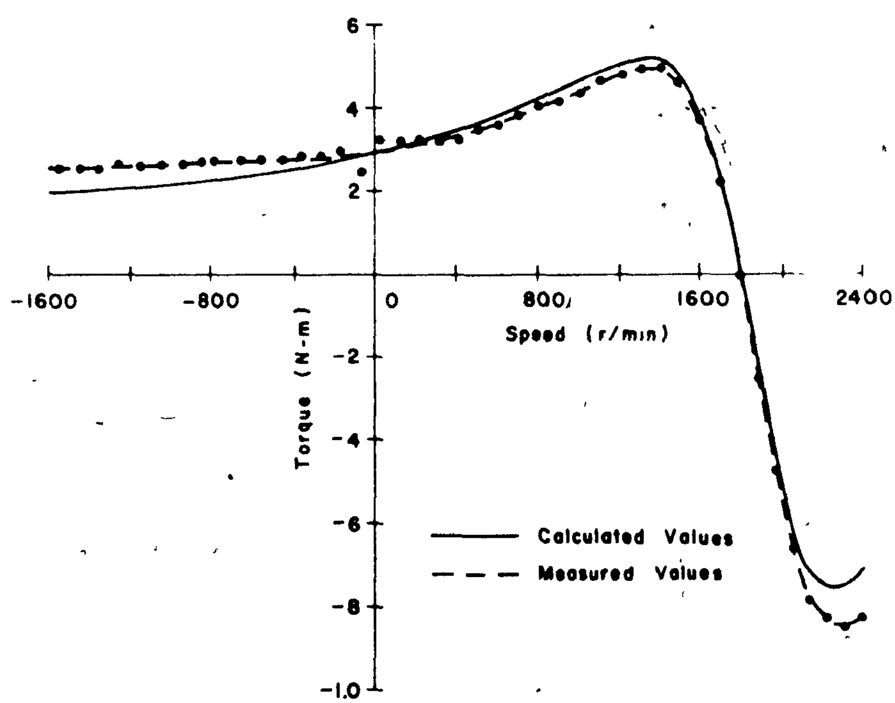

Fig. 4.12 Developed Torque vs Speed

of error function which are larger than the corresponding values of the 8-parameter model. The exception is model D in Table 4.1 but the fact that $R_{1\sigma}$ is 18% of R_1 suggests that this model may not really be satisfactory and this has been confirmed by observing that the stray loss torques implied are quite unreasonable.

Unfortunately, inspection of Table 4.2 makes it clear that unless the stalled torque is very accurately known, both the 6-parameter and 8-parameter models may yield values of $R_{1\sigma}$ which are negative. However, the 8-parameter model D is very close to the model obtained directly from the curve fitting method, using the best estimate of the stalled torque, in which the parameter $R_{1\sigma}$ is obtained indirectly from the stalled torque, the difference in the two calculated values being less than 1%.

Thus, it is unnecessary to include the stalled torque in the error function of an optimizing process provided the model includes a parameter such as $R_{2\sigma}$ which is capable of matching the calculated and measured values. The measurement of stalled torque is therefore not required when using parameter optimization to obtain values for the elements of the circuit model of a machine.

CHAPTER V

PARAMETER IDENTIFICATION FOR SQUIRREL CAGE MACHINES

5.1 Introduction

In addition to the effects which have been included in the model of the wound rotor induction machine described in Chapter 4, a squirrel cage machine may also have significant skin effect in the rotor bars. Although harmonic effects may be appreciable in squirrel cage machines, they were found to be negligible in the motor used for the experimental investigation and are considered separately in the study of pole amplitude modulated machines which have substantial harmonic content. The experimental and analytical techniques developed for the identification of the equivalent circuit parameters of a wound rotor machine can now be extended to the squirrel cage machine, for which the circuit model must include the skin effect. Also, the use of a smaller machine has enabled this study to include the effect of magnetic saturation of the main flux paths at full voltage.

5.2 The Circuit Model

The circuit which proved most successful in modelling the wound rotor machine is that shown in Figure 4.9. Inclusion of skin effect requires the introduction of at least one more parameter. Among the standard approaches, one which is suitable is the model of a double cage rotor. This requires two additional parameters and is essentially a first approximation to the ladder network representation of a deep bar secondary [28,29]. This has been rejected in favour of a single parameter alternative based on an equivalent rectangular bar [2]. The resistance, R_f, and reactance, X_f, of such a bar at frequency f are related to the zero frequency values, R_{dc} and X_{dc}, by

$$R_f = \frac{\alpha d\ (\sinh 2\alpha d + \sin 2\alpha d)}{\cosh 2\alpha d - \cos 2\alpha d} \cdot R_{dc} \tag{5.1}$$

$$X_f = \frac{\alpha d\ (\sinh 2\alpha d - \sin 2\alpha d)}{\cosh 2\alpha d - \cos 2\alpha d} \cdot R_{dc} \tag{5.2}$$

$$= \frac{3}{2\alpha d} \cdot \left[\frac{\sinh 2\alpha d - \sin 2\alpha d}{\cosh 2\alpha d - \cos 2\alpha d}\right] \cdot X_{dc} \tag{5.3}$$

where $\alpha = \sqrt{\frac{rf}{\rho} \cdot 10^7}$

d = the depth of the bar

ρ = the resistivity of the bar

r = the ratio of bar width to slot width

The rotor bars of most squirrel cage induction machines are likely to be somewhat trapezoidal in cross section, but it is convenient to consider a rectangular bar which is equivalent in the sense that the frequency dependence of resistance and reactance are similar. The depth of this equivalent rectangular bar can be taken as the additional parameter and used, in conjunction with equations 5.1 and 5.3 to modify the values of rotor resistance and reactance, R_2 and $X_{2\sigma}$ of Figure 4.9. The application of these skin effect relations to the entire secondary leakage reactance is justified if the constant portion is transformed into an equivalent primary reactance. This is done automatically by the parameter optimizing technique, described in Chapter 4, as the error function is minimized.

5.3 Experimental Results

Tests were carried out on a 2 HP squirrel cage induction motor, details of which are given in Appendix B. For this smaller machine, measurements were taken at voltage levels up to the rated value. Due to the rapid temperature rise the speed was varied over the range -1800 to +2000 rpm at approximately 450 rpm/sec. so that a run was accomplished in about 9 seconds. At full voltage the temperature rose about 40°C during this time. Analog data acquisition was employed and results transcribed from the recordings at approximately 100 rpm intervals. Due to the high values of acceleration, the recorded values differ significantly from the steady values in the region of synchronous speed. Results between 1600 and 2000rpm were therefore omitted from the computation of the error function.

In this case the only method used to determine the parameter values was the optimization process, the initial values being derived from a standard analysis of the experimental data. Similarly to the wound rotor machine, the iteration converges rapidly until the mean error becomes comparable with the instrumentation error, estimated to be of the order of 1½% due to the lower resolution of the UV recorder. Thereafter, convergence is slow, and since the computer is attempting to include the instrument characteristics, as well as those of the machine, in the model there is no point in proceeding further.

Figure 5.1 shows a typical recording, the width of which is 4.5 inches; the absence of harmonic torques may be noted. Comparison of computed and measured data for operation at 108 volts (line-to-neutral) is shown in Figure 5.2. The electrical characteristics are well reproduced except for power factors in the vicinity of synchronous speed, the errors being consistent with the high acceleration employed. The divergence between computed electromagnetic torques and the measured values is characteristic of stray loss effects and it is noteworthy that the difference is small at standstill when the stray loss torque is zero. The equivalent slot depth is 0.23 inch

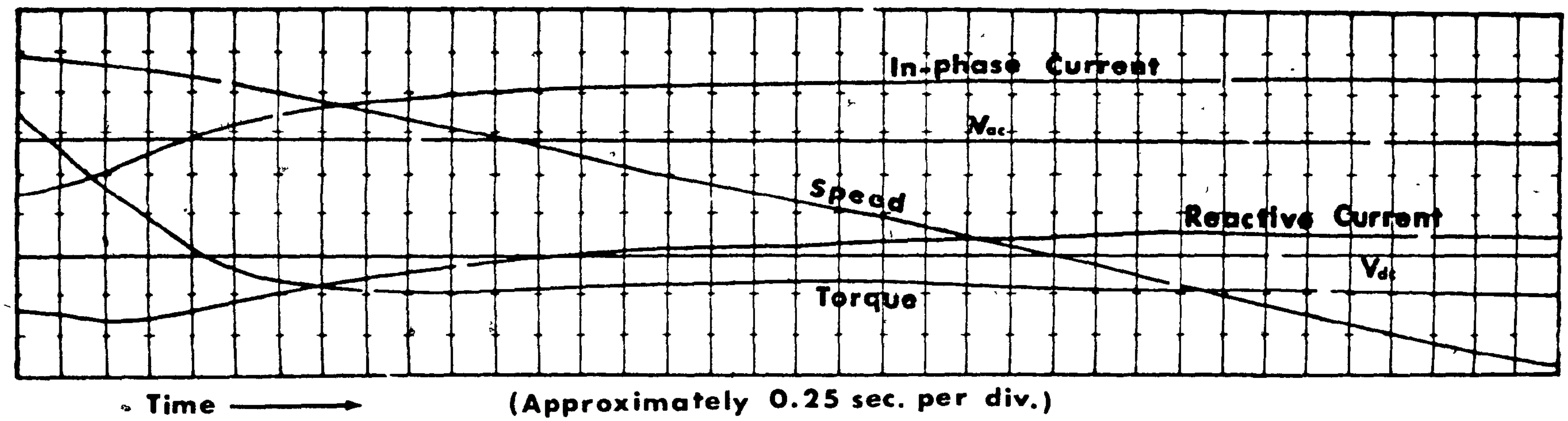

Fig. 5.1 Typical Recording

For clarity the zero and scale
for each trace have not been
added.

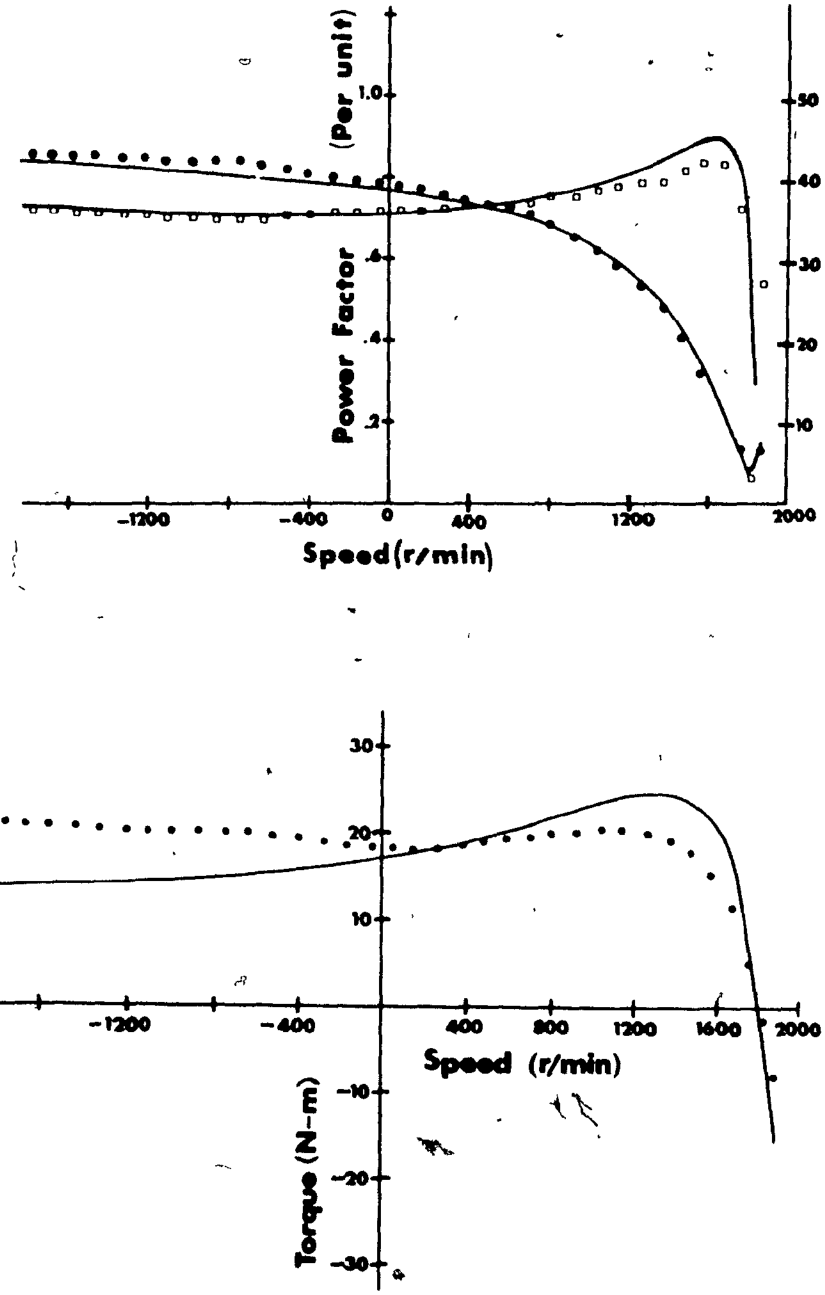

Fig. 5.2 Characteristics at 108 Volts

The lines show the calculated values; the points are the measured values.

in comparison with the actual depth of 0.47 inch, the bar having approximately a trapezoidal cross section which is detailed in Appendix B. The other parameter values, in ohms at 60 Hz normalized to a winding temperature of 50°C are

$R_1 = 1.23$

$R_{1\sigma} = 0.015$ $\qquad X_{1\sigma} = 0.955$

$R_2 = 0.655$

$R_{2\sigma} = 0.057$ $\qquad X_{2\sigma} = 0.09$

$R_0 = 1.05$ $\qquad X_0 = 31.45$

The effect of voltage on the circuit parameters, normalized to 50°C, is illustrated in Figure 5.3, the variations being consistent with the effects of magnetic saturation.

For purposes of comparison, the standard 6-parameter model, Figure 4.1(b), based on synchronous speed and blocked-rotor tests was studied. Figure 5.4 shows this to be an inadequate representation of the machine over a wide speed range. However, when the equivalent slot depth is introduced as a seventh parameter, and it alone is used to optimize the model, the agreement between computed and measured values is greatly improved. The equivalent slot depth of 0.37 inch is rather large, considering the shape of the bar, and the stray loss torque is abnormally small at negative speeds.

Although standard three-phase squirrel cage induction motors, such as the one used in the study described above, normally have negligible harmonic effects and this new approach to the measurement of parameter values is therefore widely applicable, there remains the problem of modelling the situation where harmonic content is significant. Since a pole amplitude mod-

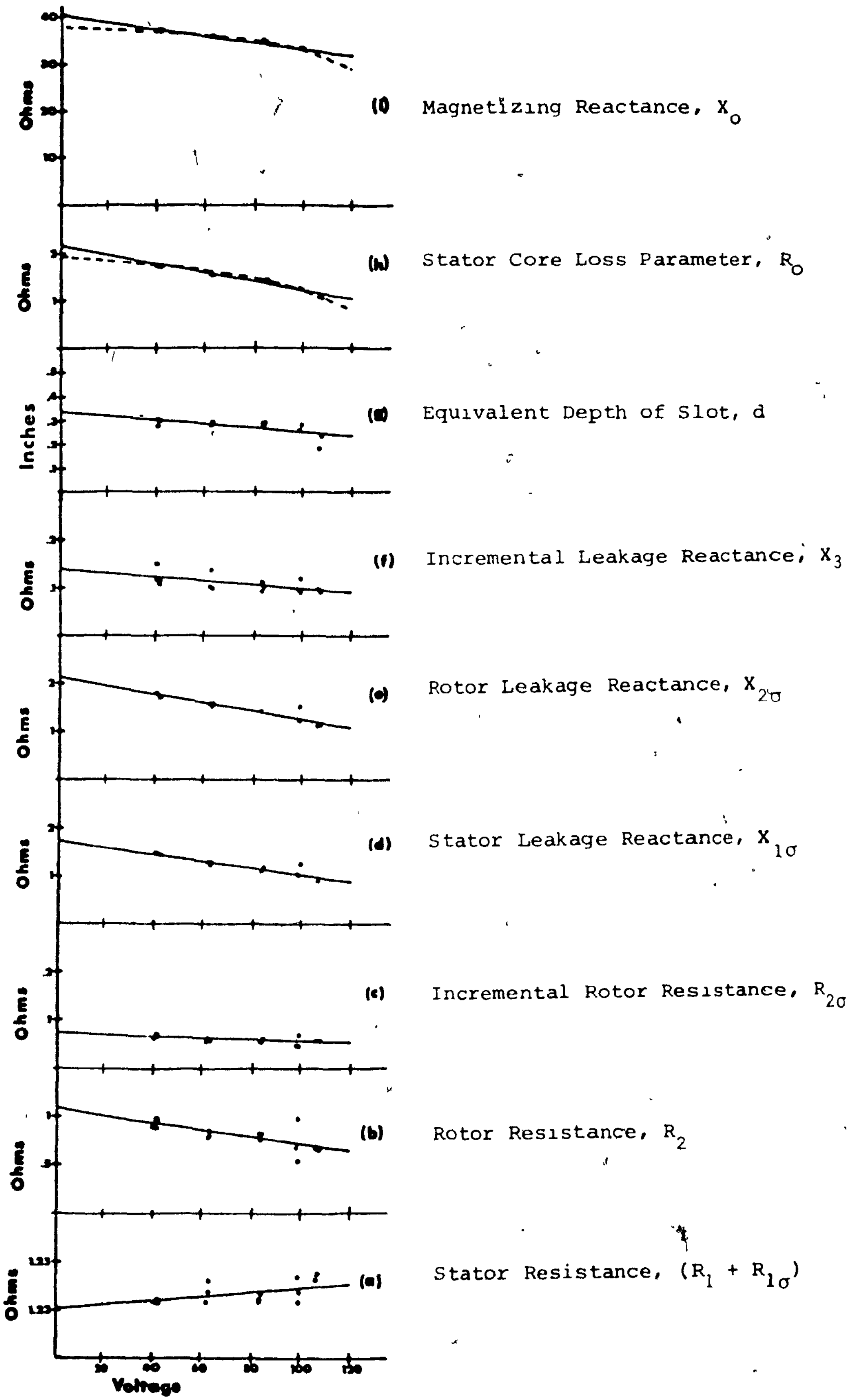

Fig. 5.3 Effect of Voltage on Parameters

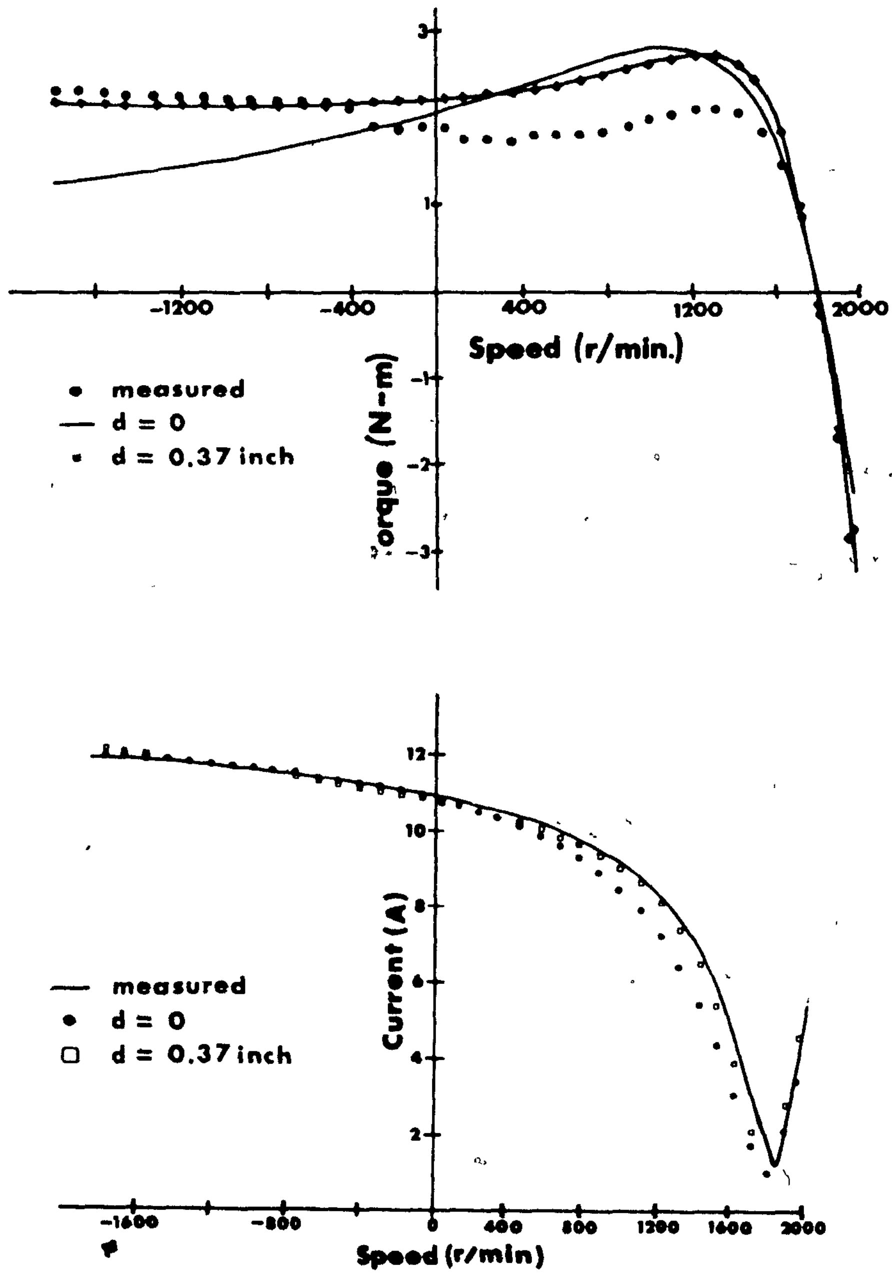

Fig. 5.4 Effect of Equivalent Slot Depth on the Conventional Model

ulated machine invariably has a high harmonic content, it is particularly suited for the study of problems in modelling when both skin effect and harmonic content are simultaneously significant.

CHAPTER VI

POLE AMPLITUDE MODULATION

6.1 Introduction

Pole-change windings have been in use for a long time, but it is only recently that the method of changing the effective number of poles was realized to have much in common with amplitude modulation[30]. As a result, it has been possible to design and manufacture induction motors for operation at two speeds whose ratios were previously considered impossible to achieve with the simple switching arrangement of reversing the connections to one-half of each phase winding. The development of these pole amplitude modulated (PAM) machines has been characterized by their inventors overcoming specific problems one at a time, with just enough theoretical background to explain the particular solution. PAM machines present both modelling and parameter identification problems in addition to those of normal machines considered in the two previous chapters. Therefore, before proceeding to develop a circuit model, it is necessary to review their theoretical background, at the same time noting the restrictions imposed by real windings.

6.2 Theoretical Considerations

Amplitude modulation of a carrier wave by a signal produces upper and lower sidebands[31]. For the induction machine, it is usual to consider modulation of the mmf waveform although, strictly, it is the current distribution in half of each phase winding which is reversed to produce the effect of modulation. If a motor is to operate satisfactorily in the modulated condition, the unwanted sideband must be brought effectively to zero. Unfortunately, the mmf waveforms are functions of both time and space, and therefore the normal techniques for single sideband transmission do not apply. However, the effect of the unwanted sideband can be made effectively zero if the mmf waveforms of each phase are co-phasal, thus producing a zero phase sequence situation. This concept was presented as a basic theorem of generalized pole amplitude modulation for 3-phase machines[32], and its extension to the more general q-phase situation is shown below.

6.3 General Theorem of Pole Amplitude Modulation

The fundamental mmf of a normal integral slot winding is given by

$$F(\theta,t) = \sum_{j=1}^{q} F \sin(\omega t - \delta_j) \sin(m\theta - \alpha_j) \tag{6.1}$$

$$\text{where } \alpha_j = \frac{2\pi(j-1)}{q} \tag{6.2}$$

is the relative position of the axis of the j^{th} of q phases of an m-pole-pair winding, and δ_j is the phase angle of the current in the j^{th} phase. Normally $\delta_j = \alpha_j$ and the resulting mmf of the polyphase winding is

$$F(\theta,t) = \frac{qF}{2} \cos(m\theta - \omega t) \tag{6.3}$$

When modulated, the distribution of the j^{th} phase mmf waveform is

$$\begin{aligned} F_j(\theta) &= F \sin(m\theta - \alpha_j) \sin(k\theta - \beta_j) \\ &= \frac{F}{2} \{\cos[(m-k)\theta - (\alpha_j - \beta_j)] - \cos[(m+k)\theta - (\alpha_j + \beta_j)]\} \end{aligned} \tag{6.4}$$

where β_j is the (space) phase angle of the modulating wave applied to the j^{th} phase and k is the expected change in the number of pole-pairs. If the values of β_j are chosen to equal α_j the resulting distribution is

$$F_j(\theta) = \frac{F}{2} \{\cos(m-k)\theta - \cos[(m+k)\theta - 4(j-1)\frac{\pi}{q}]\} \tag{6.5}$$

The lower sidebands are therefore co-phasal and the upper sidebands form a q-phase set provided q is odd. The phase angles are now $\frac{4\pi}{q}$ instead of $\frac{2\pi}{q}$ so that consecutive winding phases (1,2,3,...q) must be connected to alternate phases (1,3,...q,2,4,...q-1) of the source. For a 3-phase system this is the reverse or negative sequence.

It should also be noted that when the modulating waveforms have the same spatial sequence as that of the phase windings, modulation results in the upper sideband being effective. Conversely, when the modulating waveforms have the opposite sequence, it is the lower sideband which is effective.

6.4 Practical Limitations

The idealized pole amplitude modulation described above presupposes that the zero of each modulating wave coincides with the zero of its mmf wave. Unfortunately, this situation does not always exist as illustrated by the clock diagrams in Figure 6.1 [33]. There are three possible situations for a 3-phase winding depending on the number of pole-pairs, m, of the unmodulated winding. Figure 6.1(a) shows the distribution of a standard 8-pole winding which is typical of pole-pair numbers $m = 3i + 1$, i being an integer. For modulation by one pole-pair (i.e. $k = 1$) the angle β is $\frac{2\pi}{3}$ on the scale of θ, and if the axis A is shown, for convenience, at the beginning of phase a to signify the position of its modulating wave, the axes B and C are at the angles $\frac{2\pi}{3}$ and $\frac{4\pi}{3}$ respectively. In this case, the axis B coincides with the beginning of phase b and axis C coincides with the beginning of phase c and it is therefore feasible to modulate in the same sequence as the winding at the ideal position. However, modulation in reverse sequence $\beta = -\frac{2\pi}{3}$, requires axis C to coincide with an entry to phase b. The nearest position at

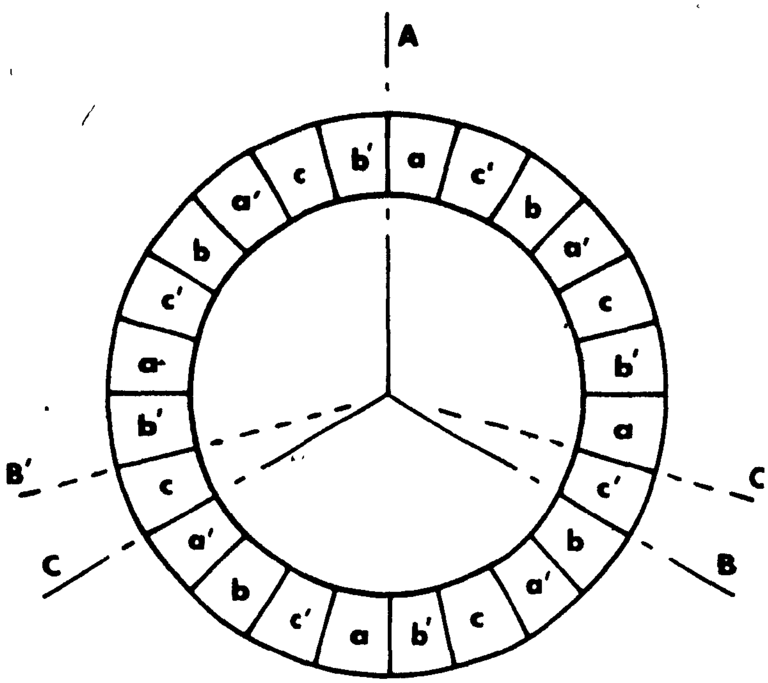

(a) m = 4

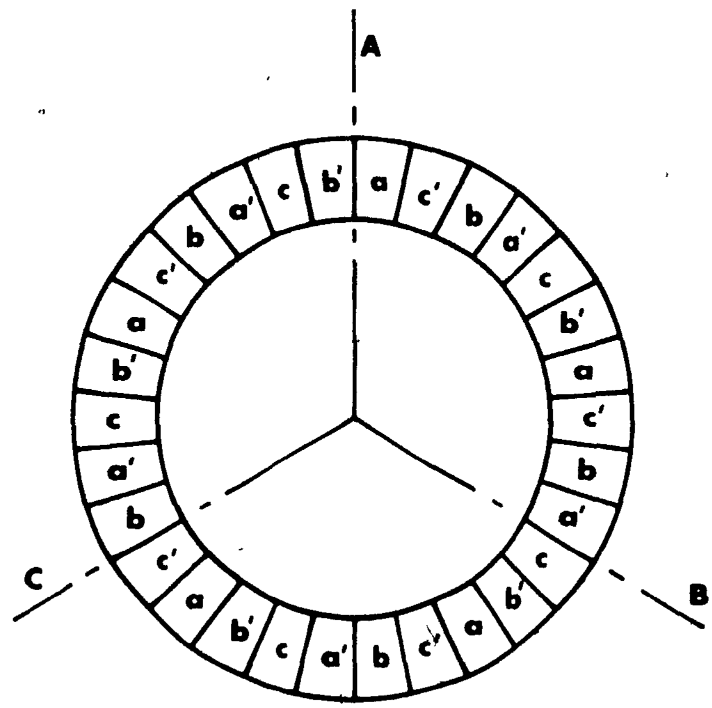

(b) m = 5

Fig. 6.1 (a & b) Clock Diagrams

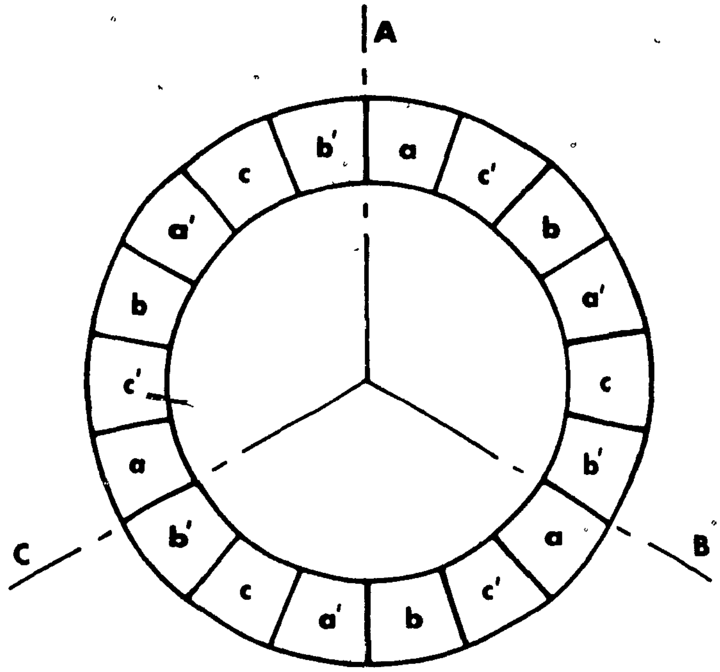

(c) m = 3

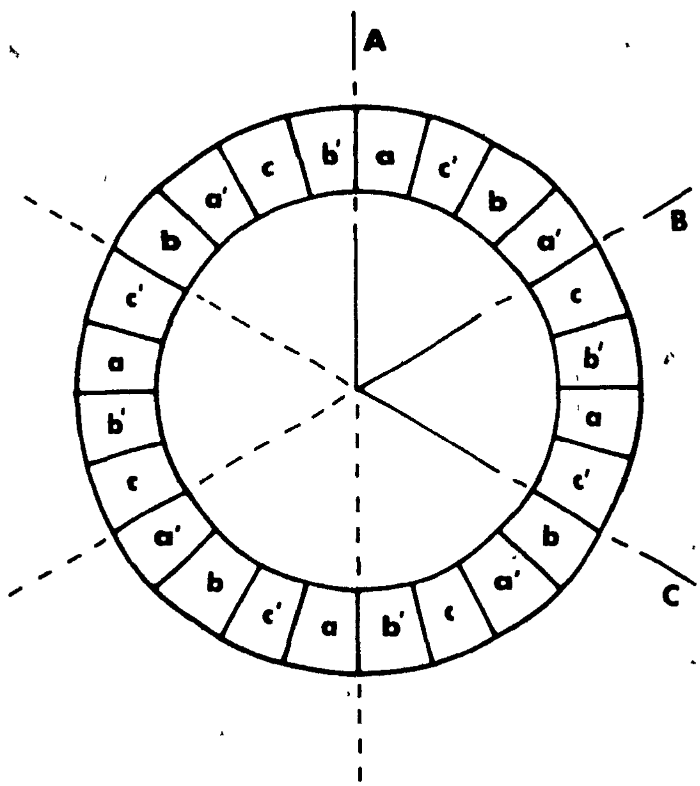

(d) m = 4 k = 2

Fig. 6.1 (c & d) Clock Diagrams

which the zero of the modulating wave can coincide with an entry to phase b is the axis B' at an angle of $(-\frac{2\pi}{3} + \frac{\pi}{3m})$. Similarly, phase c could be modulated using axis C' at the angle $(\frac{2\pi}{3} + \frac{\pi}{3m})$.

The 10-pole winding shown in Figure 6.1(b) is typical of pole-pair numbers m = 3i - 1. In this case modulation in the same sequence requires a change in the values of β, but modulation in reverse sequence can be done at the ideal values. For pole-pair numbers m = 3i such as the 6-pole distribution shown in Figure 6.1(c) the values of β must be adjusted for both modulating sequences. These angles are summarized in Table 6.1. It should be noted that these values are restricted to modulation by one pole-pair. For other values of k the situation is not necessarily the same and the position of the winding relative to the ideal modulating wave must be determined.

Application of the modulating waves at the angles given in Table 6.1 results in winding arrangements which are symmetrical. Unfortunately, the resulting mmf distributions do not form a symmetrical 3-ph set and the unwanted sidebands are no longer co-phasal, as can be seen by substituting these angles in Equation 6.5. Thus it can be seen that the phase angles of the modulated mmf distribution are determined by the angle of β of the modulating wave and not by the angle α of the winding. The result is that the application of modulating waves at other than the ideal values produces an unwanted sideband which has some positive or negative phase sequence content.

6.5 Pre-Shaping

The implicit requirement that modulation is to be achieved by a simple reversal of connections to one-half of each phase winding presents some problems since the modulating waveform is then rectangular. Typical

TABLE 6.1

SUMMARY OF ANGLES AT WHICH MODULATING WAVES AND MMF DISTRIBUTIONS HAVE COINCIDENT ZEROS

(k = 1)

m	POSITIVE SEQUENCE MODULATION		NEGATIVE SEQUENCE MODULATION	
	β_b	β_c	β_b	β_c
3i-1	$\frac{2\pi}{3} + \frac{\pi}{3m}$	$-\frac{2\pi}{3} - \frac{\pi}{3m}$	$-\frac{2\pi}{3}$	$\frac{2\pi}{3}$
3i	$\frac{2\pi}{3} - \frac{\pi}{3m}$	$-\frac{2\pi}{3} + \frac{\pi}{3m}$	$\frac{2\pi}{3} - \frac{\pi}{3m}$	$\frac{2\pi}{3} + \frac{\pi}{3m}$
3i+1	$\frac{2\pi}{3}$	$-\frac{2\pi}{3}$	$-\frac{2\pi}{3} + \frac{\pi}{3m}$	$\frac{2\pi}{3} - \frac{\pi}{3m}$

mmf waveforms are shown in Figure 6.2. The Fourier harmonic coefficients for the sidebands of the modulated waveform are low, a situation likely to result in an unsatisfactory machine. If the conditions after modulation are to approximate the ideal, the unmodulated winding connection must produce waveforms which already include the form of the modulating wave. The unmodulated waveform, in the ideal case, is then described by

$$F(\theta) = F\,\sin(m\theta - \alpha)\cdot\left|\sin(k\theta - \beta)\right| \qquad (6.6)$$

This technique has been called "pre-shaping"[34], and typical waveforms are shown in Figure 6.3.

The unmodulated waveform clearly has significant harmonic content. Harmonic analysis into a series of the form

$$F(\theta) = \sum_n (a^n \cos n\theta + b^n \sin n\theta)$$

results in the coefficients:

$$a^n = \frac{-2k}{\pi}\sum_{i=1}^{k}\left[\frac{\cos^2(m+n)\frac{\pi}{2k}\sin(m+n)(2i-1)\frac{\pi}{k}}{(m+n)^2 - k^2} + \frac{\cos^2(m-n)\frac{\pi}{2k}\sin(m-n)(2i-1)\frac{\pi}{k}}{(m-n)^2 - k^2}\right]$$

$$b^n = \frac{2k}{\pi}\sum_{i=1}^{k}\left[\frac{\cos^2(m+n)\frac{\pi}{2k}\cos(m+n)(2i-1)\frac{\pi}{k}}{(m+n)^2 - k^2} - \frac{\cos^2(m-n)\frac{\pi}{2k}\cos(m-n)(2i-1)\frac{\pi}{k}}{(m-n)^2 - k^2}\right] \qquad (6.7)$$

Due to the summations, simple expressions exist only for a limited number of conditions relating m and k. However, it can be shown that for $n = m \pm ik$, the coefficients are zero for odd values of i and therefore the upper and lower sidebands do not exist. For $n = m$, a^m is zero so that the coefficient for the physically realizable condition of $\frac{m}{k}$ an integer is

$$b^m = \frac{2}{\pi}\cdot\frac{4m^2}{4m^2 - k^2} \qquad (6.8)$$

Numerical values may appear rather low but proper comparison with the uniform sinusoid of Figure 6.3(a) should allow for the fact that with the same total

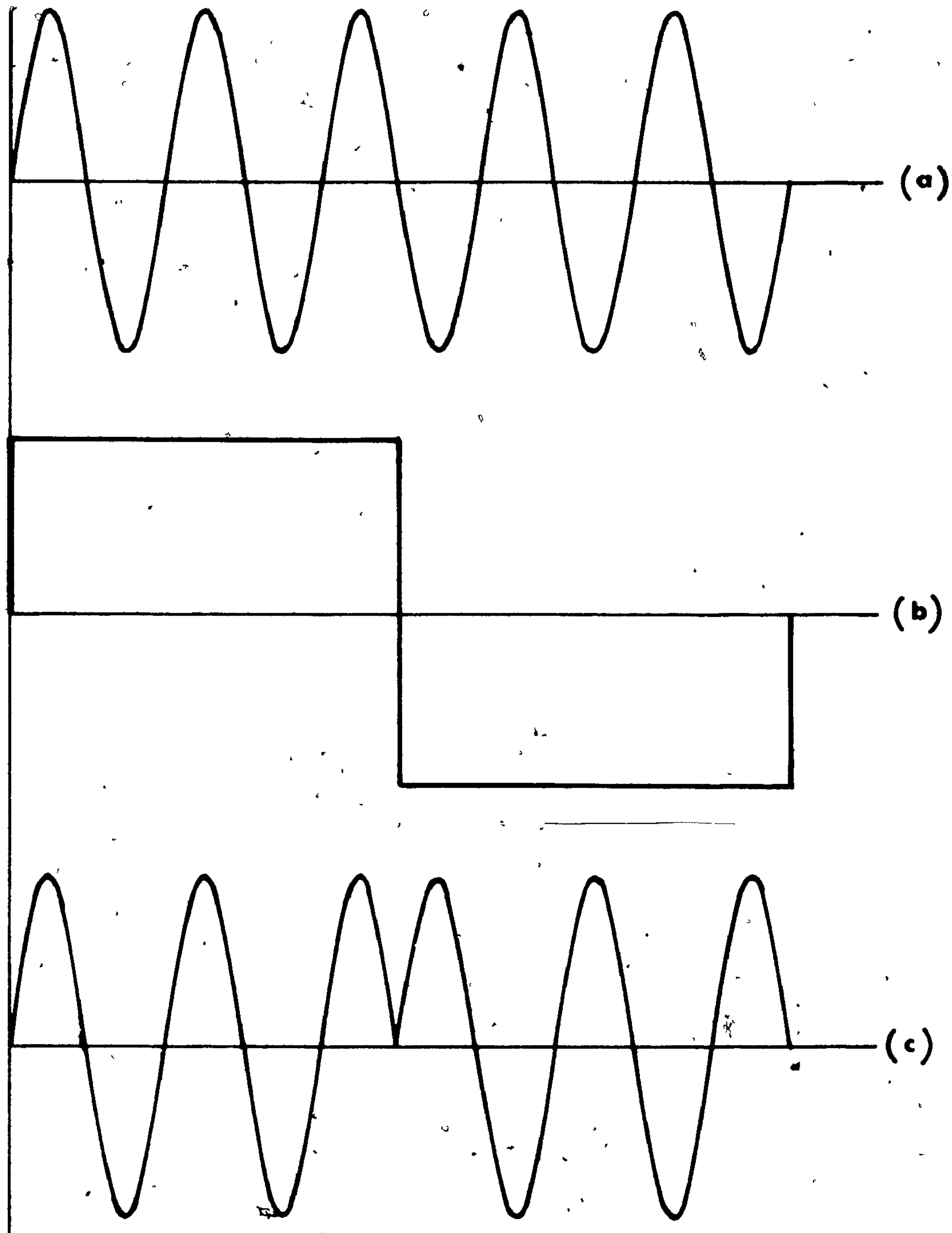

Fig. 6.2 Basic Waveforms of Regular Windings

a) The original sinusoidal wave
b) The rectangular modulating wave
c) The resulting modulated wave

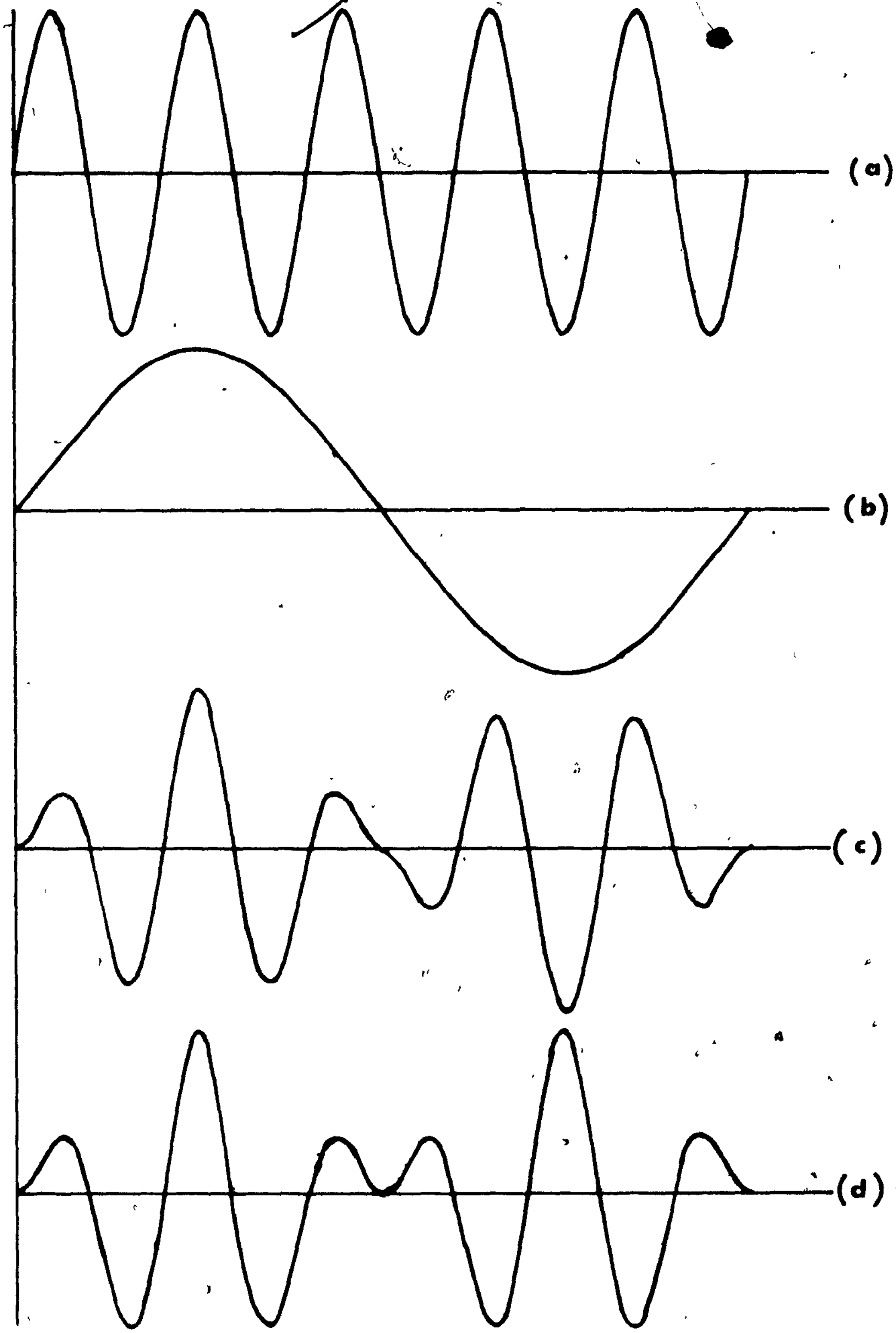

Fig. 6.3 Basic Waveforms of Pre-Shaped Windings

a) The original sinuisoidal wave
b) The desired modulating wave
c) The pre-shaped unmodulated wave
d) The resulting modulated wave

number of coils in a winding, the peak amplitude of the pre-shaped mmf wave is larger than the amplitude of the uniform sinusoid. This can be done by noting that the total area under the curve should be equal. For uniform sinusoidal distribution having unit amplitude this area is

$$A = 2m \int_{0}^{\frac{\pi}{m}} \sin m\theta \, d\theta = 4 \tag{6.9}$$

For the equivalent pre-shaped distribution of amplitude a, the area is

$$A = \sum_{i=1}^{2m} (-1)^{(i-1)} \int_{(i-1)\frac{\pi}{m}}^{i\frac{\pi}{m}} a \sin m\theta \sin k\theta \, d\theta \tag{6.10}$$

If the coefficient b^m of Equation 6.8 is applied to the pre-shaped waveform of amplitude a obtained by equating these areas, the coefficient obtained provides a valid comparison with the unit amplitude of uniform sinusoidal distribution. The ratio is close to unity and explains why pre-shaping produces a drastic improvement in the modulated performance without significant change in the unmodulated performance other than the increase in harmonic effects.

6.6 Asymmetrical Modulation

A simple extension of the technique of pre-shaping provides the solution to the problem of positioning the modulating waves at the ideal positions. Pre-shaped windings are fractional slot windings in which the belt width is proportional to the absolute value of the modulating wave. In this respect, the situation is similar to pulse width modulation. It is therefore relatively a simple matter to adjust the coil grouping so that, when required, the number of coils per group is proportional to $\sin k(\theta \pm \frac{\pi}{3m})$ rather than to $\sin k\theta$ [6]. In this manner the position of the modulating waves can be made reasonably close to the ideal values, and thus produce the required magnetic and electric symmetry.

6.7 Properties of PAM Windings

The two parts of a PAM phase winding are identical except for their location. Each of these parts can be identified as a basic segment, one being complementary to the other. From the point of view of circuit models, they can be connected in series or parallel, aiding or opposing, depending on the number of poles and the operating voltage desired.

In general, the conductor distribution pattern of a basic segment is repeated k times round the periphery of the machine, each portion occupying $\frac{\pi}{k}$. For the sake of clarity, the following discussion is limited to the case where k = 1, but can be generalized by substituting electrical for mechanical angles where appropriate.

6.7.1 The Basic Segment

Conductor and mmf distributions of a basic segment are shown in Figure 6.4. This is a basic segment of an 8-pole, full-pitch, integral-slot winding and apart from the lack of pre-shaping these distributions are typical of the case when the number of pole-pairs (unmodulated) is even.

The mmf waveform of a basic segment can be analyzed into a harmonic series containing, in general, all pole-pair numbers from one upwards.

$$F_1(\theta) = \sum_{n=1}^{\infty} F^n \sin n\theta \tag{6.11}$$

The complementary segment, identical to the first but displaced by π can be similarly analyzed giving

$$F_2(\theta) = \sum_{n=1}^{\infty} F^n \sin n(\theta + \pi) \tag{6.12}$$

When the two basic segments are connected in series aiding (i.e. the unmod-

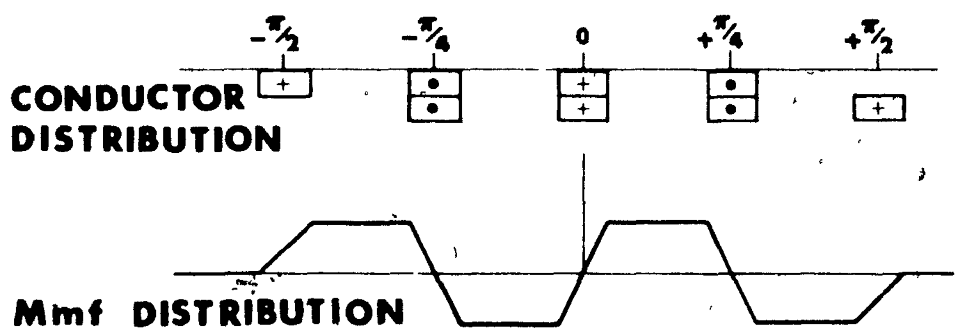

Fig. 6.4 Conductor and Mmf Distributions of a Basic Segment

ulated condition), all the odd numbered pole-pairs are suppressed. When they are connected in series opposing (i.e. the modulated condition), all the even numbered pole-pairs are suppressed.

For the situation where the winding would normally be considered as having an odd number of pole-pairs, the complementary segment mmf distribution is given by

$$F_c(\theta) = \sum_{n=1}^{\infty} -F^n \sin n(\theta + \pi) \tag{6.13}$$

In this case it is therefore the even numbered pole-pairs which are suppressed by a series aiding connection and the odd numbered pole-pairs which are suppressed by a series opposing connection.

6.7.2 Conjugate Harmonics

The discussion so far has centered on the modulation of each phase since the prime objective is a circuit model. In a normal 3-phase machine little attention is paid to third harmonic mmfs since their effects cancel out. This is not the case in a PAM winding when modulated

$$F^{3m}(\theta,t) = \sin 3m\theta \sin k\theta \sin \omega t + \sin 3(m\theta-\alpha)\sin(k\theta-\alpha)\sin(\omega t-\alpha) + \sin 3(m\theta-2\alpha)\sin(k\theta-2\alpha)\sin(\omega t-2\alpha) \tag{6.14}$$

$$= \frac{3}{4}\{\sin[(3m+k)\theta-\omega t] + \sin[(3m-k)\theta+\omega t]\} \tag{6.15}$$

The waveform of pole-pair number (3m+k) has been identified as a possible result of modulating the entire 3-phase mmf waveform by one having a number of pole-pairs equal to the sum of the unmodulated and modulated numbers[32]:

$$F(\theta,t) = \cos(m\theta-\omega t)\sin(2m+k)\theta$$

$$= \frac{1}{2}[\sin[(m+k)\theta+\omega t] + \sin[(3m+k)\theta-\omega t]$$

Such harmonics have been termed "conjugate harmonics",[6] and are readily identified when PAM winding design is based on total modulation rather than on phase-by-phase logic. Modulation by (2m+k) pole-pairs is best seen in a clock diagram and its main value lies in winding design.

CHAPTER VII

A CIRCUIT MODEL FOR POLE AMPLITUDE MODULATED INDUCTION MACHINES

7.1 Introduction

A circuit model for pole amplitude modulated machines must reflect the mmf effects which have just been described. Ideally, the model should respond to the applied constraints in the same manner as the actual machine. Because of the lack of symmetry in the windings the simple circuit model can no longer provide a suitable basis and therefore a more general orthogonal axis model must be used. As a consequence of the general theorem of pole amplitude modulation developed in the previous chapter, there is no direct way of reproducing the mmf patterns of a three phase machine using only two axes and therefore a three-axis model is required to represent the stator winding, which also has the advantage that the external constraints imposed by the connections may be applied directly.

7.2 The Primary Model

A phase winding has been shown to consist of two basic segments, whose mmf waveforms can be modelled by harmonic series. If the term "ideal winding" is considered to denote a winding with sinusoidal conductor distribution and zero resistance and leakage inductance, the electromagnetic effect of a basic segment can be modelled by a series connection of ideal windings having appropriate pole-pair numbers and turns, together with an appropriate resistance and leakage inductance. The complementary segment is displaced by $\frac{\pi}{k}$ (mechanical) and is modelled by an identical set of ideal windings correspondingly displaced as shown in Figure 7.1. As with ordinary orthogonal axis models, it is the electrical displacement between the sets of coils which is indicated.

Polarity markings for the ideal windings pose a problem since they depend on whether Equation 6.12 or 6.13 applies. The markings shown in Figure 7.1 apply to an even pole-pair number, and those on one of the segments are reversed when the number is odd.

The three-phase PAM machine has three complementary pairs of basic segments. The basic segments of the phases are not necessarily identical, especially if asymmetrical modulation has been used, nor are they necessarily inclined at exactly $\frac{2\pi}{3}$. The inclinations are readily obtained during computation of the harmonic winding factors which, in this context, include both amplitude and position of each mmf harmonic.

7.3 The Rotor Model

While wound rotors for PAM machines have been described[35], they are rare compared to the squirrel cage secondary. Only the latter have therefore been included in this study. A squirrel cage reacts as a balanced, short-circuited polyphase winding to any pole-pair number less than or equal to half its number of bars[36]. In view of the rapid convergence of the mmf harmonic series of practical primary windings, this restriction is not important so that, as shown in the next chapter, the squirrel cage can be represented by sets of quasi-stationary two-phase individually short-circuited ideal windings.

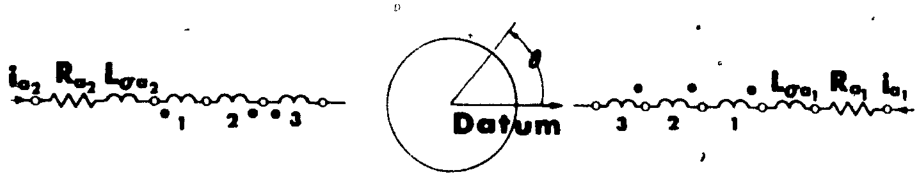

Fig. 7.1 Circuit Model of a Pair of Basic Segments

7.4 The Complete Machine Model

The complete squirrel cage PAM machine can therefore be modelled by sets of ideal windings as shown in Figure 7.2. The rotor windings are shown in their electrically orthogonal positions, however, it should be noted that physically their axes are inclined at the mechanical angles shown.

The electrical equations for the machine of Figure 7.2 may be written,

$$\begin{bmatrix} Z_{11} & Z_{12} & Z_{13} \\ Z_{21} & Z_{22} & Z_{23} \\ Z_{31} & Z_{32} & Z_{33} \end{bmatrix} \begin{bmatrix} i_1 \\ i_2 \\ i_3 \end{bmatrix} = \begin{bmatrix} v_1 \\ v_2 \\ 0 \end{bmatrix} \qquad (7.1)$$

where suffix 1 denotes the primary a_1, b_1, c_1 segments.
where suffix 2 denotes the primary a_2, b_2, c_2 segments.
where suffix 3 denotes the secondary.

The submatrices Z_{11} and Z_{22} are identical and of order 3x3. Z_{21} is the transpose of Z_{12} and is also 3x3. Z_{33} is 2hx2h where h is the number of harmonics being included in the model. Z_{13} and Z_{23} are 3x2h matrices of mutual coupling. Z_{31} and Z_{32} are equal to the respective transposes of Z_{13} and Z_{23} together with appropriate speed voltage terms. The subvectors $\mathbf{v}_1$ and v_2 each have three elements which are the voltages applied to the basic segments. The subvectors i_1 and i_2 also have three elements which are the currents in the basic segments.

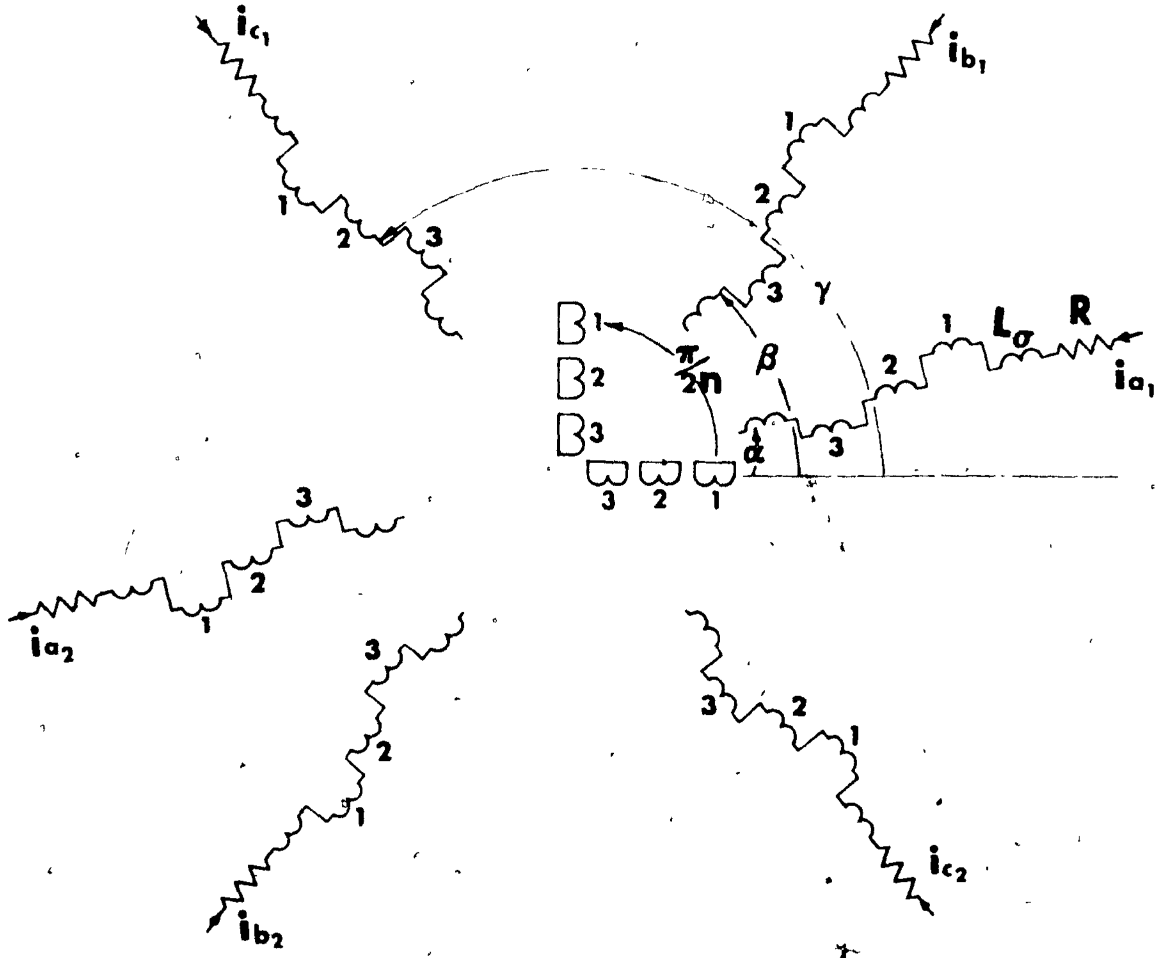

Fig. 7.2 Circuit Model of a 3-Phase Machine

The electromagnetic torque, T_e, is the quadratic product $i^t Gi$, the torque matrix, G, being the coefficient of rotor speed in the impedance matrix.

Since several sub- and super-harmonics of the desired pole-pair number are involved in any analysis, the number of simultaneous differential equations is inevitably of the order of 20. For sinusoidal steady-state conditions the equations are algebraic but nevertheless require the aid of a digital computer which yields solutions efficiently and economically. Simplification is however desirable and is often possible.

7.5 Constraints Imposed by Connections

If the winding segments are connected in parallel the constraint for an unmodulated condition is $v_2 = v_1$ and that for a modulated condition is $v_2 = -v_1$.

When the segments are connected in series the constraints are $i_2 = i_1$, if unmodulated and $i_2 = -i_1$, if modulated. In this case a $C^t ZC$ transformation reduces the number of equations by three, the connection matrix being defined by the current transformation

$$\begin{bmatrix} i_1 \\ i_2 \\ i_3 \end{bmatrix} = \begin{bmatrix} U_1 & \\ \pm U_1 & \\ & U_3 \end{bmatrix} \begin{bmatrix} i_1 \\ i_3 \end{bmatrix} \qquad (7.2)$$

where U_1 is the unit matrix of order 3 and U_3 is the unit matrix of order h, the number of harmonics being included in the model.

The constraints considered above can be applied directly to delta and four-wire star connections since the applied voltages are completely defined. The possibility of unbalance due to asymmetric conductor distribution makes the three-wire star connection more complex. The fact that the neutral current is zero can be used to reduce by one the number of current variables, thus leaving two stator currents in the case of the series connection and five for the parallel connection. Connection matrices thus defined permit solution in terms of known line voltages. The phase voltages and neutral-to-ground voltage can be obtained, if required, by substituting the currents thus found into the original equations.

7.6 Circuit Parameters

The impedance submatrices of Equation 7.1 are defined in terms of a number of circuit parameters, most of which are airgap inductances associated with the various harmonic fields. Thus

$$Z_{11} = R_{11} + L_{11}p \tag{7.3}$$

where
$$R_{11} = \begin{bmatrix} R_a & & \\ & R_b & \\ & & R_c \end{bmatrix} \tag{7.4}$$

and
$$L_{11} = \begin{bmatrix} (L_{\sigma a}+\Sigma L_a^n) & \Sigma M_{ab}^n \cos(\beta^n-\alpha^n) & \Sigma M_{ac}^n \cos(\gamma^n-\alpha^n) \\ \Sigma M_{ab}^n \cos(\beta^n-\alpha^n) & (L_{\sigma b}+\Sigma L_b^n) & \Sigma M_{bc}^n \cos(\gamma^n-\beta^n) \\ \Sigma M_{ac}^n \cos(\gamma^n-\alpha^n) & \Sigma M_{bc}^n \cos(\gamma^n-\beta^n) & (L_{\sigma c}+\Sigma L_c^n) \end{bmatrix} \tag{7.5}$$

The subscript σ indicates a leakage inductance and the superscript n indicates that the airgap inductance and angles apply to the field having n pole-pairs. The angles α, β and γ are the inclinations of the axes of windings a, b and c to the datum as indicated in Figure 7.2.

The primary mutual coupling impedances are

$$Z_{12} = Z_{21}^{t} = (-1)^{m}\Sigma \cos n\pi \begin{bmatrix} L_a^n & M_{ab}^n \cos(\beta^n-\alpha^n) & M_{ac}^n \cos(\gamma^n-\alpha^n) \\ M_{ab}^n \cos(\beta^n-\alpha^n) & L_b^n & M_{bc}^n \cos(\gamma^n-\beta^n) \\ M_{ac}^n \cos(\gamma^n-\alpha^n) & M_{bc}^n \cos(\gamma^n-\beta^n) & L_c^n \end{bmatrix} p \qquad \ldots(7.6)$$

where m is the number of pole-pairs of the unmodulated winding. The factor $(-1)^m$ resolves the problem of the polarity markings, described in Section 7.2.

All elements of the secondary self impedance matrix, Z_{33}, are zero except for h 2x2 submatrices on the leading diagonal. These terms are described in the following chapter.

The stator-rotor mutual impedance matrices, Z_{13} and Z_{23} are composed of h, 3x2 submatrices, that for the n^{th} harmonic being

$$Z_{13}^n = \begin{bmatrix} M_{ar}^n \cos \alpha^n & M_{ar}^n \sin \alpha^n \\ M_{br}^n \cos \beta^n & M_{br}^n \sin \beta^n \\ M_{cr}^n \cos \gamma^n & M_{cr}^n \sin \gamma^n \end{bmatrix} p \qquad (7.7)$$

$$Z_{23}^n = (-1)^m \begin{bmatrix} M_{ar}^n \cos (n\pi+\alpha^n) & M_{ar}^n \sin (n\pi+\alpha^n) \\ M_{br}^n \cos (n\pi+\beta^n) & M_{br}^n \sin (n\pi+\beta^n) \\ M_{cr}^n \cos (n\pi+\gamma^n) & M_{cr}^n \sin (n\pi+\gamma^n) \end{bmatrix} p \qquad (7.8)$$

where M_{ar}^n is the mutual inductance between the n^{th} harmonic winding of the a_1 segment and the n^{th} harmonic equivalent rotor winding when their axes are aligned. M_{br}^n and M_{cr}^n are similarly defined. If the turns of the equivalent rotor winding are made equal to those of the corresponding a_1 segment harmonic winding, then

$$M^n_{ar} = L^n_{br} = \sqrt{L^n_b L^n_a} \quad , \quad M^n_{cr} = \sqrt{L^n_c L^n_a} \tag{7.9}$$

The rotor-stator mutual coupling matrices, Z_{31} and Z_{32} are the transposes of Z_{13} and Z_{23} with the addition of the speed terms, $G^n_{31}\omega_m$ and $G^n_{32}\omega_m$, where

$$G^n_{31} = \begin{bmatrix} nM^n_{ar} \sin \alpha^n & nM^n_{br} \sin \beta^n & nM^n_{cr} \sin \gamma^n \\ -nM^n_{ar} \cos \alpha^n & -nM^n_{br} \cos \beta^n & -nM^n_{cr} \cos \gamma^n \end{bmatrix} \tag{7.10}$$

$$G^n_{32} = (-1)^m \begin{bmatrix} nM^n_{ar} \sin(n\pi+\alpha^n) & nM^n_{br} \sin(n\pi+\beta^n) & nM^n_{cr} \sin(n\pi+\gamma^n) \\ -nM^n_{ar} \cos(n\pi+\alpha^n) & -nM^n_{br} \cos(n\pi+\beta^n) & -nM^n_{cr} \cos(n\pi+\gamma^n) \end{bmatrix} \tag{7.11}$$

The parameters required for the formulation of the machine equations are therefore:

a) the winding segment resistances and leakage inductances,

R_a, R_b, R_c, $L_{\sigma a}$, $L_{\sigma b}$, $L_{\sigma c}$.

b) the winding egment harmonic airgap inductances

L^n_a, L^n_b, L^n_c, M^n_{ab}, M^n_{bc}, M^n_{ca}.

c) the two-axis equivalent harmonic rotor winding resistances, leakage inductances and airgap inductances,

R^n_r, $L^n_{\sigma r}$, L^n_r.

d) the rotor-stator harmonic mutual inductances,

M^n_{ar}, M^n_{br}, M^n_{cr}.

Many of these parameters are interrelated, which reduces greatly the number of unknowns. The primary airgap mutual inductances are related to the self inductances by

$$M_{xy}^{n} = \sqrt{L_x^n L_y^n} \tag{7.12}$$

The harmonic airgap inductances of a primary segment are proportional to the square of the harmonic winding factors:

$$L_x^n = Q_s (K_{wx}^n)^2 \tag{7.13}$$

where Q_s is a machine constant. Since the winding factors are readily computed, the experimental determination of a single value of L_x^n serves to determine Q_s and hence all other values of L_x^n and, from Equation 7.12, all values of M_{xy}^n.

CHAPTER VIII

A TWO-AXIS MODEL OF A SQUIRREL CAGE ROTOR

8.1 Network Equivalent of the Cage

A squirrel cage rotor comprising N bars can be considered as a network having N identical loops as shown in Figure 8.1. The N identical loops may also be considered as N phases. The total resistance of each loop is $2(R_b + R_e)$ where R_b is the resistance of one bar and R_e is the resistance of one segment of an endring. There is also a mutual resistance of $-R_b$ between the adjacent loops so that the resistance matrix is circulant having the first row given by

$$R_{1k} \doteq [2(R_b + R_e) \quad -R_b \quad 0 \quad 0 \quad \ldots\ldots\ldots \quad -R_b] \tag{8.1}$$

The inductances can be considered to have two components: one due to airgap fields and the other due to leakage fields. The latter can be described in the same way as that used for the resistances so that the leakage inductance matrix is also circulant and has the first row -

$$L_{\sigma 1k} \doteq [2(L_{\sigma b} + L_{\sigma e}) \quad -L_{\sigma b} \quad 0 \quad 0 \quad \ldots\ldots\ldots \quad -L_{\sigma b}] \tag{8.2}$$

The airgap inductances can be obtained by considering first the harmonic components of the current density distribution of one of the loops. This is represented by the pair of impulse functions shown in Figure 8.2. The n^{th} harmonic coefficients for unit current is

$$J^n = -\frac{2}{\pi}\sin\frac{n\delta_r}{2} = -\frac{2}{\pi}\sin\frac{n\pi}{N} \tag{8.3}$$

Each harmonic component may be considered to result from an equivalent sinusoidally distributed winding, carrying the same current. If this winding has w^n turns per pole, equating mmfs gives

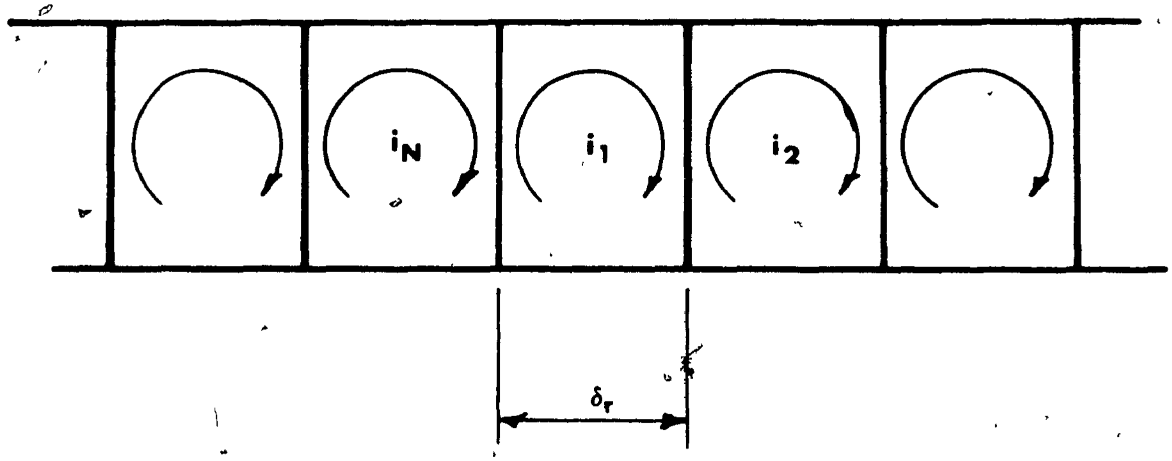

Fig. 8.1 The Squirrel Cage as a Network

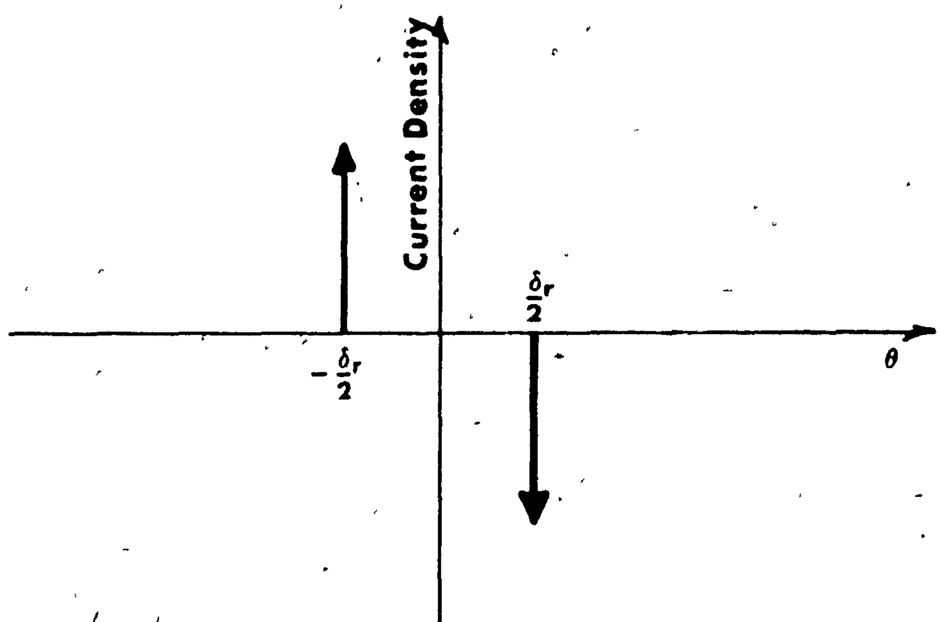

Fig. 8.2 Current Density Distribution of a Pair of Adjacent Bars

$$w^n = \frac{2}{n\pi} \sin \frac{n\pi}{N} \tag{8.4}$$

It is usually considered more convenient to use equivalent concentrated coils in circuit models. If such a coil has W^n turns per pole, its fundamental amplitude is identical provided

$$\frac{4}{\pi} W^n = w^n$$

from which $$W^n = \frac{1}{2n} \sin \frac{n\pi}{N} \tag{8.5}$$

The airgap inductance of these equivalent coils can be obtained by considering the total flux linkages which each coil produces. Thus the n^{th} harmonic component of airgap inductance is given by

$$L_r^n = Q_r \frac{1}{n^2} \sin^2 \frac{n\pi}{N} \tag{8.6}$$

where Q_r is a constant for any particular machine.

The mutual inductances are obtained by considering a pair of elemental loops, a and b, having their axes located at α and β relative to the origin of the mmf wave. The angle between them is $(\beta-\alpha)$ and the angular separation of their n^{th} harmonic equivalent windings is $n(\beta-\alpha)$. The amplitude of the mutual coupling is thus

$$L_{ab}^n = L^n \cos n(\beta-\alpha) \tag{8.7}$$

The angle $(\beta-\alpha)$ must be an integral multiple of the rotor slot pitch δ_r so that the mutual inductances with one loop are $L^n \cos n\delta_r$, $L^n \cos 2n\delta_r$ .... $L^n \cos (N-1)\delta_r$. Since $\cos (N-r)n\delta_r = \cos r\, n\delta_r$, the airgap inductance matrix is also circulant, the first row being given by

$$L_{1k}^n = L^n [1 \quad \cos n\delta_r \quad \cos 2n\delta_r \; .... \; \cos (N-1)\delta_r] \tag{8.8}$$

This completes the basic model of the squirrel cage for which each elemental loop is replaced by N identical circuits having resistance and leakage inductance components in series with a set of ideal concentrated windings each having W^n equivalent turns per pole. A circuit representation is shown in Figure 8.3.

8.2 Transformation to Two-Phase Equivalents

The basic model can now be simplified by finding a set of two-phase equivalent windings which have the same airgap harmonics. If harmonics greater than N are neglected, there are (N-1) separate two-phase systems and a zero phase sequence system[33].

The mmf distribution of the n^{th} harmonic of the k^{th} loop is

$$\mathcal{F}^n_k = \frac{4}{\pi} W^n i_k \cos n[\theta - (k-1)\delta_r]$$

$$= \frac{4}{\pi} W^n i_k [\cos n\theta \cos n(k-1)\delta_r + \sin n\theta \sin n(k-1)\delta_r] \qquad (8.9)$$

If the axes of each set of two-phase coils are chosen so that they are orthogonal with respect to their own mmf wave, the angle between them is $\frac{\pi}{2n}$ (mechanical) and the currents in coils, i^n_a and i^n_b, produce mmf waves

$$\mathcal{F}^n_a = \frac{4}{\pi} W^n_a i^n_a \cos n\theta$$

$$\mathcal{F}^n_b = \frac{4}{\pi} W^n_b i^n_b \cos n(\theta - \frac{\pi}{2n}) \qquad (8.10)$$

$$= \frac{4}{\pi} W^n_b i^n_b \sin n\theta$$

The two-phase currents which produce the same mmf distribution as rotor currents, i_k, are

$$i^n_a = \frac{W^n}{W^n_a} \sum_{k=1}^{N} i_r \cos n(k-1)\delta_r$$

$$(8.11)$$

$$i^n_b = \frac{W^n}{W^n_b} \sum_{k=1}^{N} i_r \sin n(k-1)\delta_r$$

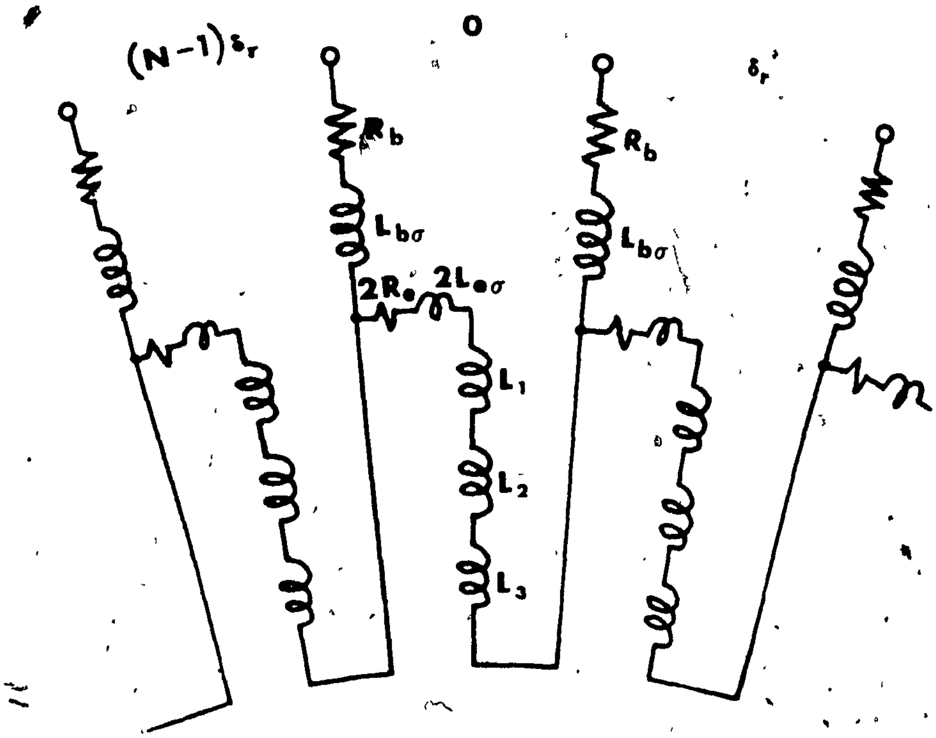

Fig. 8.3 Circuit Equivalent of the N-loop Network

Fortunately, the number of linearly independent currents required to duplicate the mmf wave is limited. This can be shown by considering two harmonics of order n_1 and n_2 such that

$$n_2(k-1)\delta_r = n_1(k-1)\delta_r + 2\pi K \tag{8.12}$$

where K is an integer. If the turns are chosen such that

$$\frac{W^{n_2}}{W_a^{n_2}} = \frac{W^{n_1}}{W_a^{n_1}} \tag{8.13}$$

the currents are equal. Dividing Equation 8.12 by $(k-1)\delta_r$ and noting that $\delta_r = \frac{2\pi}{N}$ gives

$$n_2 = n_1 + N \tag{8.14}$$

if K is chosen to equal (k-1). Thus there are N separate pairs of currents which may be required to reproduce the mmf wave.

This number can be further reduced by noting that if $n_2 = N - n_1$,

$$n_2(k-1)\delta_r = N(k-1)\delta_r - n_1(k-1)\delta_r \tag{8.15}$$

Since $N(k-1)\delta_r$ is an integral multiple of 2π

$$\cos n_2(k-1)\delta_r = \cos n_1(k-1)\delta_r$$

$$\text{and } \sin n_2(k-1)\delta_r = -\sin n_1(k-1)\delta_r \tag{8.16}$$

The currents are therefore paired in the sense that

$$i_a^{(N-n)} = i_a^n$$

$$i_b^{(N-n)} = -i_b^n \tag{8.17}$$

When N is odd the only unpaired currents are

$$i_a^N = \frac{W^N}{W_a^N}\sum_{k=1}^{N} i_r$$

$$i_b^N = 0 \tag{8.18}$$

so that the number of currents required is $\frac{1}{2}(N + 1)$ on axis a and $\frac{1}{2}(N - 1)$ on axis b. When N is even the last of the paired sets is

$$\left.\begin{aligned} i_a^N &= i_a^{N/2} \\ i_b^N &= -i_b^{N/2} = 0 \end{aligned}\right\} \qquad (8.19)$$

and the number of currents required is $\frac{1}{2}N$ on axis a and $\frac{1}{2}N - 1$ on axis b. The arrangement of coils on the two axes is shown in Figure 8.4.

8.3 Impedance Transformation

The currents in the two-phase equivalent coils are therefore related to the currents in the actual cage by

$$i_{ab} = T\, i_N = WS\, i_N \qquad (8.20)$$

where i_{ab} and i_N are the corresponding current vectors, and

$$W = \begin{bmatrix} \frac{w_a^1}{w^1} & & & & & \\ & \frac{w_b^1}{w^1} & & & & \\ & & \frac{w_a^2}{w^2} & & & \\ & & & \frac{w_b^2}{w^2} & & \\ & & & & \ddots & \\ & & & & & \frac{w_a^N}{w^N} \end{bmatrix} \qquad (8.21)$$

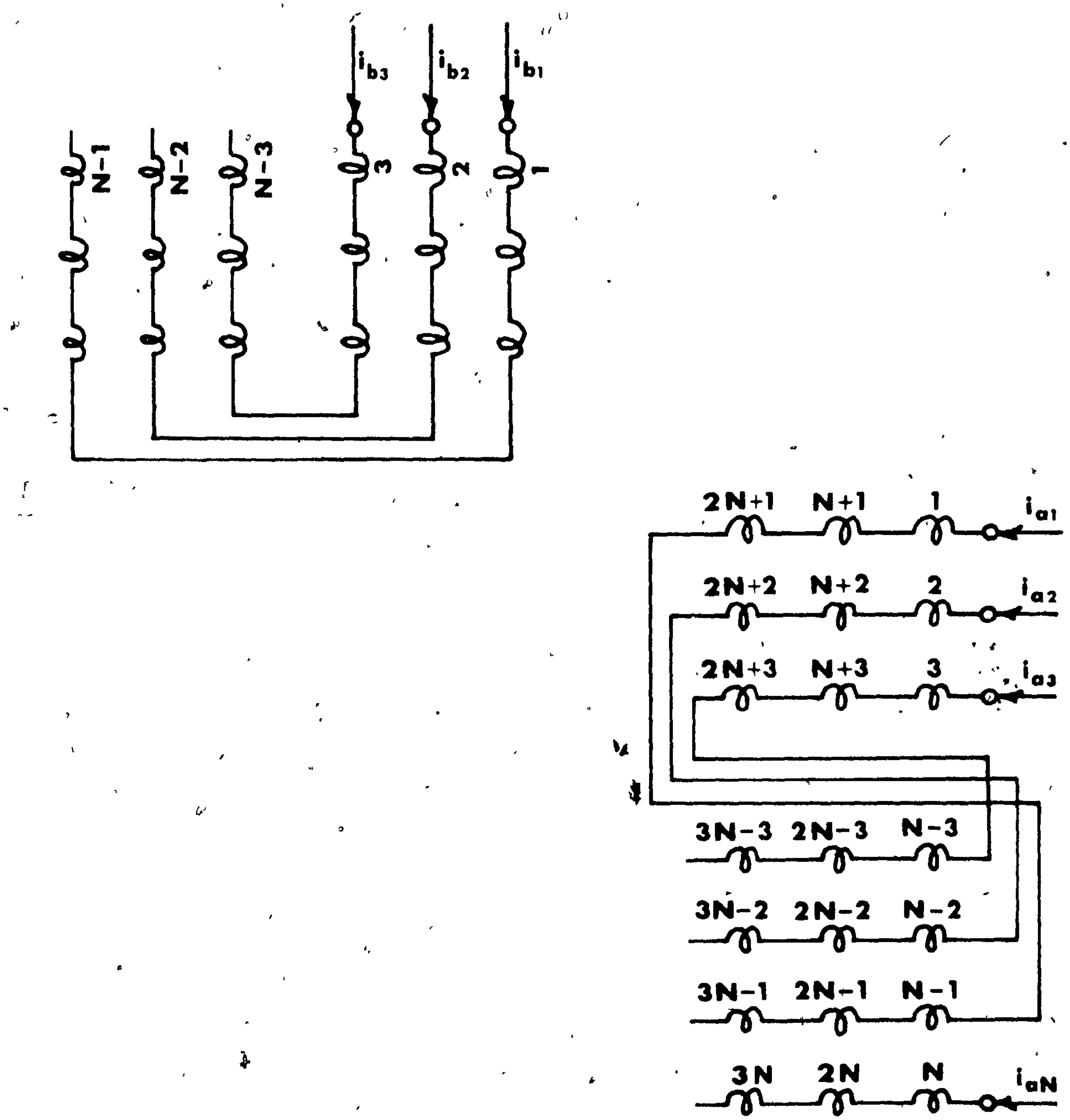

Fig. 8.4 Two-axis Arrangement of Equivalent Coils

$$S = \begin{bmatrix} 1 & \cos\delta_r & \cos 2\delta_r & \cdots & \cos(N-1)\delta_r \\ & \sin\delta_r & \sin 2\delta_r & \cdots & \sin(N-1)\delta_r \\ 1 & \cos 2\delta_r & \cos 4\delta_r & \cdots & \cos 2(N-1)\delta_r \\ & \sin 2\delta_r & \sin 4\delta_r & \cdots & \sin 2(N-1)\delta_r \\ \cdot & & & & \\ \cdot & & & & \\ \cdot & & & & \\ 1 & 1 & 1 & & 1 \end{bmatrix} \tag{8.22}$$

Both W and S are shown for the case of an odd value of N. The product of T and its transpose is the diagonal matrix,

$$H = \begin{bmatrix} \left(\frac{W_a^1}{W^1}\right)^2 \frac{N}{2} & & & & & \\ & \left(\frac{W_b^1}{W^1}\right)^2 \frac{N}{2} & & & & \\ & & \left(\frac{W_a^2}{W^2}\right)^2 \frac{N}{2} & & & \\ & & & \left(\frac{W_b^2}{W^2}\right)^2 \frac{N}{2} & & \\ & & & & \ddots & \\ & & & & & \left(\frac{W_a^N}{W^N}\right)^2 \frac{N}{2} \end{bmatrix} \quad \ldots \text{(8.23)}$$

which also is shown for an odd value of N.

The connection matrix, C, is used to derive the original variables from the transformed variables.

$$i_N = C\ i_{ab} = T^{-1}\ i_{ab} \tag{8.24}$$

and

$$C = S^t\ W^t\ H^{-1} \tag{8.25}$$

The impedances can now be transformed using this connection matrix. Since the impedance matrix is cyclic-symmetric, the transformed matrix is sparse[37,38], comprising 2x2 submatrices for each harmonic two-phase set, arrayed along the leading diagonal. The n^{th} harmonic submatrix is

$$Z_r^n = \begin{bmatrix} R_r^n + (L_{\sigma r}^n + L_r^n)p & n\omega_m(L_{\sigma r}^n + L_r^n) \\ -n\omega_m(L_{\sigma r}^n + L_r^n) & R_r^n + (L_{\sigma r}^n + L_r^n)p \end{bmatrix} \tag{8.26}$$

where

$$\begin{aligned} R_r^n &= 2[R_e + R_b(1 - \cos n\delta_r)] \\ L_{\sigma r}^n &= 2[L_{\sigma e} + L_{\sigma b}(1 - \cos n\delta_r)] \end{aligned} \tag{8.27}$$

and L_r^n is defined by Equation 8.6.

As in the case of the stator model, the determination of one of the harmonic parameters permits ready computation of the complete series. The bar and endring components can be obtained by determing the distribution of rotor resistance and leakage reactance between the bars and endrings from the dimensions of the machine.

CHAPTER IX

EXPERIMENTAL VERIFICATION OF THE MODEL

9.1 Introduction

An essential part of the process of developing a new model is that of providing an assessment of its accuracy. Details of the two machines used for this investigation are given in Appendix B. However, there are some aspects of their specifications which are worth amplifying because of the nature of the PAM machine.

9.2 The Test Machines

The machines have frames normally used for 10 HP motors. Each stator has 54 slots and the only difference between the windings is the coil span; one is 6 slots, the other 10 slots. With standard integral-slot windings they can be considered as normal 8-pole and 6-pole motors, rated at 220 volts, 3 phases, 60 Hz. The same rotor is used in each machine. With these coil spans the first machine can be connected for 6/8 poles, series delta/parallel star and the second machine for 6/4 poles, series delta/parallel star. Connections from all stator coils were brought out to a terminal board so that the winding connections could readily be changed. This panel is shown in Figure 9.1.

Since both machines have six poles when unmodulated, the windings inevitably require asymmetrical modulation. This choice was deliberate in order to present the most complex form of the problem of modelling a PAM machine.

Fig. 9.1 View of Terminal Panel

Details of the winding for the 6/8-pole machine may be found in Reference [5]. The winding for the 6/4-pole machine is similar, the sequence of the modulating waves being reversed. The 6/8-pole machine has average winding factors greater than 0.1 for pole-pair numbers 1,3,5,7,11,13,15 and 21, with numbers 5 and 15 being essentially zero phase sequence, for the unmodulated connection. For the modulated connection the corresponding pole-pair numbers are 2,4,6,14,24, with number 2 being essentially zero sequence as it ought to be. The 6/4-pole machine has average winding factors greater than 0.1 for pole-pair numbers 1,3,7,9,13 and 19, with numbers 1,7,9,13 and 19 being essentially zero sequence, for the unmodulated connection, and numbers 2,4,8,14 and 18, with number 4 being essentially zero phase sequence as it ought to be, for the modulated connection. If this information is obtained separately, the number of harmonics included in the model can be reduced, thus economizing on computer space and time to solve the equations.

9.3 Parameter Determination

Parameter values for the investigation were determined experimentally by operating the machines with a standard integral-slot, 6-pole winding and, where necessary, modifying them to take account of the different winding factors of the PAM winding.

The voltages used were approximately 10% of the rated value. This was due primarily to the maximum available current being 50A. However, it should be noted that harmonic torques are relatively largest when the core is unsaturated [39], and it is desirable from this point of view to use relatively low voltage levels. As a result, use of additional parameters modelling second order effects, as in Chapter V, is unwarranted and the only refinement to the proposed model for a PAM machine is the use of the equivalent rotor slot depth to adjust the rotor bar resistance and leakage inductance to account for skin effect based on Equations 5.1 and 5.3.

9.4 Experimental Results

The characteristics were obtained by means of the digital data acquisition system. However, in this case the data was acquired point by point to ensure that the harmonic torques were defined without excessive memory requirements.

Comparisons of measured and computed characteristics are shown for each machine with

(a) the PAM winding when unmodulated (Figures 9.2 and 9.4)

(b) the PAM winding when modulated (Figures 9.3 and 9.5)

Also shown is a comparison of measured and computed characteristics of one of the machines with a standard integral slot winding (Figure 9.6). As might be expected, the best agreement has been obtained with the integral-slot winding. However, the shapes of the PAM characteristics have been correctly computed, the effects of the harmonic mmfs being clearly seen. In particular, the computed harmonic torques are correctly proportioned and the overall difference between measured and computed characteristics is typical of stray-loss effects which are somewhat larger than those attainable with an integral-slot winding.

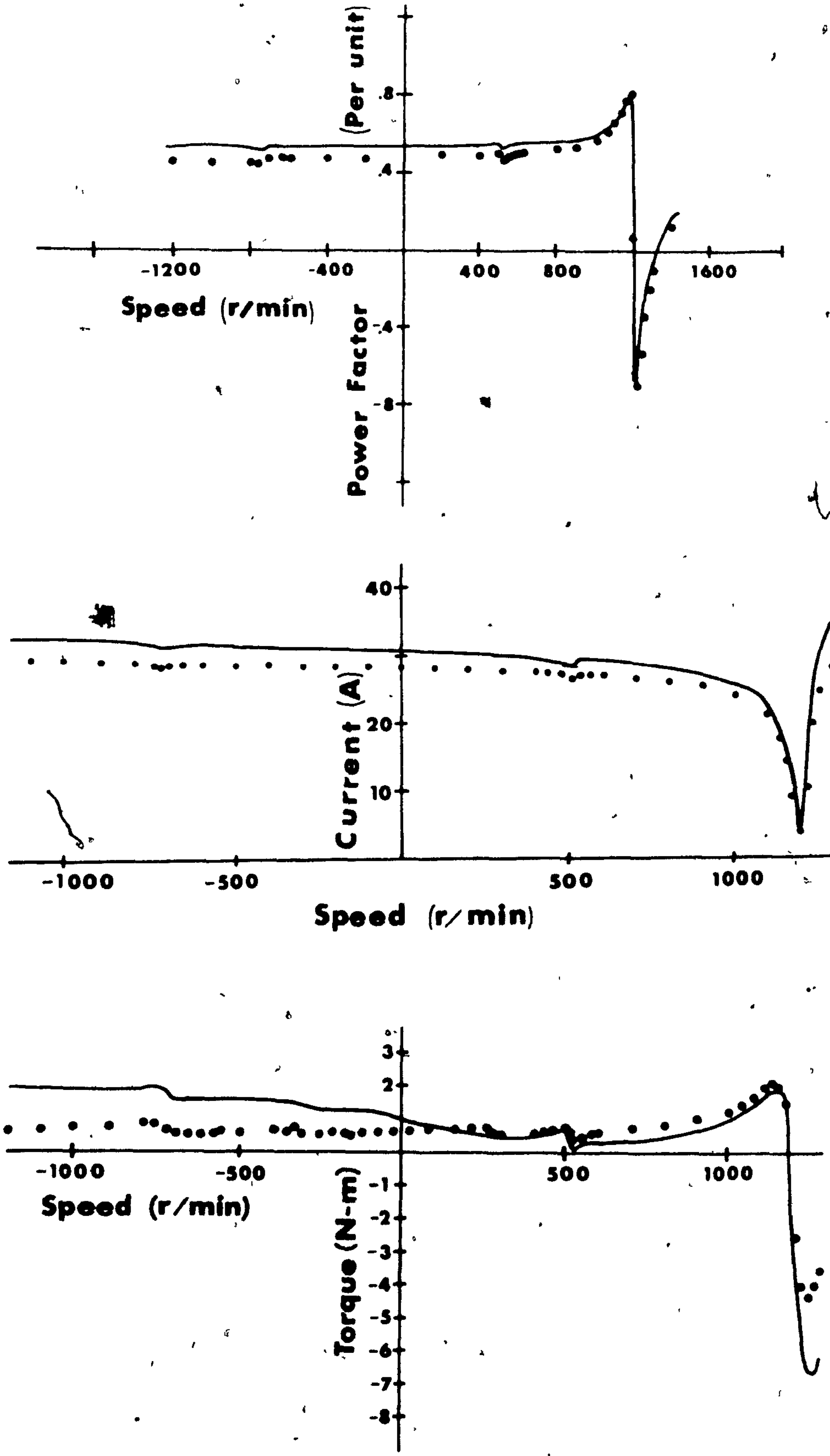

Fig. 9.2 Characteristics of the 6/8-pole Machine, Unmodulated Connection

—— measured

● calculated

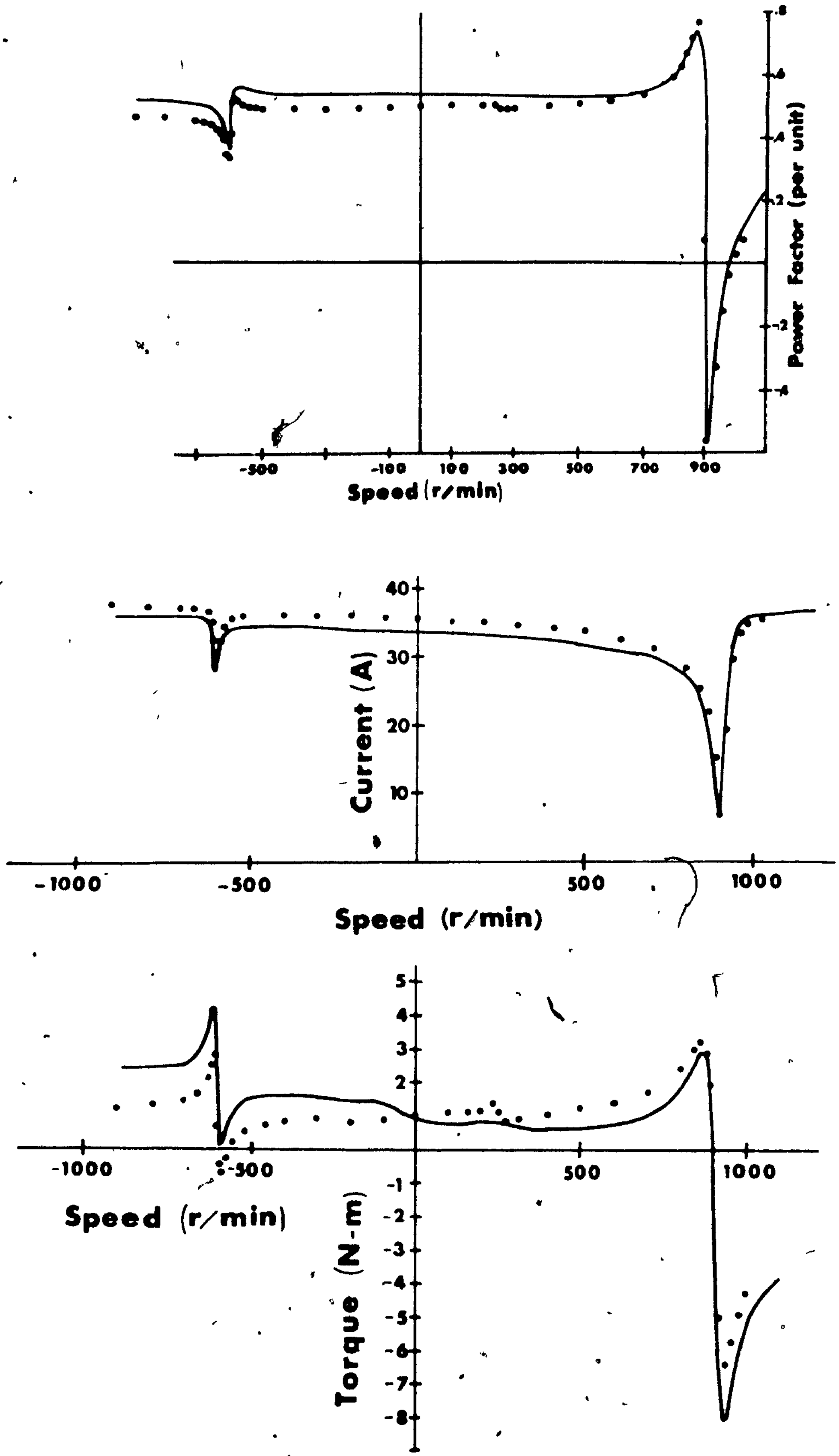

Fig. 9.3 Characteristics of the 6/8-pole Machine, Modulated Connection.

—— measured

• calculated

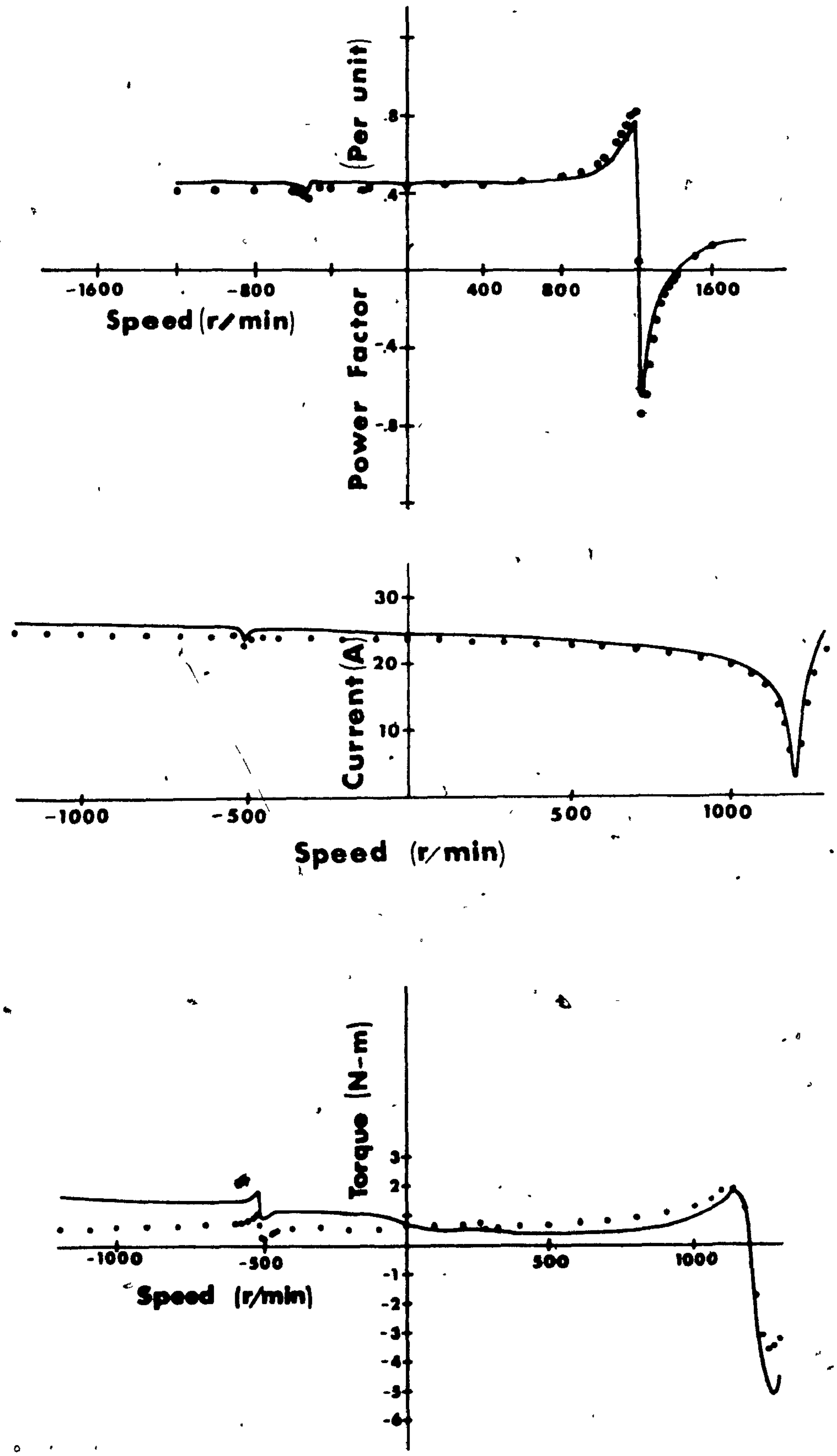

Fig. 9.4 Characteristics of the 6/4-pole Machine, Unmodulated Connection.
—— measured
● calculated

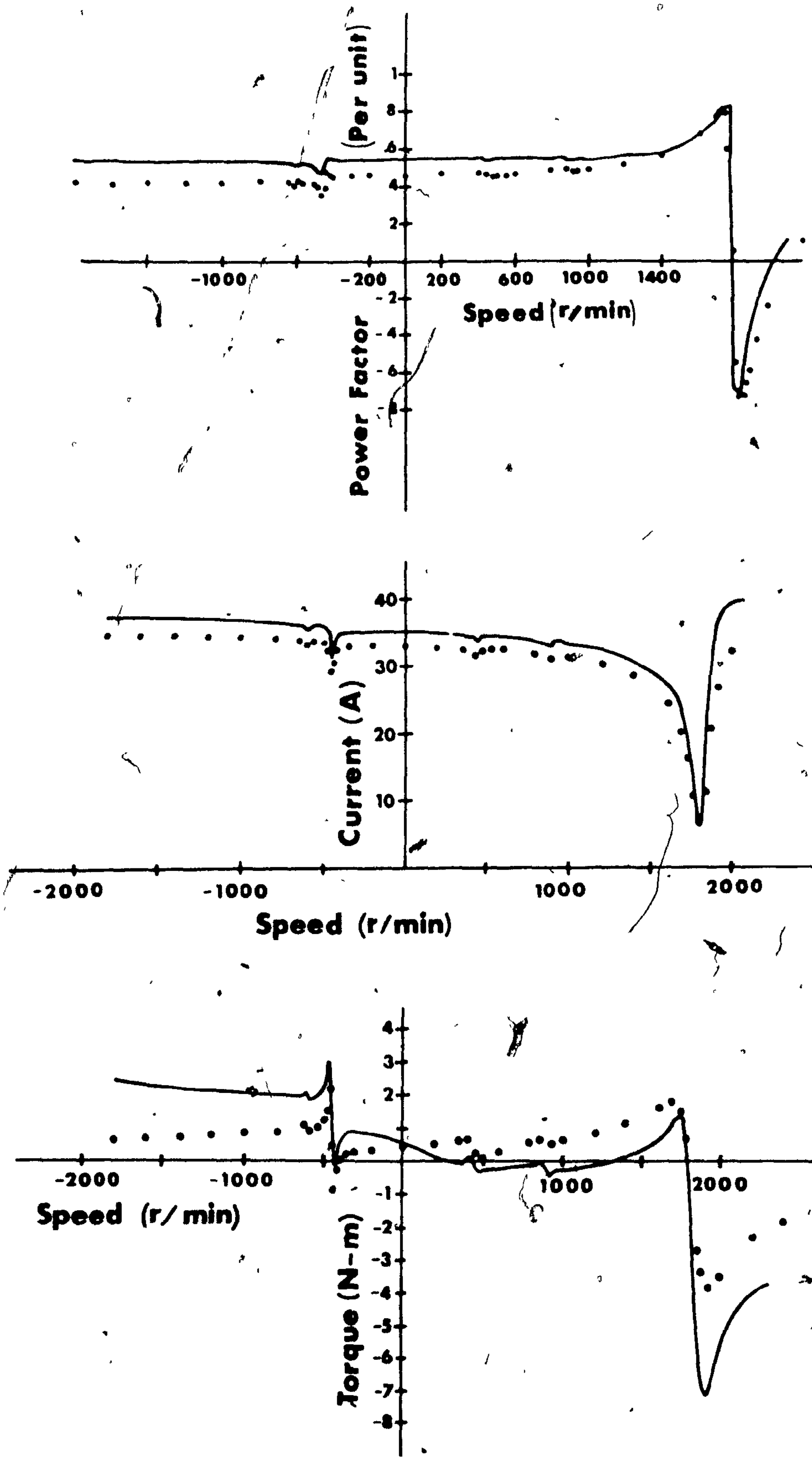

Fig. 9.5 Characteristics of the 6/4-pole Machine, Modulated Connection

—— measured

● calculated

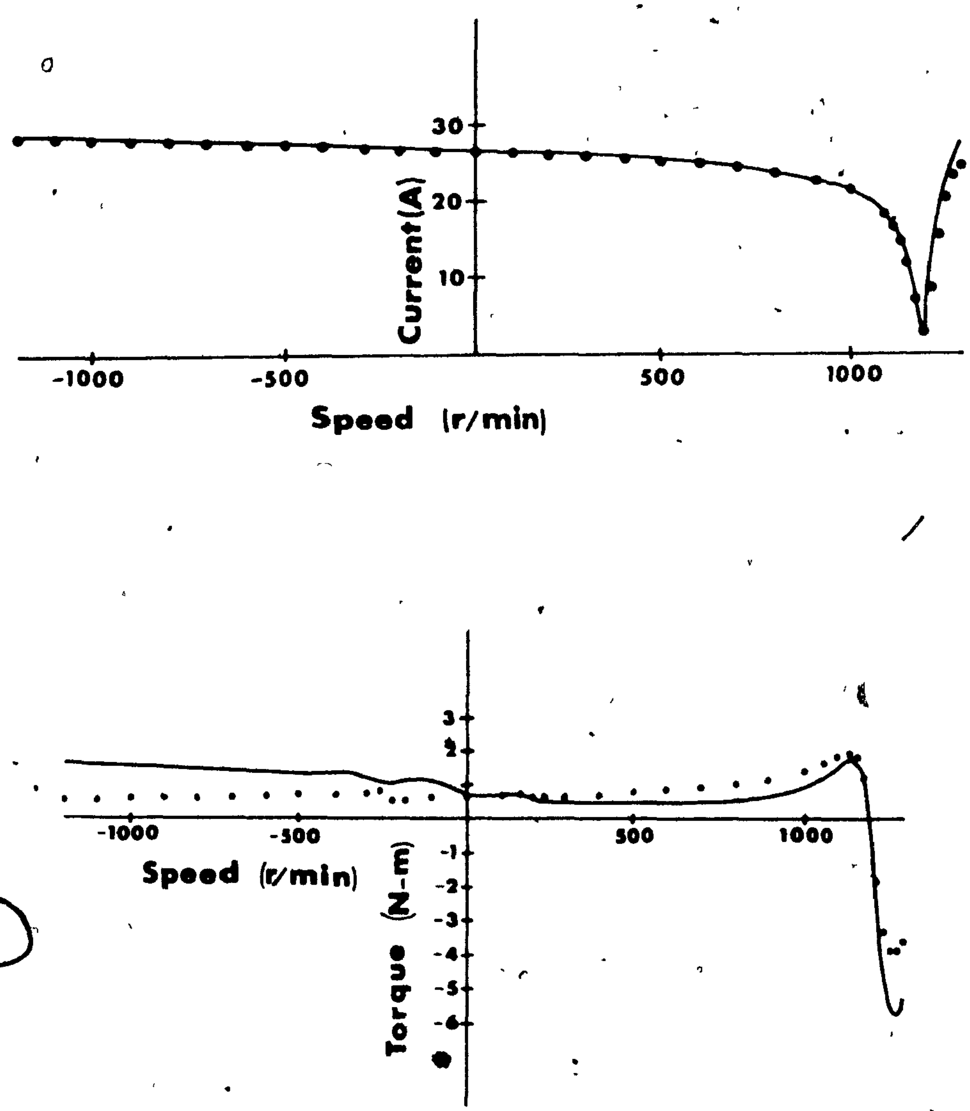

Fig. 9.6 Characteristics of the First Machine with a Standard Integral Slot Winding
— measured
• calculated

CHAPTER X

CONCLUSIONS

10.1 Standard Machines

The feasibility and conditions required for the use of optimizing techniques as an aid to induction machine parameter identification have been established for situations where the harmonic content is low. The same basic circuit model can be used for both wound and squirrel cage rotors. No knowledge of the geometry of the bars is necessary since it is the depth of an equivalent rectangular bar which is used as the additional parameter to model skin effect. In choosing an initial value it is advisable to choose a depth which is appropriate to the size of machine, and after the first set of data has been processed a better value is then available to initiate the processing of subsequent data. The initial values of the main parameters shown in Figure 4.9 are obtained from a standard analysis of data at zero and synchronous speeds; those modelling second order effects, $R_{2\sigma}$ and X_3, are given arbitrary small values.

The conditions necessary for the successful application of an optimizing technique to the determination of parameter values are the same for both the wound rotor and squirrel cage machines. The thermal model must be obtained and used to estimate the temperature variations during tests, this requiring only two short-term cooling curves. It is advisable to repeat a set of measurements at the same voltage with a view to averaging the resulting parameter values. The optimizing process should not be continued to drive the error function below a value compatible with the accuracy of the instrumentation. This is the main reason for the choice of error function to correspond to the normal form of expressing the error of the instruments used. Nevertheless, if the optimization is stopped after the same number of searches, the parameter values are virtually independent of the function used. There is no need to measure the stalled torque nor to include it in the error function provided the circuit model includes the resistive parameter, $R_{2\sigma}$, which is capable of matching the calculated and measured values.

The use of an automatic data acquisition system in addition to digital computation facilities enables the parameter values to be obtained relatively quickly, especially if a ramp velocity source is available. However, it is necessary to acknowledge the impossibility of repeating a measurement at an individual point which is apparently in error. Repetition of a set of measurements for the purpose of averaging the resulting parameter values is not difficult as the time required to acquire four sets of data for the wound rotor machine is less than one hour. For measurements at full voltage the main limitation is the time required for the machine to cool between sets of measurements. Unfortunately, such repeated measurements increase the cost of computation. An alternative approach is to arrange the programming to ignore such points in the computation of the error function, this procedure being required in any case for the points close to synchronous speed at which the ramp may have an appreciable effect on the current.

Although digital data acquisition is very helpful in that it already has the measured data in a form suitable for processing by digital computer, it is not essential for the application of an optimizing technique. The success of the squirrel cage machine investigation shows that a standard multichannel optical recorder has sufficient resolution to be used for the basic data acquisition in this approach to parameter identification, although some of the measured characteristics, after transcription to digital form, would be smoother with better resolution. The main effect of the lower resolution is that the value of error function which is compatible with the instrumentation error is higher, and therefore the resulting model may not appear to be as good. It seems reasonable to conclude, therefore, that provided the capabilities of the instrumentation, whether digital or analog, are assessed realistically, the process of parameter optimization produces quickly and economically a model which is appreciably better then the conventional model shown in Figure 4.1.

The speed of data acquisition makes it feasible to obtain reliable models at normal voltage levels. Although the voltage with the wound rotor machine was limited to less than half of the rated value, there were indications of magnetic saturation. However, with the smaller squirrel cage machine, which was operated at voltage levels up to its rated value, the effects were quite pronounced, and consistent with the onset of magnetic saturation. The leakage reactances, $X_{1\sigma}$ and $X_{2\sigma}$, decrease as the voltage increases, the effect being perhaps greater than is normally supposed. Certainly, reliable figures for stalled currents at full voltage demand that the values used for these reactances correspond to saturated conditions. The magnetizing reactance, X_0, decreases as expected. Since the error function is insensitive to changes in this parameter, the change is derived mainly from the measurement of input admittance at synchronous speed as the voltage is varied. The value of X_3, modelling the reduction in leakage reactance due to saturation of the teeth whether or not the main core is saturated, shows the reduction anticipated.

The most notable trend among the resistive parameters is that of R_2, the rotor resistance. The reduction in value as the voltage is increased is greater than expected. A slight increase is indicated in the value of the stator resistance, $R_1 + R_{1\sigma}$, the difference between low voltage and rated voltage being approximately 1%.

The trend in the equivalent depth of rotor bar shows that skin effect becomes less pronounced at higher voltages. Blocked rotor measurements, if taken at full voltage, provide an adequate model if data over a range of speeds cannot be obtained. However, since there is also a considerable change in the value of the rotor resistance with voltage, parameter values based on stalled conditions at low voltage may be considerably in error.

Perhaps the most surprising conclusion relates to the second order effects. Initially it was anticipated that experimental determination of appropriate parameter values to model these effects would be the result of using better data acquisition methods. The results have demonstrated that, not only can they be modelled successfully, but they are in fact necessary for satisfactory parameter optimization and therefore they must be included in the model.

10.2 Pole Amplitude Modulated Machines

The study of pole amplitude modulated machines has demonstrated that, whereas a dynamic circuit model has no particular advantage over a conventional model in situations such as those considered above where the phase windings are identical with low harmonic content and the system voltages are balanced, the model developed in Chapter VII is capable of predicting, with reasonable accuracy and simplicity, the characteristics of these machines in which the harmonic content is high and the windings are asymmetrical. If the torques associated with stray losses are kept in mind, there should be no difficulty in interpreting the computed torque-speed characteristic to estimate the actual characteristic. In the case of the 6/4-pole machine such a procedure would indicate that it is unlikely to develop sufficient torque to accelerate to its intended operating speed in the modulated condition, a situation which can be confirmed by inspection of the measured characteristic.

The basic parameter values used are essentially the standard ones obtainable from measurements at synchronous and zero speeds. The only additions are the choice of equivalent slot depth from operation with the integral slot winding, and the distribution of rotor resistance and leakage reactance between the endrings and bars from the dimensions of the machine. It can therefore be seen that this model requires very little information in addition to that which is normally available. Although the main emphasis has been on the measurement of basic parameter values it may be noted that the procedure is applicable, with only minor modification, at the design stage since the additions noted above are based on the internal dimensions of a machine.

To reduce the cost of computation it is advisable, first, to obtain the winding factors so that in the main program only those harmonics likely to have a significant effect are included in the model. If the symmetrical components of the winding factors are obtained at the same time, it is possible to determine the synchronous speeds of the harmonics and to arrange the programming to use smaller increments of speed in these regions. With such precautions, the central memory field length required for the main program used in this study is less than 21,000 words when dimensioned to include ten harmonic rotor windings in the model.

The application of dynamic circuit theory to PAM induction motors has therefore been shown to be a powerful tool for their analysis. As a result, it is now possible to obtain accurate quantitative information about the torque-speed characteristics of alternative designs. The programming is not excessively long and characteristics may be obtained simply and economically.

10.3 Suggestions for Further Development

Although developed specifically for PAM induction motors because of their high harmonic content, this dynamic circuit model is applicable to other similar situations. It may reasonably be expected to provide the basis of an investigation into some of the parasitic torques observed in induction motors which may be operated at different voltages by series or parallel connections of sections of the phase windings [40,41]. Since single phase PAM induction motors also have been developed and their characteristics reported [42], further development of the model for this situation should prove useful. In general, the main value of the model probably lies in the modelling of machines having irregular windings, whether intentionally [43], or in error.

For simpler situations where the phase windings are balanced and regular, parameter optimization has proved to be a valuable improvement on standard methods for the measurement of parameter values. In describing the instrumentation, reference was made to the possibility of automatic determination of parameter values. As a result of the experience gained with the automatic data acquisition system, this seems theoretically feasible provided the experimental procedure is almost entirely controlled by the digital processor. Nevertheless, it would seem wise to provide for some inspection of key characteristics to be sure that irrelevant perturbations are minimal and may safely be disregarded. Unfortunately, it is doubtful if the costs of such measurements could reasonably be considered economical.

REFERENCES

[1] P.L. Alger, "The Nature of Induction Machines", New York, Gordon and Breach, 1965, p. 325.

[2] Ibid. pp. 265 - 269.

[3] S. Chang and T. Lloyd, "Saturation Effect of Leakage Reactance", Trans. AIEE, Vol. 68, part II, pp. 1144 - 1147, 1949.

[4] B.J. Chalmers, "Saturated Leakage Reactances of Cage Induction Motors", Proc. IEE, Vol. 116, No. 8, Aug. 1969.

[5] P.L. Alger, "The Nature of Induction Machines", New York, Gordon and Breach, 1965, pp. 192 - 193.

[6] G.H. Rawcliffe and W. Fong, "Two-speed Induction Motors using Fractional-slot Windings", Proc. IEE, Vol. 112, No. 10, pp. 1899 - 1916, Oct. 1965.

[7] R.E.G. Ratcliffe, "The PAM Motor and its Application in Industry and Power Plants", Conference record of the 4th Annual Meeting of the IEEE Industry and General Applications Group, Detroit, Michigan, U.S.A., pp. 547 - 554, 12 - 16, Dec. 1969.

[8] M.G. Say, "The Performance and Design of Alternating Current Machines", 3rd edition, London, Pitman, 1958; pp. 269 - 270.

[9] H.K. Messerle, "Dynamic Circuit Theory", Oxford, Pergamon Press, 1965.

[10] G. Kron, "Tensors for Circuits", 2nd edition, New York, Dover, 1959.

[11] G.A. Battersby, "Analysis of Asymmetrical Induction-Motor Windings", Proc. IEE, Vol. 112, No. 11, Nov. 1965.

[12] S. Vibulsreth, "Magnetic Stress Anisotropy Torquemeters", M. Eng. Thesis, McGill University, 1970.

[13] "Applications Manual for Computing Amplifiers", 2nd edition, George A. Philbrick Researches, Inc., Boston, 1966, pp. 74 - 75.

[14] W.T. Martiny, R.M. McCoy and T.H. Margolis, "Thermal Relationships in an Induction Motor Under Normal and Abnormal Operation", Trans. AIEE, Vol. 80, Part III, pp. 66 - 78, 1961.

[15] J.F. Heidbreder, "Induction Motor Temperature Characteristics", Trans. AIEE, Vol. 77, part III, pp. 800 - 804, 1958.

[16] A. Tustin and J.J. Bates, "Temperature Rises in Electrical Machines on Variable Load and with Variable Speed", Proc. IEE, Vol. 103, part A, No. 11, pp. 483 - 492, October 1956.

[17] J.J. Bates and A. Tustin, "Temperature Rises in Electrical Machines as Related to the Properties of Thermal Networks", Proc. IEE, Vol. 103, part A, No. 11, pp. 471 - 482, October 1956.

[18] R.D. Slater, "Constant Speed Solutions to the Evaluation of Induction-Motor Transient Torque Peaks", Proc. IEE, Vol. 114, No. 10, pp. 1429 - 1435, October 1967.

[19] R.D. Slater, W.S. Wood, F.P. Flynn and R. Simpson, "Digital Computation of Induction-Motor Transient Torque Patterns", Proc. IEE, Vol. 113, No. 5, pp. 819 - 822, May 1966.

[20] A.E. Fitzgerald and C. Kingsley, "Electric Machinery", New York, McGraw-Hill, second edition, 1961, pp. 479 - 482.

[21] D. O'Kelly, "Eddy-Current and Hysteresis Effects in Rotating Machines", Proc. IEE, Vol. 116, No. 3, pp. 391 - 395, March 1969.

[22] F.F. Martin, "Computer Modeling and Simulation", New York, Wiley, 1968, pp. 280 - 281.

[23] D. Morris, "Some Tests of an Exact Practical Equivalent Theory of the Induction Motor", Proc. IEE, Vol. 97, part II, no. 55, pp. 767-778, December 1950.

[24] G.C. Goodwin, "Application of Curvature Methods to Parameter and State Estimation", Proc. IEE, Vol. 116, No. 6, pp. 1107 - 1110, June 1969.

[25] R. Fletcher and C.M. Reeves, "Function Minimization by Conjugate Gradients", Computer Journal, Vol. 7, No. 2, pp. 149 - 154, 1964.

[26] G.A. Bekey and W.J. Karplus, "Hybrid Computation", New York, Wiley, 1968, pp. 276 - 278.

[27] K.J. Binns, "Cogging Torques in Induction Machines", Proc. IEE, Vol. 115, No. 12, December 1968, pp. 1783 - 1789.

[28] P. Silvester, "Dynamic Resistance and Inductance of Slot-Embedded Conductors", IEEE Trans. on Power Apparatus and Systems, Vol. PAS-87, pp. 250 - 256, January 1968.

[29] E.A. Klingshirn and H.E. Jordan, "Simulation of Polyphase Induction Machines with Deep Rotor Bars", IEEE Trans. on Power Apparatus and Systems, Vol. PAS-89, pp. 1038 - 1043, July/August 1970.

[30] G.H. Rawcliffe, R.F. Burbidge, and W. Fong, "Induction-Motor Speed Changing by Pole-Amplitude Modulation", Proc. IEE, Vol. 105A, pp. 411 - 419, August 1958.

[31] B.P. Lathi, "Communication Systems", New York, Wiley, 1968, pp. 148 - 181.

[32] G.H. Rawcliffe and W. Fong, "Close-Ratio Two-Speed Single-Winding Induction Motors", Proc. IEE, Vol. 110, No. 5, pp. 916 - 934, May 1963.

[33] G.H. Rawcliffe and W. Fong, "Clock Diagrams and Pole-Amplitude Modulation", Proc. IEE, Vol. 118, No. 5, pp. 675 - 680, May 1971.

[34] G.H. Rawcliffe and W. Fong, "Speed-Changing Induction Motors: Further Developments in Pole-Amplitude Modulation", Proc. IEE, Vol. 107A, No. 36, pp. 513 - 528, December 1960.

[35] G.H. Rawcliffe and W. Fong, "Slip-Ring P.A.M. Induction Motors for Two Synchronous Speeds", IEEE Trans. on Power Apparatus and Systems, Vol. PAS-90, No. 2, pp. 495 - 499, March/April 1971.

[36] T.H. Barton and J.C. Dunfield, "Polyphase to Two-Axis Transformation for Real Windings", IEEE Trans. on Power Apparatus and Systems, Vol. PAS-87, No. 5, pp. 1342 - 1346, May 1968.

[37] J.C. Sabonnadiere and M. Poloujadoff, "Multiple Eigenvalues and Corresponding Eigenvectors in the Study of Symmetrical and Related Components", The Matrix and Tensor Quarterly, Vol. 18, No. 2, pp. 44 - 54, December 1967.

[38] T.H. Barton and M. Poloujadoff, "A Generalized Symmetrical Component Transformation for Cylindrical Electrical Machines", IEEE Trans. on Power Apparatus and Systems, Vol. PAS-91, No. 5, September/October 1972, pp. 1781 - 1786.

[39] M.S. Erlicki, "Parasitic Torques of Saturated Asynchronous Motors", IEEE Trans. on Power Apparatus and Systems, Vol. PAS-91, No. 4, pp. 1501 - 1505, July/August 1972.

[40] K. Oberretl, "New Facts about Parasitic Torques in Squirrel Cage Induction Motors", Bull. Oerlikon, No. 348, pp. 130 - 155, May 1962.

[41] E.R. Laithwaite, "Differences Between Series and Parallel Connection in Machines with Asymmetric Magnetic Circuits", Proc. IEE, Vol. 112, No. 11, pp. 2074 - 2082, November 1965.

[42] M.R. Krishnamurthy and K.C. Rajaraman, "Three-Speed Single-Winding Single-Phase Induction Motor", Proc. IEE, Vol. 112, No. 6, pp. 1135 - 1143, June 1965

[43] W. Fong, "Polyphase Symmetrisation: A New Method for the Design of Electrical-Machine Windings", Proc. IEE, Vol. 115, No. 8, pp. 1123 - 1134, August 1968.

APPENDIX A

Determination of Parameter Values by Curve Fitting

The use of a curve fitting technique to obtain parameter values is a process having two distinct parts. First, it is necessary to interpret the experimental data in terms of the modified Morris model of Figure 4.4. However, in order to obtain a suitable polynomial it is necessary to neglect the rotor core loss parameters R_{c1} and R_{c2}. This model is then transformed to the more conventional form of Figure 4.9.

The Modified Morris Model Relationships

Comparison of Figures 4.3 and 4.4 gives

$$R_m + j\,X_m = R + R_{1\sigma} + R_o + j(X_{1\sigma} + X_o)$$

$$k e^{j\theta} = \frac{R_o + j\,X_o}{R_m + j\,X_m} \qquad \text{....A-1}$$

$$R_e + j\,X_e = \frac{(R_1 + R_{1\sigma} + j\,X_{1\sigma})(R_o + j\,X_o)}{R_m + j\,X_m}$$

The components of Z_σ are:

$$R_\sigma = \frac{1}{k^2}\left[\frac{R_{c1}s + R_{c2}}{R_{c1}s + R_{c2} + R_2} \cdot \frac{R_2}{s} \cos 2\theta + (R_s \cos 2\theta + X_s \sin 2\theta) - X_3 \sin 2\theta\ |s|\right]$$

....A-2

$$X_\sigma = \frac{1}{k^2}\left[\frac{-(R_{c1}s + R_{c2})}{R_{c1}s + R_{c2} + R_2} \cdot \frac{R_2}{s} \sin 2\theta + (X_s \cos 2\theta - R_s \sin 2\theta) - X_3 \cos 2\theta\ |s|\right]$$

....A-3

where $$R_s = R_e + R_{2\sigma}\frac{|s|}{s}$$

....A-4

$$X_s = X_e + X_{2\sigma}$$

If R_σ and X_σ are multiplied by s, and restricted to positive values of slip at which the effect of R_{c1} and R_{c2} is negligible, these equations become

$$R_\sigma s = a_o + a_1 s + a_2 s^2$$
$$X_\sigma s = b_o + b_2 s + b_2 s^2 \qquad \text{....A-5}$$

where

$$a_o = R_2' \cos 2\theta$$
$$b_o = - R_2' \sin 2\theta$$
$$a_1 = R_s' \cos 2\theta + X_s' \sin 2\theta$$
$$b_1 = X_s' \cos 2\theta - R_s' \sin 2\theta \qquad \text{....A-6}$$
$$a_2 = - X_3' \sin 2\theta$$
$$b_2 = - X_3' \cos 2\theta$$

and

$$R' = \frac{R_2}{k^2} \text{ etc.}$$

Thus, if the measured data is processed to give values of $R_\sigma s$ and $X_\sigma s$ over a range of values of slip, a quadratic curve fitting procedure may be used to determine values for a_o, b_o, a_1, b_1, a_2, b_2. The equations may then be solved yielding:

$$\tan 2\theta = - \frac{b_o}{a_o}$$

$$R_2' = \frac{a_o}{\cos 2\theta}$$

$$R_s' = a_1 \cos 2\theta - b_1 \sin 2\theta \qquad \text{...A-7}$$

$$X_s' = b_1 \cos 2\theta + a_1 \sin 2\theta$$

$$X_3' = - \frac{b_2}{\cos 2\theta}$$

To divide R_s' into its components R_e' and $R_{2\sigma}'$ it is necessary to consider the stalled torque:

$$T_s = \frac{q\, I_{\sigma s}^2 \quad (R_2' + R_{2\sigma}')}{\omega_s} \qquad \text{....A-8}$$

where q is the number of phases

ω_s is the synchronous speed

and $I_{\sigma s}$ is the value of I_σ when stalled.

Thus measurement of the stalled torque gives

$$R_{2\sigma}' = \frac{T_s \omega_s}{q\, I_{\sigma s}^2} - R_2' \qquad \text{....A-9}$$

and $$R_e' = R_s' - R_{2\sigma}' \qquad \text{....A-10}$$

Transformation to Conventional Form

Although the model can be used in this form, it suffers from the fact that some of its parameters cannot be associated directly with physical concepts such as the resistance of a particular winding or with the leakage flux. It is therefore desirable to transform this model to the form of Figure 4.9. This can be done by further consideration of the relationships between the parameters of Figures 4.3 and 4.4, given in equation A-1.

$$k_e^{j\theta} = \frac{1}{Z_m^2} \left[(R_o R_m + X_o X_m) + j(R_m X_o - R_o X_m) \right] \qquad \text{....A-11}$$

where $$Z_m^2 = R_m^2 + X_m^2$$

and is obtained from measurements at synchronous speed.

Also, $$\tan\theta = \frac{R_m X_o - R_o X_m}{R_o R_m + X_o X_m} \qquad \text{....A-12}$$

$$R_e = \frac{1}{Z_m^2} \left[(R_{11} R_o - X_{1\sigma} X_o)\, R_m + (R_{11} X_o + X_{1\sigma} R_o)\, X_m \right]$$

$$\text{....A-13}$$

$$X_e = \frac{1}{Z_m^2} \left[(R_{11} X_o + X_{1\sigma} R_o)\, R_m - (R_{11} R_o - X_{1\sigma} X_o)\, X_m \right]$$

where $R_{11} = R_1 + R_{1\sigma}$

If the ratio of X_o to R_o is defined as a factor F_o, an expression for R_o can be obtained by first noting:

$$X_{1\sigma} = X_m - X_o$$

$$R_{11} = R_m - R_o \qquad \text{....A-14}$$

$$R_e = \frac{1}{Z_m^2}\left[- G_o R_o^2 + Z_m^2 R_o\right]$$

where $G_o = 2\, F_o X_m - (F_o^2 - 1) R_m$

and thus $G_o R_o^2 - Z_m^2 R_o + Z_m^2 R_e = 0 \qquad \text{....A-15}$

However it must now be noted that although Z_m and G_o can be obtained from measurements, it is R_e' rather than R_e which is known from equation A-10. If equation A-1 is further rearranged to give

$$k^2 = \frac{R_o^2 + X_o^2}{R_m^2 + X_m^2} = \frac{R_o}{Z_m^2}(1 + F_o^2)$$

substitution of $R_e' k^2$ for R_e in equation A-15 yields

$$R_o = \frac{Z_m^2}{G_o + (1 + F_o^2)\, R_e'} \qquad \text{....A-16}$$

Having determined R_o, the remaining parameters are readily obtained:

$$X_o = R_o F_o$$

$$X_{1\sigma} = X_m - X_o$$

$$R_1 = R_m - R_o$$

$$k^2 = \frac{R_o^2 + X_o^2}{Z_m^2} \qquad \text{....A-17}$$

$$R_2 = R_2' \, k^2$$

$$X_{2\sigma} = X_s - X_e$$

$$R_{2\sigma} = R'_{2\sigma}\ k^2$$

$$X_3 = X'_3\ k^2$$

This completes the derivation of the model, but some consideration should be given to the sensitivity of the parameter values to measurement errors. The factor F_o is likely to be sensitive to error in the angle θ since it is small. This, however, does not lead to significant error in the core loss parameter, R_o, which is quite insensitive to error in the angle θ. The main problem caused by the difficulty in obtaining a reliable figure for this angle is that the values of $X_{1\sigma}$ and $X_{2\sigma}$ are extremely sensitive. During computation the value of θ is therefore adjusted to produce a specified ratio of $X_{1\sigma}$ to $X_{2\sigma}$. This extreme sensitivity is a direct result of the fact that the ratio of $X_{1\sigma}$ to $X_{2\sigma}$ has little effect on the external characteristics of an induction machine.

APPENDIX B

Details of Machines

Wound Rotor Machine

Rating:	7 1/2 HP, 220 V, 60 Hz, 1725 rpm.	
	Full load stator current	20.4 A
	Rotor voltage	170 V
	Rotor current	21.3 A

Squirrel Cage Machine

Rating:	2 HP, 208 V, 60 Hz, 1700 rpm.	
	Full load stator current	6.9 A

Stator slot dimensions: Figure B - 1

Rotor slot dimensions: Figure B - 2

Pole Amplitude Modulated Machines

Rating (both machines): 10 HP, 220 V, 60 Hz

Stator details:

	Stator No. 1	Stator No. 2
Stack Length	5 inch	5 inch
Turns per coil	5	5
Conductor size	2 #13	2 #13
Coil span	1 - 7	1 - 11
Length of mean turn	22.5 inch	27.0 inch
Number of Slots	54	54
Slot dimensions	Figure B-3	Figure B-3
Airgap	0.0175 inch	0.0175 inch

Rotor details:

Outer diameter	8.465 inch
Skew	0.9 rotor slot pitch
Slot dimensions	Figure B-4
Number of slots	42

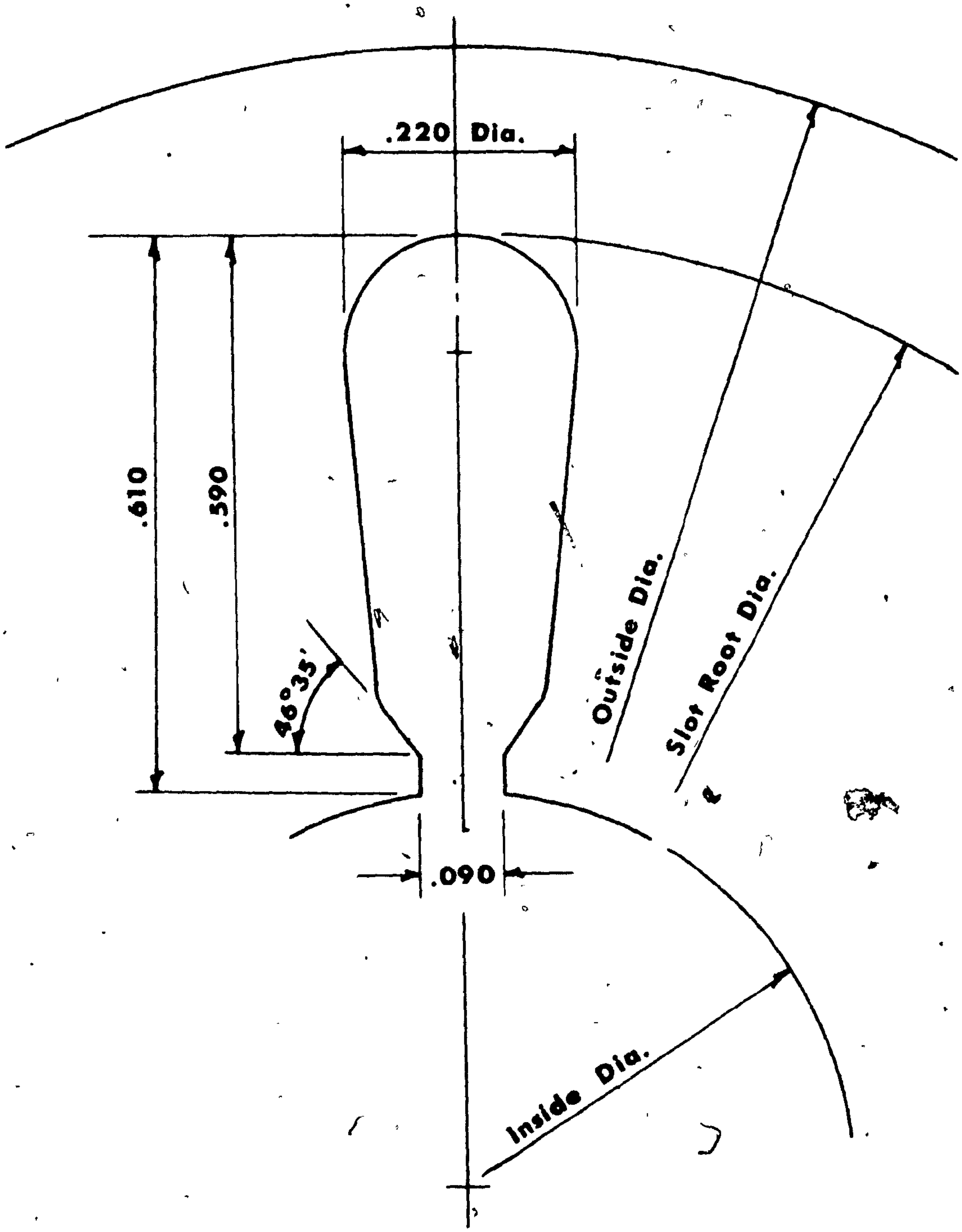

Fig. B-1 Detail of Stator Slot of 2 HP Machine

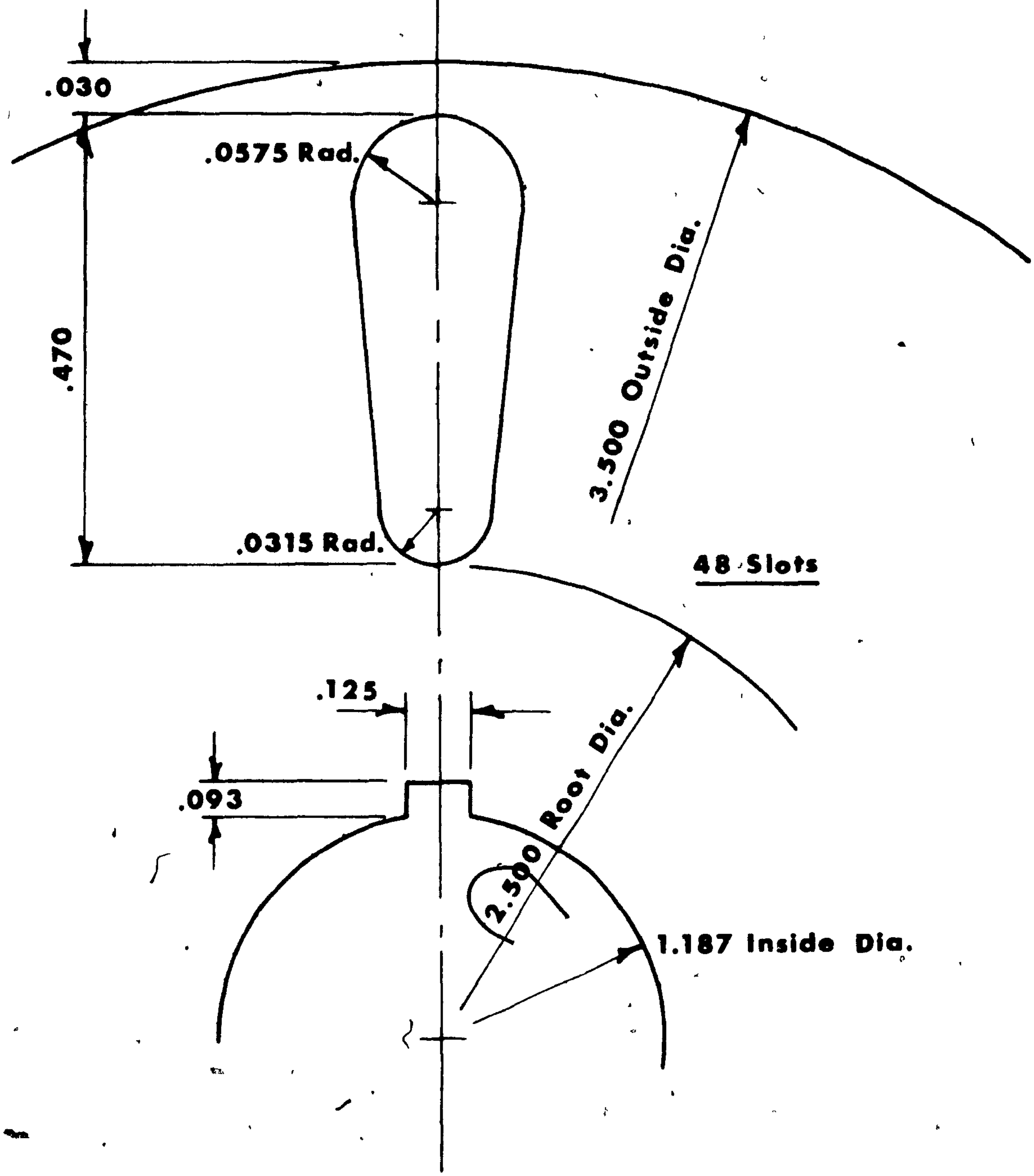

Fig. B-2 Detail of Rotor Slot of 2 HP Machine

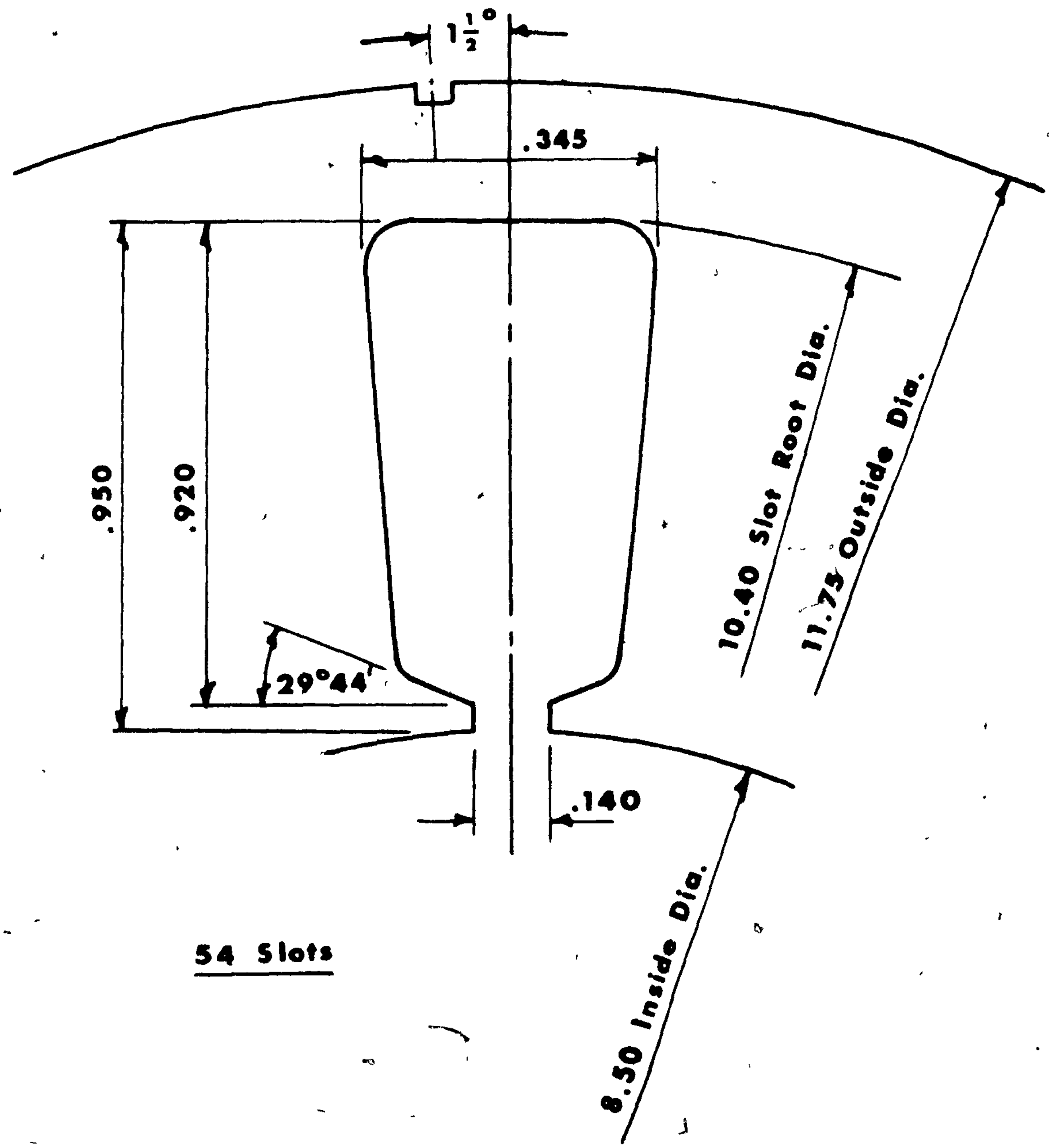

Fig. B-3 Detail of Stator Slot of 10 HP Machine

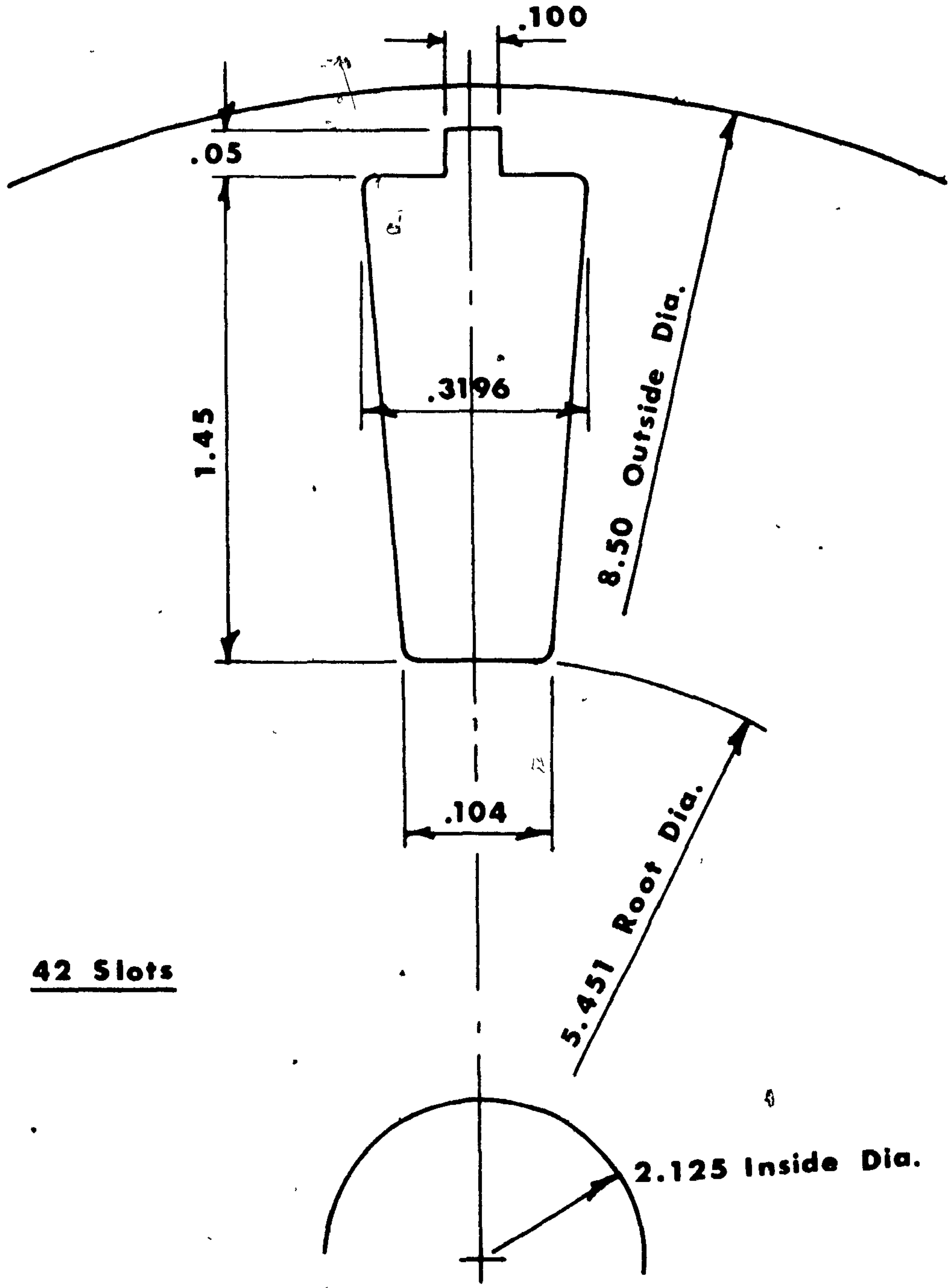

Fig. B-4 Detail of Rotor Slot of 10 HP Machine